HAYNES International

A Guide to the Metallurgical, Corrosion, and Wear Characteristics of the Wrought Nickel and Cobalt Alloys

Written by: Dr. Paul Crook

HAYNES International

A Guide to the Metallurgical, Corrosion, and Wear Characteristics of the Wrought Nickel and Cobalt Alloys

Contents

Introduction

The wrought, corrosion-resistant, nickel-based alloys are vitally important in a number of industries, particularly chemical processing, petrochemical, agrichemical, and pharmaceutical. They exhibit much higher resistance than the stainless steels to many of the key industrial chemicals, and most are inherently resistant to chloride-induced localized attack and stress corrosion cracking. The closely-related, wrought, corrosion-resistant, cobalt-based alloys are used more sparingly, on account of their cost; nevertheless, they provide the added benefit of resistance to certain forms of wear that can be encountered in these same industries.

The purpose of this manual is to describe the characteristics and attributes of these materials in detail, and, in doing so, pass on much of Haynes International's practical knowledge in the fields of aqueous corrosion, wear, and metallurgy (of those wrought, nickel and cobalt alloys designed for moderate temperature use).

For perspective, it should be mentioned that within the realm of nickel and cobalt alloys, these represent just a portion. For example, an equal or greater number of such alloys were designed for, and are used at, high temperatures (>500°C), notably in flying and land-based gas turbines. Furthermore, numerous wear-resistant cobalt alloys with insufficient ductility for wrought processing are used in the form of castings and weld overlays, in hostile, moderate and high temperature environments.

Nickel Alloy Background

Nickel is an ideal base for alloys resistant to aqueous corrosion, for the following reasons:

1. There is a plentiful supply of nickel, at a reasonable price.
2. It is inherently more resistant to corrosion than iron.
3. It exhibits a ductile, face-centered cubic structure (known as "gamma" phase, and which is similar to the favored "austenite" in stainless steels) throughout its solid range.
4. Beneficial elements, in particular chromium, copper, and molybdenum, are highly soluble in nickel (i.e. they can be added in significant quantities without causing the precipitation of second phases in the microstructure).
5. As a result of their high ductility, they are very amenable to wrought processing (hot and cold), fabrication, and welding.

Chromium, copper, molybdenum, and iron are among the elements added to nickel, to enhance its corrosion resistance, or (in the case of iron) to reduce costs.

The primary role of chromium in nickel-based alloys is to enable the formation of protective ("passive"), chromium-rich (oxide or hydroxide) surface films in corrosive solutions of an oxidizing nature. Such solutions induce cathodic reactions of high potential involving oxygen, whereas solutions of a reducing nature induce lower potential cathodic reactions involving hydrogen evolution.

Pure nitric acid solutions are oxidizing, as are many impure solutions of other acids. Impurities with strong oxidizing tendencies include ferric ions and dissolved oxygen. As with steels, which are only regarded as "stainless" when chromium contents exceed approximately 13 wt.%, the corrosion-resistant nickel alloys also require a threshold chromium content to enable passivation in oxidizing solutions. This is believed to be around 15 wt.%. More typical in the most versatile nickel alloys are contents ranging from 16 to 23 wt.%.

Copper, which is mutually soluble in nickel (i.e. all mixtures of the two elements exhibit a single FCC structure, in the absence of other alloying elements), enhances the resistance of nickel in seawater and reducing acids, especially hydrofluoric. It is used in small quantities in some of the chromium-bearing alloys of nickel, but is a major constituent of several corrosion-resistant nickel alloys (associated with the MONEL® trademark), with copper contents at around 30 wt.%.

Molybdenum ennobles nickel and therefore enhances its resistance to reducing acids, i.e. those that induce a cathodic reaction involving the release of hydrogen. Such acids include hydrochloric and sulfuric, the most commonly encountered industrial corrosives. Since atoms of molybdenum are relatively large, it also strengthens the gamma solid solution. Tungsten (from the same group of elements, and with an even larger atomic size) is used as a partial substitute for molybdenum in some alloys. The solubilities of molybdenum and tungsten, especially in the presence of other elements such as chromium, are limited. However, molybdenum levels of 15 to 20 wt.% are possible in chromium-bearing nickel alloys, and molybdenum contents of 30 wt.% are feasible in nickel alloys with only minor additions of other elements.

As already mentioned, the reason for adding iron is usually economic, either to allow the use of less expensive charge materials during melting, or to produce materials which bridge the cost/performance gap between the corrosion-resistant nickel-based alloys and the austenitic and duplex (austenitic/ferritic) stainless steels. One of the problems of adding iron is that it reduces the solubilities (in the nickel-rich, gamma solid solution) of more beneficial elements, such as chromium and molybdenum, thus restricting the use of these elements, or causing the presence of second phases deleterious to ductility and/or corrosion resistance.

Other elements sometimes added to the wrought, corrosion-resistant nickel alloys (albeit in small amounts) include:

1. Aluminum, either for oxygen control during melting, or (at slightly higher levels) to induce the precipitation of fine “gamma-prime” particles in the microstructure, for strengthening purposes. While gamma-prime (as a second phase) reduces corrosion resistance to some extent, gamma-prime strengthened versions of various nickel alloys have been commercially successful.
2. Manganese, for sulfur control during the melting process.
3. Titanium, to tie up any residual carbon (and/or nitrogen) in the form of stable carbides and/or carbo-nitrides, or to participate in the formation of fine, strengthening, gamma-prime precipitates.
4. Niobium (columbium), which can also tie up residual carbon, and (at slightly higher levels) give rise to an alternate, fine, strengthening precipitate known as “gamma-double prime”.

Carbon and silicon are undesirable residuals in most wrought, corrosion-resistant, nickel-based alloys, and sophisticated techniques (such as argon-oxygen decarburization, or AOD) are employed during melting to minimize the contents of these two elements. They are undesirable because they are not very soluble in nickel, and can give rise to deleterious precipitates, particularly at the grain boundaries, both during hot working and welding (of annealed material).

A key step in the production and fabrication of these alloy is solution annealing, followed by rapid cooling (quenching). This enables the dissolution of unwanted second phase precipitates (due to over-alloying, or the presence of residuals, such as carbon and silicon) that might have occurred during hot (or warm) working, and the “locking-in” of this largely, single-phase structure. Meta-stability is generally only a problem in the heat-affected zones of subsequent welds, where grain boundary precipitation can give rise to preferential attack of the boundaries in certain corrosive media. Structural changes during service are of little concern, since the intended use temperatures of these materials are below those required to cause significant diffusion.

Cobalt Alloy Background

Despite their close proximity in the Periodic Table, there are substantial differences between the atomic structures and characteristics of nickel and cobalt. Like nickel, cobalt is inherently resistant to corrosion, and can accommodate high levels of beneficial elements. However, cobalt exhibits two atomic forms:

1. A low temperature hexagonal close packed (HCP) form.
2. A high temperature face-centered cubic (FCC) form.

The transformation temperature of pure cobalt is 417°C. Alloying elements such as nickel, iron, and carbon (within its limited soluble range) are known as FCC stabilizers, and suppress the transformation temperature. Chromium, molybdenum, and tungsten, on the other hand, are HCP stabilizers and increase the transformation temperature.

In reality, the transformation is extremely sluggish, and not easily brought about by either heating or cooling. Indeed, after solidification from the molten state (or after solution annealing and quenching, in the case of wrought products), cobalt and cobalt alloys (with elevated transformation temperatures) normally exhibit metastable FCC structures at room temperature. However, partial transformation to HCP is easily induced by cold-work (i.e. plastic deformation at room temperature).

The transformation of cobalt and cobalt alloys under the action of mechanical stresses is believed to progress by the creation of wide stacking faults (the FCC form of the materials having very low stacking fault energies) and by subsequent coalescence. Extensive micro-twinning is also observed in plastically-deformed, cobalt-based alloys.

Chromium provides the same benefits to cobalt as it does to nickel, i.e. it is key to the formation of protective films/scales in both corrosive fluids and high-temperature gases. Moreover, it influences the driving force for structural change in cobalt and its alloys, which in turn affects their mechanical and wear behavior.

The primary role of nickel (if present) in the cobalt-based is to stabilize the FCC form. This negatively impacts wear performance, but provides many benefits, especially ease of wrought processing (at sufficiently high nickel contents).

Molybdenum and tungsten are both strong, solid-solution strengthening agents in cobalt-based alloys. They also result in higher transformation temperatures, which increase resistance to those forms of wear that involve a micro-fatigue component (such as metal-to-metal sliding and cavitation erosion). Molybdenum is used in those cobalt alloys designed primarily for resistance to aqueous corrosion and wear. Tungsten is used in those wrought cobalt alloys designed for high temperature use and those cast (and weld overlay), high-carbon alloys designed primarily for wear resistance in hostile environments.

In the cast (and weld overlay) cobalt alloys with relatively high carbon contents (i.e. from 0.5 to 3.5 wt.%), chromium, molybdenum, and tungsten also encourage the formation of carbides within the microstructure. These carbides (chromium-rich M_7C_3 and $M_{23}C_6$, and molybdenum/tungsten-rich M_6C) are very beneficial under low stress (two-body) abrasion conditions.

As with the nickel-based alloys, iron can be used to reduce cost, particularly if it allows the use of ferro-compounds or iron-contaminated scraps in the charge materials during melting. However, it can also be used as an alternate FCC stabilizer (rather than nickel), to decrease the transformation temperature and make the alloys more amenable to wrought processing and fabrication.

The solubility of carbon in cobalt is higher than that in nickel; thus, there is less need to minimize carbon in wrought, corrosion- and wear-resistant, cobalt-based alloys. Furthermore, carbon is an important minor addition to the wrought, high temperature alloys (both of cobalt and nickel), and a major addition to those cast and weld overlay, cobalt alloys designed primarily for resistance to wear. Its purpose in the high temperature alloys is for strengthening, through the formation of sparsely dispersed carbides. Its purpose in the wear-resistant alloys is to generate high volume fractions of carbide in their microstructures, to increase their cutting and deformation resistance.

Nickel Alloy Groups

There are many commercially-available, wrought, corrosion-resistant, nickel-based alloys. To understand their characteristics and metallurgy, it is convenient to group them compositionally. The main groups, as defined by alloying elements present at levels of 10 wt.% or above, are as follows:

1. Commercially-Pure Nickel (Ni)
2. Nickel-Copper (Ni-Cu)
3. Nickel-Chromium (Ni-Cr)
4. Nickel-Molybdenum (Ni-Mo)
5. Nickel-Chromium-Molybdenum (Ni-Cr-Mo)
6. Nickel-Chromium-Iron (Ni-Cr-Fe)
7. Nickel-Iron-Chromium (Ni-Fe-Cr)

The general attributes of each group are listed in the following table, along with the names of some representative alloys:

Group	Examples	Attributes
C-P Nickel	Nickel 200 alloy	Very resistant to caustic alkalis. Useful electrical and magnetic properties.
Ni-Cu	MONEL® alloy 400 alloy	Very resistant to seawater and hydrofluoric acid. Moderately resistant to sulfuric acid.
Ni-Cr	HASTELLOY® G-35® alloy	Very resistant to oxidizing acid solutions.
Ni-Mo	HASTELLOY® B-3® alloy	Very resistant to hydrochloric acid and sulfuric acid.
Ni-Cr-Mo	HASTELLOY® C-276 alloy	Resistant to both oxidizing and reducing acid solutions. Very resistant to chloride-induced pitting, crevice attack and stress corrosion cracking.
Ni-Cr-Fe	HASTELLOY® G-30® alloy	Very resistant to oxidizing solutions. Moderately resistant to chloride-induced pitting, crevice attack and stress corrosion cracking.
Ni-Fe-Cr	INCOLOY® alloy 825	Resistant to oxidizing solutions. Some resistance to sulfuric acid and chloride-induced localized attack.

Compositional details of several materials from each group are given in the table below. For completeness, some casting equivalents are included (although their characteristics are generally affected by microstructural inhomogeneity, and elevated residual element contents).

				Composition wt.% (values denoted with * are maxima, and ** are minima)											
Group	Alloy	UNS No.	Form	Ni	Cu	Mo	Cr	Fe	W	Mn	Si	C	Al	Ti	Other
Ni	200	N02200	Wrought	99.5	0.1	-	-	0.2	-	0.2	0.2	0.08	-	-	-
	201	N02201	Wrought	99.5	0.1	-	-	0.2	-	0.2	0.2	0.01	-	-	-
	301	N03301	Wrought	96.5	0.1	-	-	0.3	-	0.2	0.5	0.2	4.4	0.6	-
	CZ-100	N02100	Cast	95**	1.25*	-	-	3*	-	1.5*	2*	1*	-	-	-
Ni-Cu	400	N04400	Wrought	66.5	31.5	-	-	1.2	-	1	0.2	0.2	-	-	-
	K-500	N05500	Wrought	66.5	29.5	-	-	1	-	0.8	0.2	0.1	2.7	0.6	-
	M-35-1	N24135	Cast	BAL.	29.5	-	-	3.5*	-	1.5*	1.25*	0.35*	-	-	Nb 0.5*
Ni-Mo	B-2	N10665	Wrought	69	0.5*	28	1*	2*	0.5*	1*	0.1*	0.01*	-	-	-
	B-3®	N10675	Wrought	65**	0.2*	28.5	1.5	1.5	3*	3*	0.1*	0.01*	0.5*	-	-
	N-7M	N30007	Cast	BAL.	-	31.5	1*	3*	-	1*	1*	0.07*	-	-	-
	N-12MV	N30012	Cast	BAL.	-	28	1*	5	-	1*	1*	0.12*	-	-	Co 2.5*, V 0.4

Ni-Cr	600	N06600	Wrought	76	0.2	-	15.5	8	-	0.5	0.2	0.08	-	-	-
	625	N06625	Wrought	61	-	9	21.5	2.5	-	0.2	0.2	0.05	0.2	0.2	Nb + Ta 3.6
	690	N06690	Wrought	58**	0.5*	-	29	9	-	0.5*	0.5*	0.05*	-	-	-
	725	N07725	Wrought	57	-	8	21	7.5	-	0.35*	0.2*	0.03*	0.35*	1.5	Nb 3.5
	G-35®	N06035	Wrought	58	0.3*	8.1	33.2	2*	0.6*	0.5*	0.6*	0.05*	0.4*	-	-
	ALLCORR	N06110	Wrought	BAL.	-	10	31	-	2	-	-	0.02	0.25	0.25	Nb 0.4
Ni-Cr-Mo	C-4	N06455	Wrought	65	0.5*	16	16	3*	-	1*	0.08*	0.01*	-	0.7*	-
	C-22®	N06022	Wrought	56	0.5*	13	22	3	3	0.5*	0.08*	0.01*	-	-	V 0.35*
	C-22HS®	-	Wrought	61	0.5*	17	21	2*	1*	0.8*	0.08*	0.01*	0.5*	-	-
	C-276	N10276	Wrought	57	0.5*	16	16	5	4	1*	0.08*	0.01*	-	-	V 0.35*
	C-2000®	N06200	Wrought	59	1.6	16	23	3*	-	0.5*	0.08*	0.01*	0.5*	-	-
	59	N06059	Wrought	BAL.	-	16	23	1.5*	-	0.5*	0.1*	0.01*	0.25	-	-
	686	N06686	Wrought	BAL.	-	16	21	5*	3.7	0.75*	0.08*	0.01*	-	0.15	-
	CW-2M	N26455	Cast	BAL.	-	16.25	16.25	2*	1*	1*	0.8*	0.02*	-	-	-
	CW-6M	N30107	Cast	BAL.	-	18.5	18.5	3*	-	1*	1*	0.07*	-	-	-
	CW-12MW	N30002	Cast	BAL.	-	17	16.5	6	4.5	1*	1*	0.12*	-	-	V 0.3
	CX-2MW	N26022	Cast	BAL.	-	13.5	21.5	4	3	1*	0.8*	0.02*	-	-	V 0.35*
Ni-Cr-Fe	G-3	N06985	Wrought	44	2	7	22	19.5	1.5*	1*	1*	0.015*	-	-	Co 5*, Nb 0.5*
	G-30®	N06030	Wrought	43	2	5.5	30	15	2.5	1.5*	0.8*	0.03*	-	-	Co 5*, Nb 0.8
	G-50®	N06950	Wrought	50**	0.5*	9	20	17	1*	1*	1*	0.02*	0.4*		Co 2.5*, Nb 0.5*
Ni-Fe-Cr	825	N08825	Wrought	42	2.2	3	21.5	30	-	0.5	0.2	0.05*	0.1	0.9	-
	925	N09925	Wrought	44	2.2	3	21	22**	-	1*	0.5*	0.03*	0.3	2.2	Nb 0.5*

Cobalt Alloy Groups

There are relatively few wrought, corrosion- and wear-resistant, cobalt-based alloys. On the other hand, there are many cast, wear-resistant, cobalt-based alloys (closely associated with the STELLITE® tradename) that, despite their high carbon contents, possess a modicum of resistance to aqueous corrosion. This manual is concerned with the former materials. However, the cast alloys will be referred to often, since they provide a well-known frame of reference.

There are essentially three types of wrought, cobalt alloys used to resist aqueous corrosion. All contain high levels (20 wt.% or more) of chromium, and significant molybdenum and/or tungsten contents.

First are those derived from the cast, tungsten-bearing, high-carbon alloys, exemplified by HAYNES® 6B alloy (also known as STELLITE® 6B alloy). With a 1 wt.% carbon content, this alloy can be hot worked, but cannot be cold worked. Wrought processing enables the breaking down of large carbide particles (within the cast, ingot structure) into a discontinuous dispersion of equiaxed carbide particles; this results in enhanced ductility, increased resistance to corrosion, and excellent resistance to low stress abrasion, relative to compositionally-similar, cast and weld overlay materials.

Second are those tungsten-bearing, low-carbon, wrought materials designed for high temperature service, but whose resistance to aqueous corrosion is so high that they have found use in low temperature applications also. The primary example is HAYNES® 25 alloy, which is approved for biomedical use.

Third are those molybdenum-bearing alloys with carbon contents of about 0.35 wt.% or less, and designed to excel in both corrosive solutions and systems subject to wear. The prime example is ULTIMET® alloy, which exhibits a unique blend of properties, including high resistance to aqueous corrosion and wear, relatively high ductility, and excellent weldability.

The nominal compositions of several wrought, corrosion-resistant, cobalt alloys are given in the following table, along with those of several cast, cobalt alloys, for comparison.

Group	Alloy	UNS No.	Form	Composition, wt.% (values denoted with * are maxima)									
				Co	Ni	Cr	Mo	W	C	Fe	Si	Mn	Other
Tungsten-Bearing High-Carbon	6B	R30016	Wrought	58	2.5	30	1.5*	4	1	3*	0.7	1.4	-
	1	R30001 W73001**	Cast Weld Overlay	BAL	1.5	30	0.5	13	2.5	3*	1.3	0.5	-
	6	R30006 W73006**	Cast Weld Overlay	BAL	3*	29	1.5*	4.5	1.2	3*	1.5*	1*	-
	12	R30012 W73012**	Cast Weld Overlay	BAL	3*	29.5	1*	8.25	1.5	3*	1.2	1*	-
Tungsten-Bearing Low-Carbon	25	R30605	Wrought	51	10	20	1*	15	0.1	3*	0.4*	1.5	-
Molybdenum-Bearing Low-Carbon	ULTIMET®	R31233	Wrought	54	9	26	5	2	0.06	3	0.3	0.8	N 0.08
	F75	R30075	Cast	BAL	1*	28.5	6	0.2*	0.35*	0.75*	1*	1*	Al 0.3* B 0.01* N 0.25*

**Welding filler metal designations, with slight compositional modifications

Metallurgical Primer

Before discussing the metallurgy of the nickel and cobalt alloys, it is important that certain metallurgical terms are understood. First and foremost, it should be understood that an *alloy* is a mixture of metals, possibly containing small quantities of non-metals, such as carbon. The predominant metal in the alloy is known as the *base*.

A *solid solution* is an alloy in the solid state having a single atomic structure or *phase*. *Second phases* are possible when the combined levels of alloying additions to the base exceed their solubility limits. So, as with a liquid solution, there are natural limits to how much can be dissolved in a metallic material of a given atomic structure, and as with a liquid solution, the higher the temperature, the more can be dissolved. Fortunately, it is possible to create supersaturated solid solutions by heat treating materials at high temperatures where the solubilities are higher, then rapidly cooling the materials to room temperature, or at least below 500°C, where the diffusion of atoms (the main catalyst for microstructural change) is no longer appreciable. Holding alloys at high temperatures, to dissolve unwanted second phases in their microstructures, is known as *solution annealing*. Rapid cooling, to lock in the high temperature microstructure, is known as *quenching*, and is best performed in cool water.

The problem with such supersaturated materials is that they are prone to second phase *precipitation* during excursions above 500°C, when diffusion becomes appreciable. Such excursions are common during welding, for example. Unfortunately, precipitates tend to nucleate and grow at microstructural imperfections, such as grain boundaries. These then become prone to preferential corrosion attack.

Not all second phase precipitates are detrimental. Those that precipitate homogeneously (i.e. throughout the microstructure, rather than just at the grain boundaries) can be used to strengthen materials. This is known as *precipitation-hardening* or *age-hardening*. The heat treatments used to induce such precipitates often involve multiple steps in the temperature range 500°C to 800°C.

The microstructures of wrought and cast alloys comprise numerous *grains*, within which the crystal structure is aligned in a certain direction. However, these grains can sub-divide under the action of mechanical stress or temperature by a process known as *twinning*, whereby bands of material within a grain can realign.

Grain boundaries (of irregular geometry) and *twin boundaries* (which are straight and parallel) are very important microstructural features, since they are preferred nucleation sites for second phase precipitates.

The *major* alloying elements determine the general behavior of a material. However, *minor* alloying elements are also important. Some minor elements are there to ensure successful melting and processing; some are used to fine-tune performance in specific environments. Others are added to induce hardening precipitates.

Except in the case of the few precipitation-hardenable nickel alloys designed to resist aqueous corrosion, strengths are determined largely by the major alloying elements. These provide solid solution strengthening. Large atoms such as molybdenum are particularly effective strengtheners.

To maximize the corrosion resistance of the nickel alloys, many are deliberately overalloyed and reliant upon the previously mentioned process of solution annealing and quenching to optimize their microstructures. Even those that are not overalloyed are prone to second phases, due to the presence of insoluble residuals, such as carbon.

Nickel Alloy Metallurgy

The purpose of this part of the manual is to provide information on the physical metallurgy of the four groups of wrought, corrosion-resistant, nickel alloy with which Haynes International is associated (i.e. the Ni-Cr, Ni-Mo, Ni-Cr-Mo, and Ni-Cr-Fe groups). For completeness, however, microstructures of materials from the other three groups will be shown and commented upon.

As already discussed, the atomic structure of pure nickel is face-centered cubic (FCC), otherwise known as gamma phase within the realm of nickel alloy metallurgy. Commercially-pure nickel (Ni), of which there are several grades, and the nickel-copper (Ni-Cu) alloys generally exhibit stable FCC microstructures, although (due to the insolubility of impurity carbon in wrought products from these two groups), carbides, or even free carbon, can be observed in grain boundaries or dispersed throughout these materials. The presence of carbides is evident in the following microstructures of annealed sheets of Nickel 200 and MONEL® alloy 400:

Microstructure of Ni-200 Sheet (with evidence of grain boundary carbide precipitation)

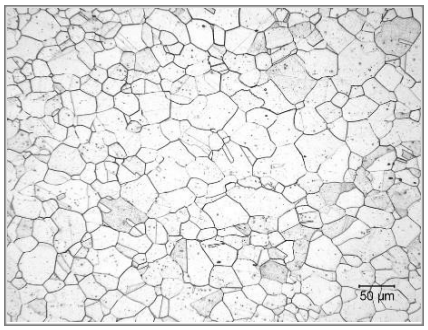

Microstructure of MONEL® alloy 400 sheet (with evidence of free carbon dispersoids)

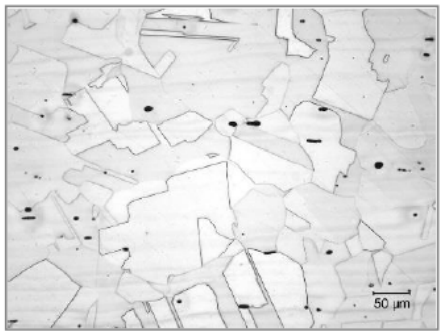

Incidentally, unless otherwise stated, the optical photomicrographs exhibited in this manual involved the following metallographic procedures:

1. Polish the mounted sample to 0.5 μm alumina.
2. Swab with cotton under running water.
3. While still wet, immerse in a solution of 95 ml of reagent grade (37 wt.%) hydrochloric acid + 5 g oxalic acid (added in crystalline form).
4. Electrolytically etch at 5 V, making the sample the anode.
5. Break contact upon visually detecting a change in reflectivity.
6. Agitate sample vigorously in etchant, to remove superfluous film.
7. Remove under running water.
8. Clean with methanol.
9. Dry under hot air.

This etchant is known as the "All Purpose Etch" at Haynes International.

It is appropriate to combine the discussions of alloys from the Ni-Cr and Ni-Cr-Mo groups, since some of the commercially-important, wrought, corrosion-resistant Ni-Cr alloys contain significant levels of molybdenum, so that the same phase diagrams are relevant.

The 850°C section of the Ni-Cr-Mo phase diagram, shown below, provides some indication of the solubilities of chromium and molybdenum in nickel, in the absence of other alloying elements. It indicates that, at this temperature, and with a chromium content of 30 wt.%, then the molybdenum content must be less than 10 wt.%, to maintain a single-phase (FCC) structure. Conversely, if the molybdenum content is 25 wt.%, then the chromium content should be less than 10 wt.%.

850°C Section of the Ni-Cr-Mo Ternary System (*Raghavan et al, 1984*)

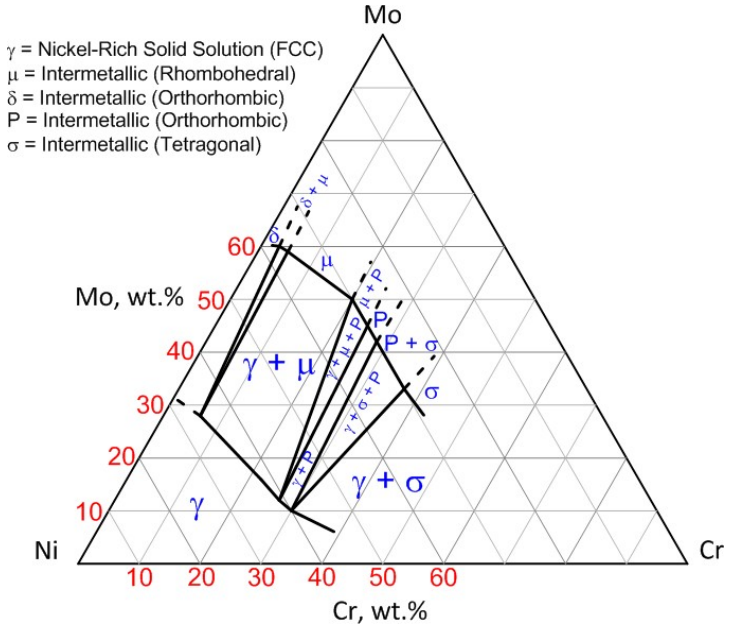

Several Ni-Cr and Ni-Cr-Mo materials (for example HASTELLOY® C-4, C-22HS®, HYBRID-BC1®, Alloy 59, and G-35® alloys) are effectively ternary systems. All except C-4 alloy (which is well within the gamma phase field, and consequently relatively stable) are close to the gamma phase field boundary. This is due to a trend whereby designers of such materials have chosen to maximize the contents of chromium and molybdenum, for enhanced corrosion resistance, while using solution annealing and quenching to maintain an (albeit meta-stable) single-phase (FCC) microstructure.

Such an approach is limited by the need to avoid continuous precipitation of second phases (such as μ phase) in the grain boundaries during subsequent thermal cycles (for example, during welding).

To complicate matters, other second phases are possible in the Ni-Cr and Ni-Cr-Mo alloys. They can occur at temperature ranges below or (less likely) above 850°C. They can result from the presence of residual elements (notably carbon). Alternatively, they can be triggered by other alloying additions.

With regard to second phases associated with different temperatures, an ordered phase of the type A_2B, or in this case $Ni_2(Cr, Mo)$, can occur in the range 300°C to 650°C by long-range ordering (*Raghavan et al, 1982*). The driving force for this ordering reaction depends upon the atomic ratios of the various alloying elements. The precipitation reaction is homogeneous, with no preferential precipitation at the grain boundaries or twin boundaries. At low temperatures within the range, the reaction is impeded by low diffusion rates; however, at temperatures closer to 650°C, the reaction can be strong enough to be used as a strengthening process (*Pike et al, 2003*). Indeed, this is the reaction used to strengthen C-22HS® alloy.

The most important second phase resulting from residual (unwanted) elements is M_6C carbide, which is prevalent in the high-molybdenum alloys, even at very low residual carbon levels (0.005 wt.% or less). *Hodge, 1973* indicates that M_6C forms in the temperature range 650°C to 1038°C in C-276 alloy (as compared with a range of 760°C to 1093°C for μ phase). The same reference indicates that the kinetics of carbide formation are faster than those of μ phase.

The microstructure of G-35® alloy, a representative of the Ni-Cr group (containing 33.2 wt.% chromium and 8.1 wt.% molybdenum) is shown in the following figure. It is generally free of second phase precipitates, although some are evident in selected grain boundaries. These are likely carbide precipitates, since the maximum carbon content in G-35® alloy is high (0.05 wt.%), relative to the wrought Ni-Cr-Mo alloys, for which the maximum carbon content is typically 0.01 wt.%.

Microstructure of Mill Annealed G-35® Sheet

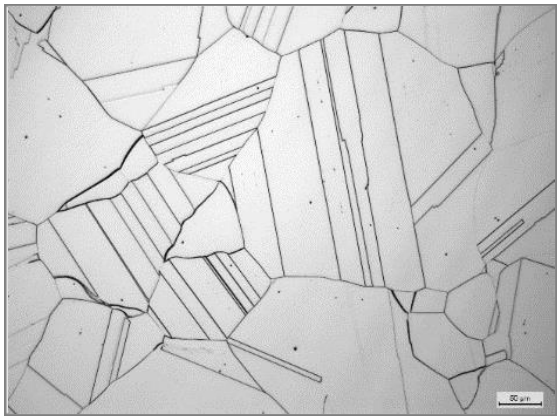

To evaluate the propensity for second phase precipitation (i.e. thermal stability) in alloys of this kind, it is usual to subject them to long-term aging treatments, at different elevated temperatures (normally above 500°C, where diffusion of elements becomes appreciable). Such temperatures are well beyond the use temperatures of the corrosion-resistant nickel alloys, and the exposure times infinitely higher than those experienced during welding; nevertheless, they provide a glimpse of the "true" stability of the material. Below are microstructures (photographed using an optical microscope) of G-35® alloy, after aging for 8,000 hours at 538°C (1000°F), 649°C (1200°F), and 760°C (1400°F). Higher magnification, secondary electron images of the samples aged at 649°C and 760°C, taken on a scanning electron microscope, are also shown (*Srivastava and Crook, 2016*).

Microstructure of Mill Annealed G-35® Sheet After Aging for 8000 h at 538°C (1000°F)

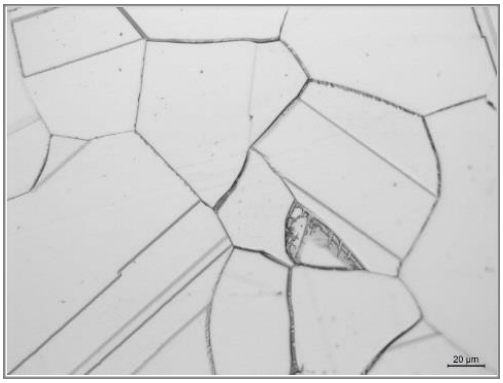

Microstructure of Mill Annealed G-35® Sheet After Aging for 8000 h at 649°C (1200°F)

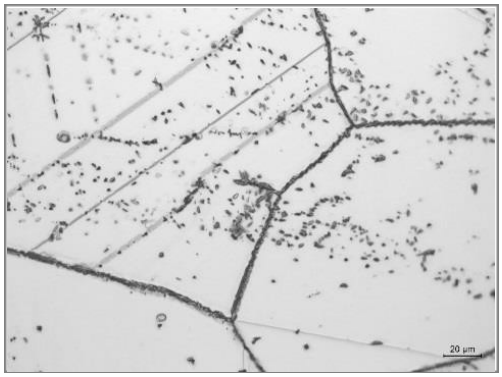

Secondary Electron Image of Mill Annealed G-35® Sheet After Aging for 8000 h at 649°C (1200°F)

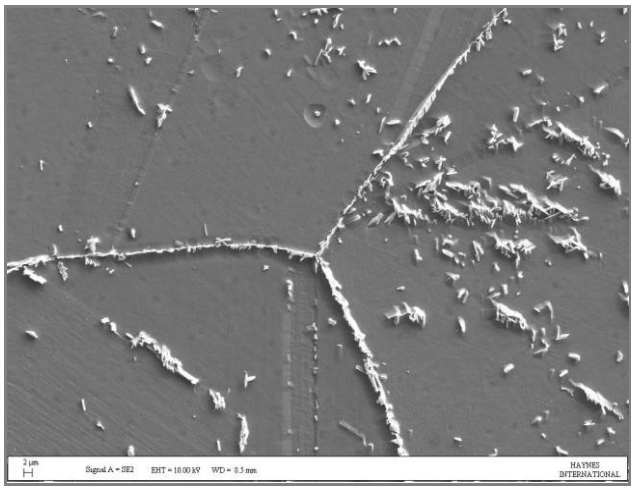

Microstructure of Mill Annealed G-35® Sheet After Aging for 8000 h at 760°C (1400°F)

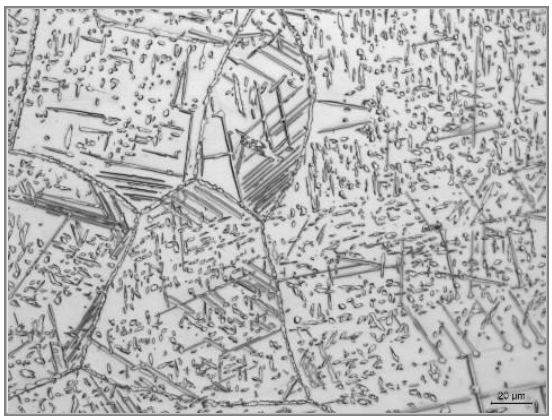

Secondary Electron Image of Mill Annealed G-35® Sheet After Aging for 8000 h at 760°C (1400°F)

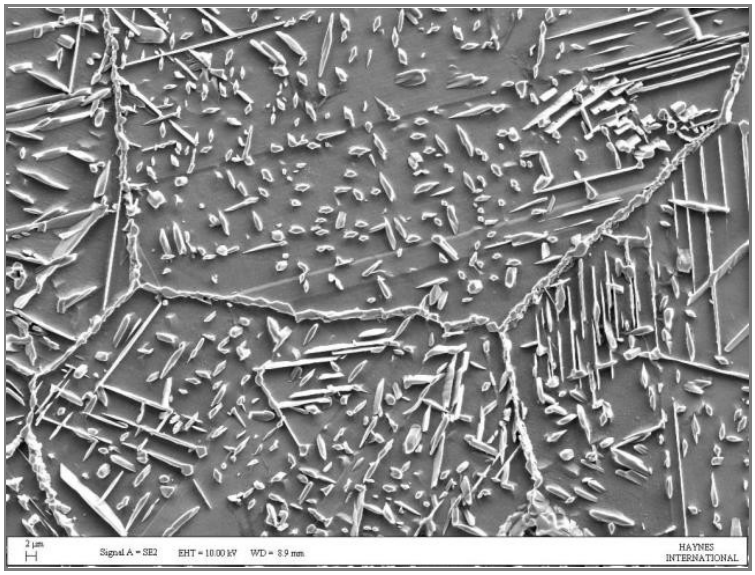

The optical photomicrograph of the microstructure after aging at 538°C indicates some second phase precipitation in the grain boundaries. The optical photomicrograph and secondary electron image of G-35® alloy aged at 649°C indicate more extensive grain boundary precipitation, together with some intra-granular, second phase precipitates. After long-term aging at 760°C, the alloy exhibits a large amount of inter- and intra-granular precipitation, and notably an array of acicular particles within the grains.

Energy-dispersive X-ray (EDX) analyses revealed that the second phases present in G-35® alloy, after long-term exposure at 649°C and 760°C, are:

1. A chromium-rich (about 90 wt.%), nickel-free phase (presumed to be alpha-chromium).
2. A phase containing about 45 wt.% chromium, 30 wt.% nickel, and 23 wt.% molybdenum.
3. Four phases containing various levels of carbon (1, 3, 6, and 11 wt.%), with varying levels of other elements.

The annealed microstructure of HASTELLOY® C-276 alloy is shown in the optical photomicrograph below. It features "clean" (i.e. precipitate-free, or undecorated) grain boundaries, and, like G-35® alloy, annealing twins. The small, black particles dispersed throughout the microstructure are most likely oxide impurities. Although photographs of long-term aged microstructures are unavailable for C-276 alloy, it is known that μ phase and carbides occur in C-276, as already discussed.

Microstructure of Mill Annealed C-276 Sheet

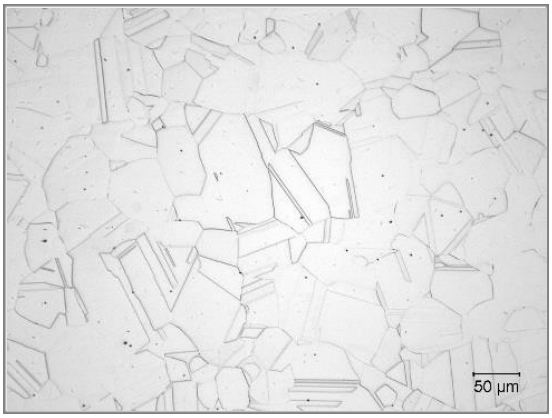

Most of the Ni-Cr-Mo materials are microstructurally similar to C-276 alloy. However, whereas C-276 alloy and others are not particularly prone to the A_2B ordering reaction in the temperature range 300°C to 650°C, C-22HS® alloy is very prone, as already discussed. HYBRID-BC1® alloy, which is strictly a Ni-Mo-Cr alloy, since its molybdenum content is higher than its chromium content, is also very prone. Fortunately, optical photomicrographs and secondary electron

images for long-term aged HYBRID-BC1® alloy are available, and illustrate the effects of A_2B ordering extremely well, as shown below.

Microstructure of Mill Annealed HYBRID-BC1® Sheet

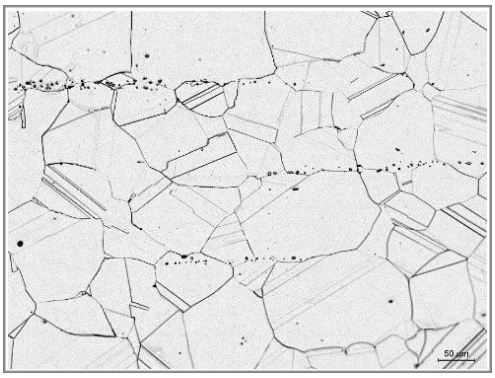

Microstructure of Mill Annealed HYBRID-BC1® Sheet After Aging for 8000 h at 538°C (1000°F)

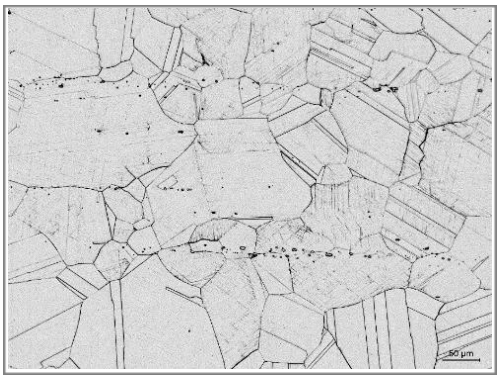

Microstructure of Mill Annealed HYBRID-BC1® Sheet After Aging for 8000 h at 649°C (1200°F)

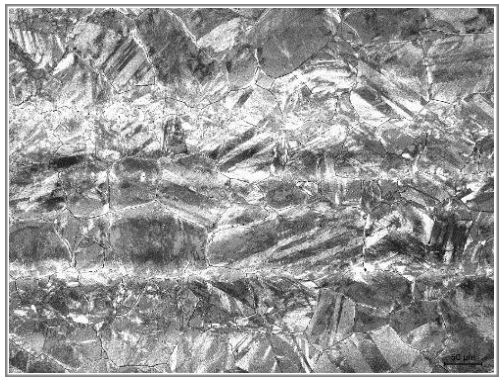

Secondary Electron Image of Mill Annealed HYBRID-BC1® Sheet After Aging for 8000 h at 649°C (1200°F)

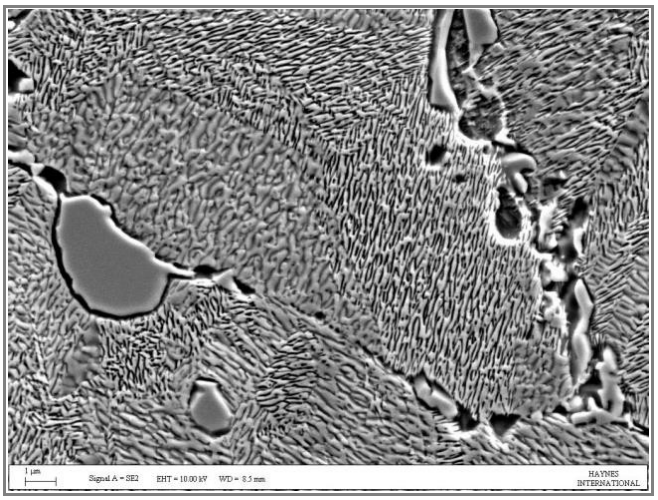

Microstructure of Mill Annealed HYBRID-BC1® Sheet After Aging for 8000 h at 760°C (1400°F)

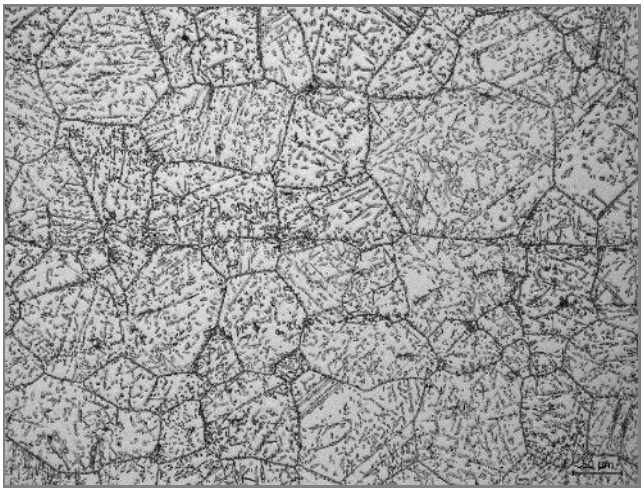

Secondary Electron Image of Mill Annealed HYBRID-BC1® Sheet After Aging for 8000 h at 760°C (1400°F)

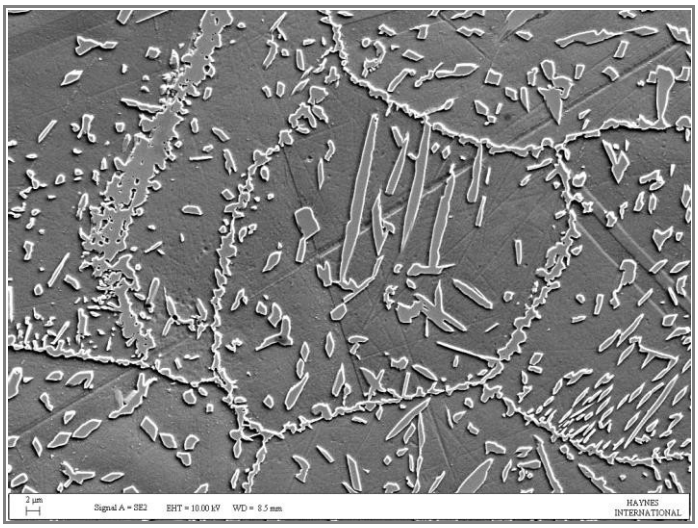

The presence of A_2B in HYBRID-BC1® alloy after long-term aging at 649°C (1200°F) is shown to great effect in the above photomicrographs, particularly in the secondary electron image taken using a scanning electron microscope (SEM). The difference between the optical photomicrographs taken after aging at 538°C (1000°F) and 649°C (1200°F) is very striking, given that they were etched under the same conditions. Obviously, the driving force for the ordering reaction is very temperature-dependent, due to an exponential increase in diffusion rates over this temperature range.

Incidentally, the second-phase particle stringers evident in the mill annealed and 538°C aged microstructures of HYBRID-BC1® alloy are due to residual segregation (banding) effects. Banding is common in high molybdenum and/or tungsten alloys, since these elements diffuse slowly due to their large atomic sizes.

As regards the much larger second-phase precipitates evident in the grain boundaries, and within the grains, of HYBRID-BC1® alloy after long term exposure at 760°C (1400°F), these were identified by EDX as:

1. A phase containing about 55 wt.% molybdenum, 33 wt.% nickel, and 12 wt.% chromium.
2. A phase containing about 43 wt.% molybdenum, 33 wt.% nickel, and 22 wt.% chromium.

In summary, commercial wrought nickel alloys containing significant quantities of chromium and molybdenum (whether from the Ni-Cr or Ni-Cr-Mo groups) are typically metastable within their normal operating temperature range (i.e. R.T. to 427°C). By virtue of solution annealing and rapid cooling, they exhibit a microstructure that is predominantly gamma (FCC) phase, although minor amounts of precipitation are possible in grain boundaries, and small oxide particles can be seen, sparsely peppered throughout the material.

Most of these materials are designed such that short-term thermal excursions above 500°C (as encountered during welding) do not cause continuous precipitation of second phases (carbides or intermetallics) in the grain boundaries. However, long-term exposures reveal their equilibrium, multiple phase nature.

Turning now to the nickel-molybdenum (Ni-Mo) alloys, they are metallurgically complex, and prone to second phases that severely impair both their mechanical properties and resistance to stress corrosion cracking. With molybdenum contents between 28 and 31.5 wt.%, they can exhibit three phases, as indicated in the following binary phase diagram, if not fully solution annealed and rapidly quenched to lock in the FCC phase stable at temperatures above 900°C (which in this diagram is confusingly designated alpha phase, rather than the usual gamma phase). Beta is the ordered body-centered tetragonal intermetallic, Ni_4Mo, and gamma is the ordered orthorhombic intermetallic, Ni_3Mo. Beta and gamma phases are both very detrimental, if they form, causing loss of ductility and susceptibility to hydrogen embrittlement and chloride stress corrosion cracking. The formation of beta phase is much more rapid than the formation of gamma phase.

Nickel-Rich Portion of Ni-Mo Binary System (*Ref. Gutherie and Stansbury, 1961*)

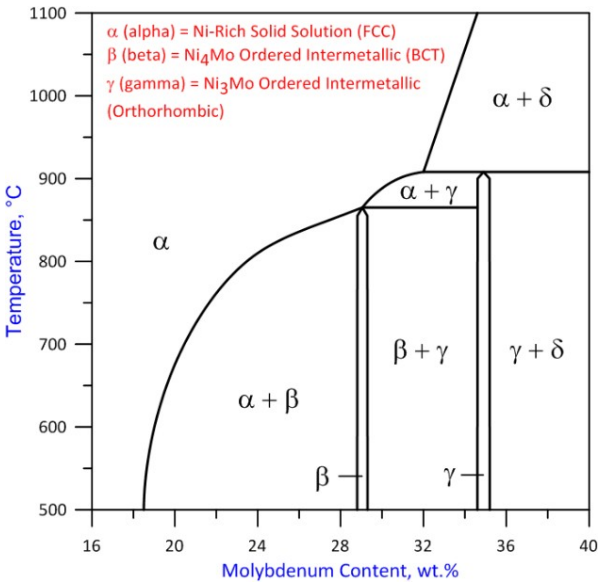

The microstructure of HASTELLOY® B-3® alloy is shown below. The straight parallel lines are twin boundaries (caused by realignment of the atomic structures within individual grains, during annealing) and the random lines are the alloy grain boundaries. The grey streaks that run across the photograph are etching effects due to remnant segregation from the cast ingot, and the fine black particles are oxide inclusions. Though not very evident, a few second phase particles (probably carbides that did not dissolve during the annealing process) are present. Preparation of the sample involved sectioning, mounting, and polishing, followed by etching in a mixture of chromic and hydrochloric acids.

Microstructure of Mill Annealed B-3® sheet

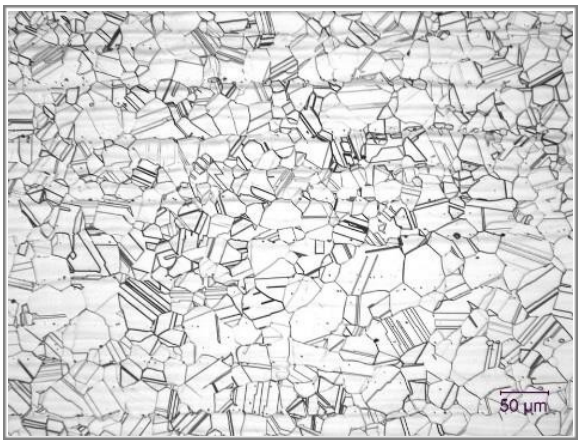

With regard to the time required to induce deleterious Ni_3Mo and Ni_4Mo precipitates in the Ni-Mo alloys, the figure below shows the Time-Temperature-Transformation Chart for B-2 and B-3® alloys (*Klarstrom, 1993*). It demonstrates how small changes in the composition of Ni-Mo alloys can have significant effects upon the various possible transformations. The main compositional differences between B-2 and B-3® alloys are deliberate 1.5 wt.% additions of both chromium and iron to B-3® alloy, along with a 0.5 wt.% increase in molybdenum content. Interestingly, the original HASTELLOY® B alloy was less prone to the rapid precipitation of deleterious Ni_3Mo and Ni_4Mo precipitates, apparently as a result of its deliberate 5 wt.% iron addition, the intention of which was to allow the use of ferro-molybdenum in its manufacture. However, HASTELLOY® B alloy was more prone to carbide precipitation in the grain boundaries due to its higher carbon allowance, since it pre-dated the advent of the argon-oxygen decarburization process in the mid-1960's, which enabled the attainment of very low carbon contents in the nickel-based corrosion-resistant alloys.

Time-Temperature-Transformation Chart for B-2 and B-3® Alloys (*Ref: Klarstrom, 1993*)

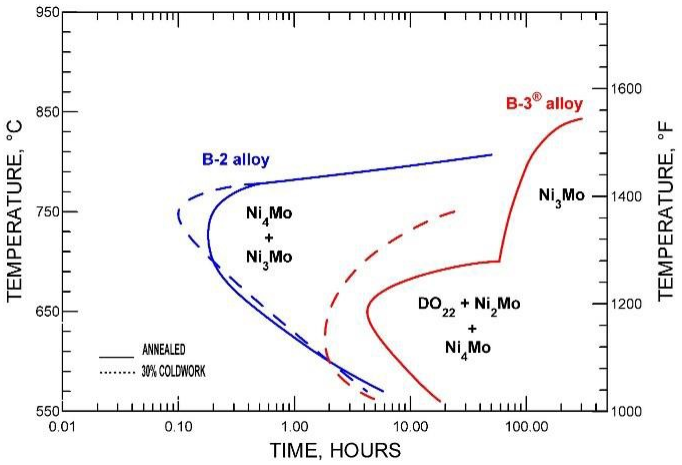

With regard to the Ni-Cr-Fe and Ni-Fe-Cr materials, the most relevant phase diagram is the 800°C section of the Ni-Cr-Fe ternary system, constructed by Raynor and Rivlin (shown below).

800°C Section of the Ni-Cr-Fe Ternary System (*Raynor and Rivlin, 1981*)

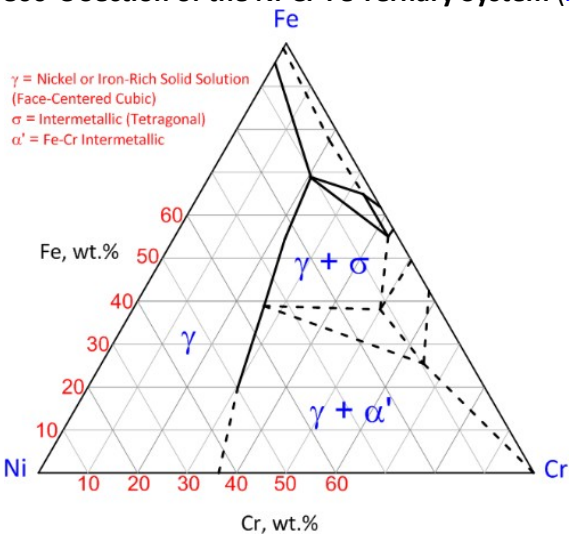

However, it should be noted that the Ni-Cr-Fe corrosion-resistant alloys typically contain significant quantities of molybdenum as well, rendering this diagram less relevant. What can be stated is that iron limits the solubility of molybdenum in wrought nickel-based alloys, and promotes the presence of sigma (σ) phase in overalloyed materials.

In general, the wrought, Ni-Cr-Fe and Ni-Fe-Cr materials can be thought of in the same way as the Ni-Cr and Ni-Cr-Mo alloys. That is, they can be slightly overalloyed (super-saturated) to maximize their corrosion-resistance, but care must be taken during solution annealing and rapid cooling to ensure an optimum (predominantly gamma phase, but possibly

metastable) microstructure within the service temperature range. Also, welding should not result in a continuous grain boundary precipitation of one or more second phases; otherwise, preferential grain boundary attack can occur in certain solutions. Ni-Cr-Fe and Ni-Fe-Cr alloys intended for corrosion service also benefit from ultra-low carbon and silicon contents, since these insoluble, residual elements can cause the precipitation of deleterious carbides and intermetallics, respectively.

To enable a microstructural comparison between G-30® alloy (from the Ni-Cr-Fe group) and G-35® alloy (from the Ni-Cr group), annealed and aged microstructures of the former are shown in the following photomicrographs.

Microstructure of Mill Annealed G-30® Sheet

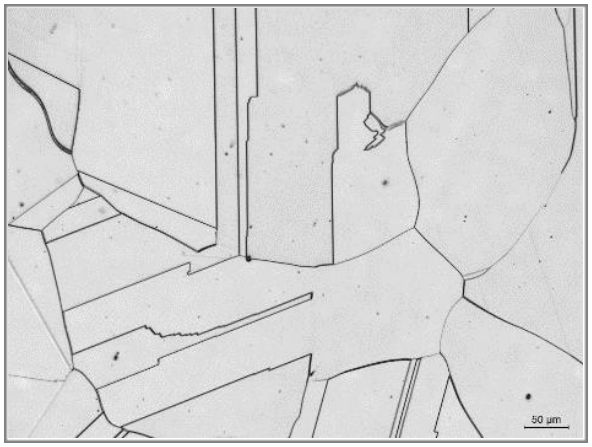

Microstructure of Mill Annealed G-30® Sheet After Aging for 8000 h at 538°C (1000°F)

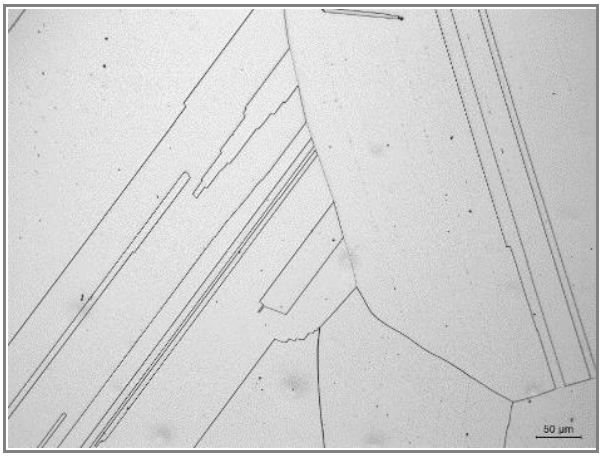

Microstructure of Mill Annealed G-30® Sheet After Aging for 8000 h at 649°C (1200°F)

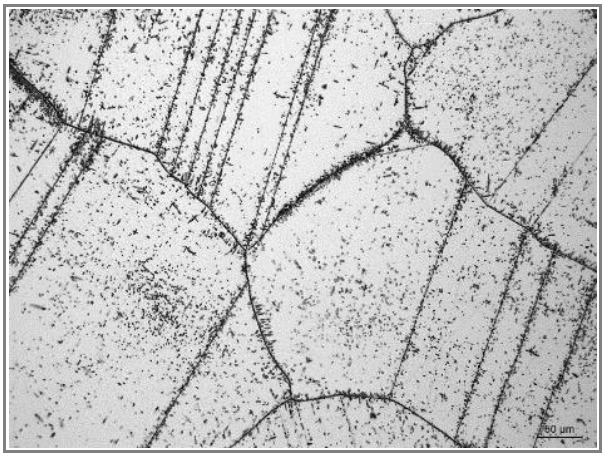

Secondary Electron Image of Mill Annealed G-30® Sheet After Aging for 8000 h at 649°C (1200°F)

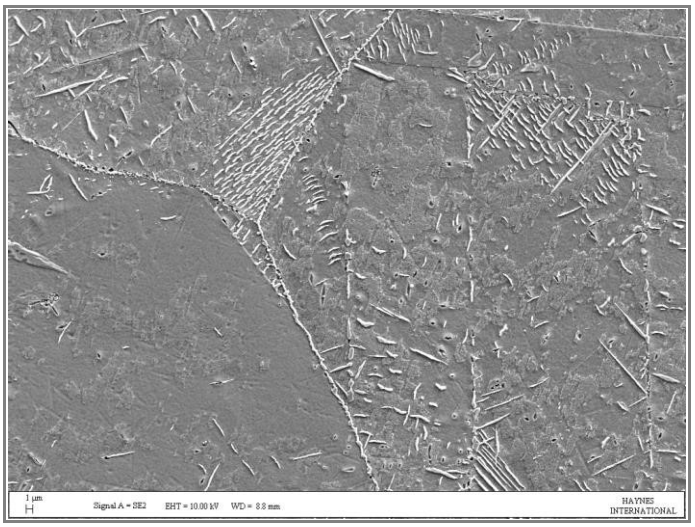

Microstructure of Mill Annealed G-30® Sheet After Aging for 8000 h at 760°C (1400°F)

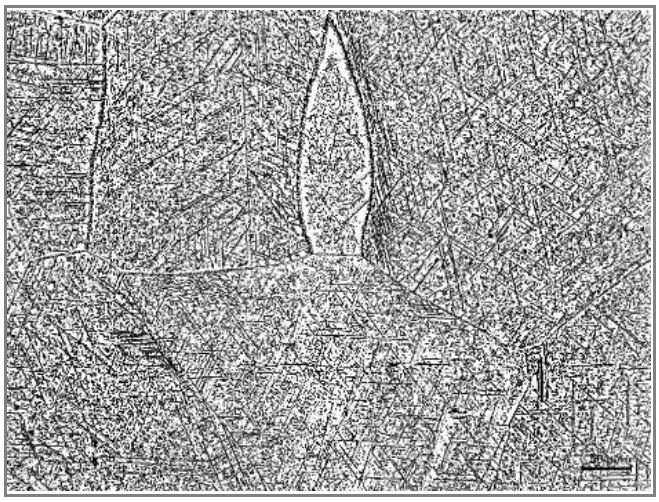

Secondary Electron Image of Mill Annealed G-30® Sheet After Aging for 8000 h at 760°C (1400°F)

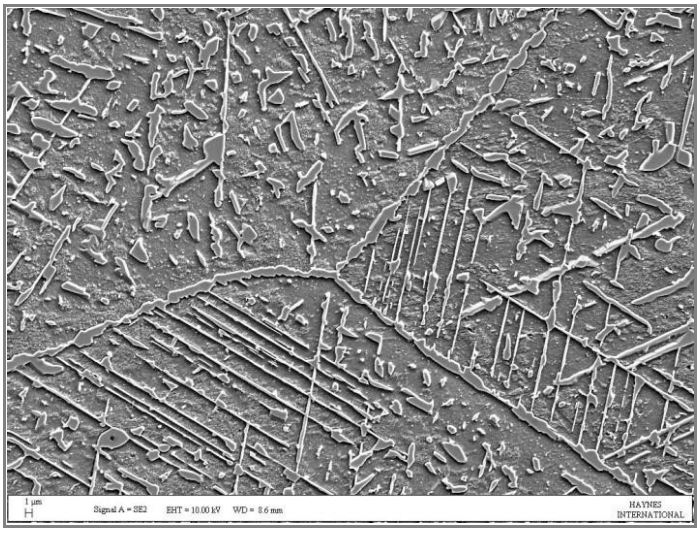

EDX analyses indicate the presence of three second phases in G-30®alloy, after long-term aging at 649°C and 760°C. One contains about 80 wt.% chromium, and is believed to be alpha chromium. The second contains approximately 40 wt.% chromium, 25 wt.% nickel, 14 wt.% molybdenum, 7 wt.% tungsten, and 12 wt.% iron. The third, most likely a carbide, contains about 4.5 wt.% carbon, 65 wt.% chromium, 10 wt.% molybdenum, and 5 wt.% tungsten.

To complete the section on metallurgy of the wrought, corrosion-resistant, nickel-based alloys, it is appropriate to illustrate the mill annealed microstructure of a Ni-Fe-Cr alloy. A photomicrograph of 825 alloy is therefore shown below. Its fine grain size is either a result of special sheet processing, and/or the presence of an appreciable carbon content, resulting in a titanium carbide dispersion, which would encourage grain boundary pinning.

Microstructure of Mill Annealed 825 Alloy

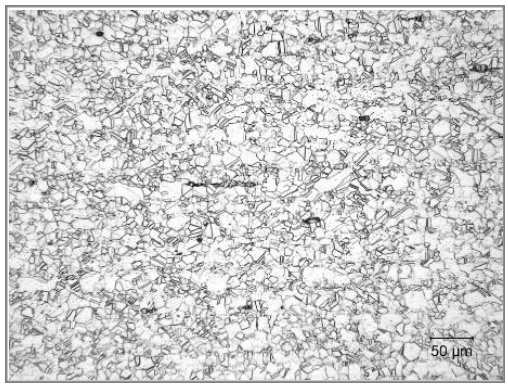

Cobalt Alloy Metallurgy

The unique metallurgical characteristics of the wrought, corrosion- (and wear-) resistant cobalt-based alloys were outlined earlier in this manual, so only a few additional details will be provided here. Considering first the tungsten-bearing, high carbon alloys, the microstructure of HAYNES® 6B (STELLITE® 6B) alloy is illustrated below. Note the large, discrete carbide particles; their size and morphology not only provide the wrought product with significantly enhanced ductility (as compared with cast equivalents), but also result in higher resistance to low stress abrasion (if the abrading particles are larger than the carbides, and can "skate" over them). According to *Antony and Silence, 1979*, the weight percentage of carbides in 6B alloy is approximately 12.5, of which about 90% is M_7C_3 and about 10% is $M_{23}C_6$.

Microstructure of Wrought HAYNES® 6B Plate

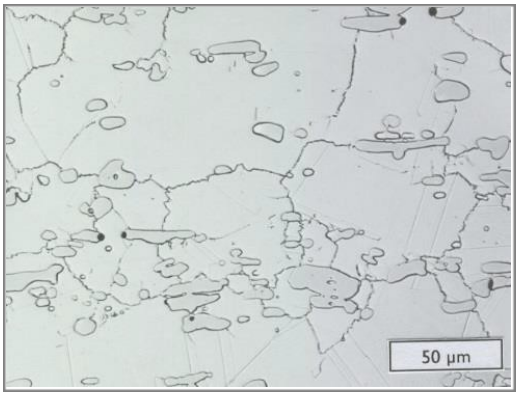

With regard to the cast equivalents, these are used, more often than not, in weld overlay form. The microstructure of such a weld overlay is shown below. Note that the carbides are much finer, and dispersed in a hypoeutectic fashion.

Microstructure of Weld Overlay STELLITE® 6 Alloy as Applied by Plasma Transferred Arc Welding

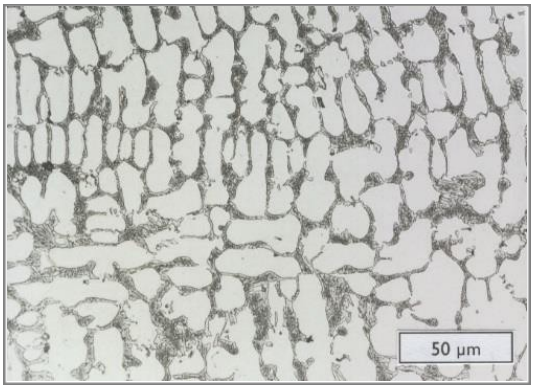

The microstructure of wrought ULTIMET® alloy (a representative of the molybdenum-bearing, low-carbon cobalt alloys) is very similar to that of the Ni-Cr and Ni-Cr-Mo alloys, in the solution annealed and quenched condition, as shown below. This is by design, to provide optimum resistance to corrosion. Its outstanding wear characteristics derive not from the presence of hard particulates in the material, but to microstructural changes (under stress) at the atomic level (twinning and the formation of HCP platelets); these induce high work hardening rates, and provide high resistance to sub-surface fracture.

Microstructure of Wrought Plate of ULTIMET® Alloy

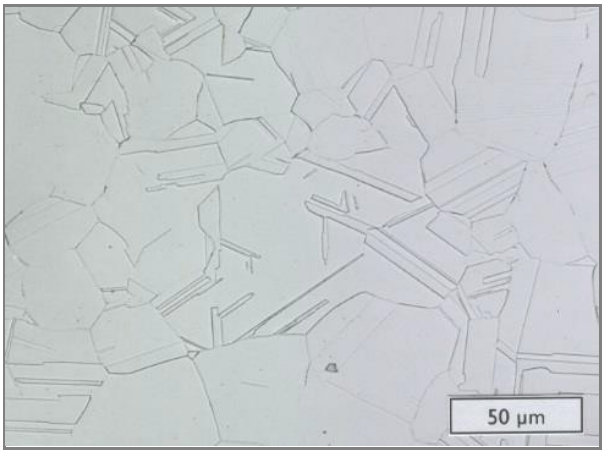

Aqueous Corrosion Background

Corrosion in aqueous solutions is an electrochemical process, involving ions (electrically charged atoms) and the transfer of electrical charges at the metallic surfaces. Anodes and cathodes occur locally on the surfaces; metal is removed at the anodes (in the form of positively charged ions, i.e. $M > M^{+}$). Electrons flow within the metallic material from anodic sites to cathodic sites, and vice versa in the aqueous solution. The principle cathodic reaction during corrosion by acids is the reduction of positively charged hydrogen ions to regular hydrogen atoms (i.e. $H^{+} > H$), and subsequently hydrogen molecules (gas). Hence the term reducing acid solution. An oxidizing acid solution is one that induces a cathodic reaction of higher potential; oxidizing acids tend to induce passivation (passivity), whereby protective films form on the metallic surfaces. These films can be multi-layered and can be oxides, hydroxides, or oxy-hydroxides.

The corrosion performance of even one metallic material is a very complex issue, given that there are many forms of corrosion, each dependent upon temperature, concentration, and the chemical purity of the solution. To simplify matters, therefore, this section deals with each form of corrosion in turn, with particular emphasis on the key industrial, inorganic chemicals, and upon the characteristics of each of the major alloy families (within the realm of corrosion-resistant, nickel- and cobalt-based alloys). The emphasis on inorganic chemicals is a reflection of their ionic nature, hence ability to induce an electrochemical (corrosive) process.

Uniform Corrosion in Hydrochloric Acid

Hydrochloric is a reducing acid. It pervades the chemical processing industries (CPI), both as a feedstock and by-product. It is extremely corrosive to most metals and alloys. As will be discussed, many nickel-based corrosion alloys (particularly those with high molybdenum contents) are able to withstand pure hydrochloric acid, within specific concentration and temperature ranges. Be aware, however, that the concentration and temperature dependencies can be strong with certain alloys, and that upset conditions in industry can result in significantly higher corrosion rates when these alloys are pushed close to their limits. Furthermore, some nickel alloys, notably those in the nickel-molybdenum family, are negatively affected by the presence of oxidizing impurities (which can occur in “real world” solutions of hydrochloric acid). Industrial field trials are therefore important, prior to use.

The alloys with the highest resistance to pure hydrochloric acid are those of the nickel-molybdenum family, whose molybdenum contents are close to 30 wt.%. Within this family, the wrought material with the highest level of corrosion resistance plus thermal stability is HASTELLOY® B-3® alloy. The corrosion rates of B-3® alloy in pure, reagent-grade hydrochloric acid are shown in the figure below, as a function of concentration and temperature. Such charts (known as “Iso-Corrosion Diagrams”) will be used frequently in this manual, so some explanation is in order.

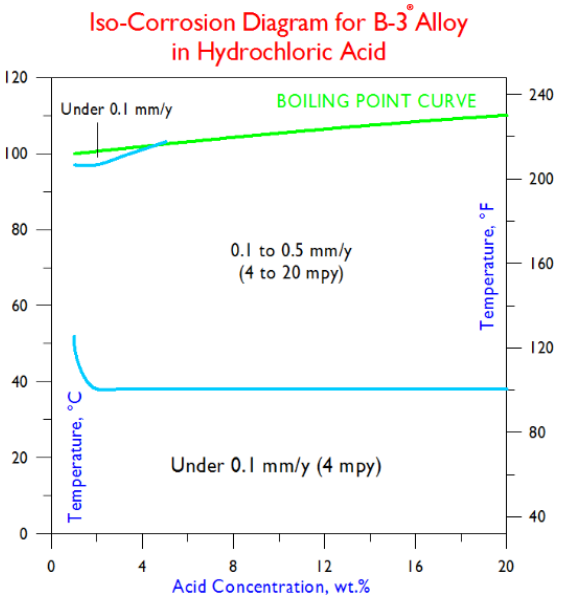

These diagrams were constructed mathematically from numerous laboratory data points, and each one defines, for a given alloy and solution, the “very safe”, “moderately safe”, and “unsafe” concentration/temperature regimes. These correspond to the corrosion rate ranges 0 to 0.1 mm/y, 0.1 to 0.5 mm/y, and over 0.5 mm/y. For those more familiar with the traditional American units (mils per year, or mpy), 0.1 mm/y is equivalent to 4 mpy, and 0.5 mm/y is equivalent to 20 mpy. It is noteworthy that, like all the materials in the nickel-molybdenum family, B-3® alloy is able to withstand pure hydrochloric acid at all temperatures up to the boiling point curve, within the 0 to 20 wt.% concentration range. Tests of the type used to create these diagrams (involving unpressurized glass flask/condenser systems) are only accurate in hydrochloric acid up to a concentration of 20 wt.% (the azeotrope). At higher concentrations, hydrogen chloride gas can escape, resulting in concentration instability and the possibility of erroneous results.

Below is a graph illustrating the effects of oxidizing impurities (ferric ions and cupric ions) upon the performance of B-3® alloy in hydrochloric acid (in this case boiling 2.5% HCl). For comparison, HASTELLOY® HYBRID-BC1® alloy, which contains 15 wt.% chromium in addition to a relatively high molybdenum level, is shown.

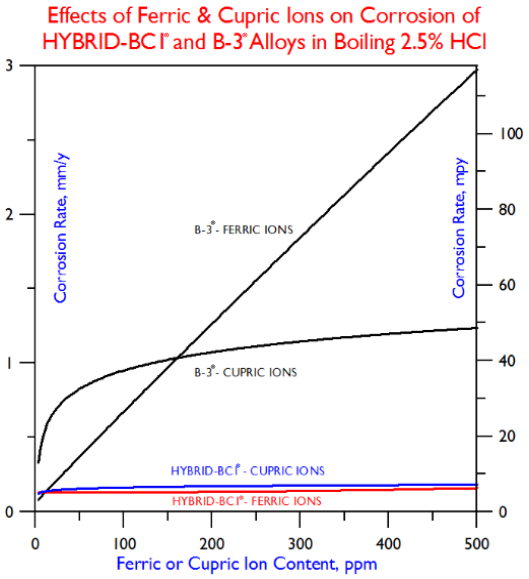

The alloys with the next highest resistance to pure hydrochloric acid are those of the nickel-chromium-molybdenum family, whose molybdenum contents range from about 13 to 22 wt.% (in some cases augmented by tungsten, which is half as effective as molybdenum on a wt.% basis). The most widely used, wrought material in this family is HASTELLOY® C-276 alloy, which contains 16 wt.% of both chromium and molybdenum, plus 4 wt.% tungsten. Its iso-corrosion diagram for pure hydrochloric acid is shown below.

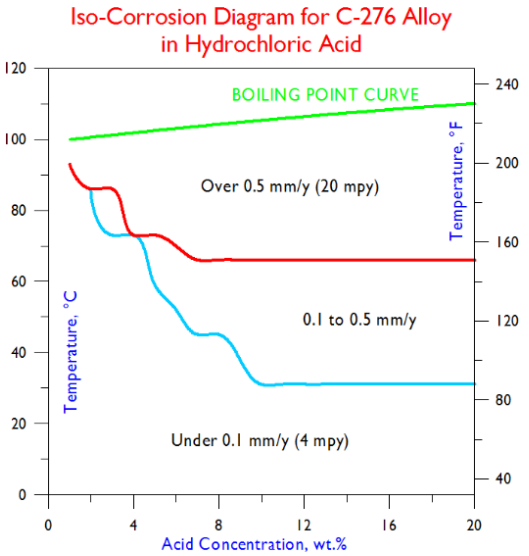

From the above diagram it is evident that the 16 wt.% molybdenum alloys exhibit strong temperature dependencies, especially at lower concentrations. The importance of molybdenum in resisting pure hydrochloric acid is illustrated in the next figure, which shows the corresponding iso-corrosion diagram for HASTELLOY® HYBRID-BC1® alloy, a material which contains 22 wt.% molybdenum (and 15 wt.% chromium, but no tungsten). Note the much broader "very safe" and "moderately safe" regimes, and generally higher temperature capabilities.

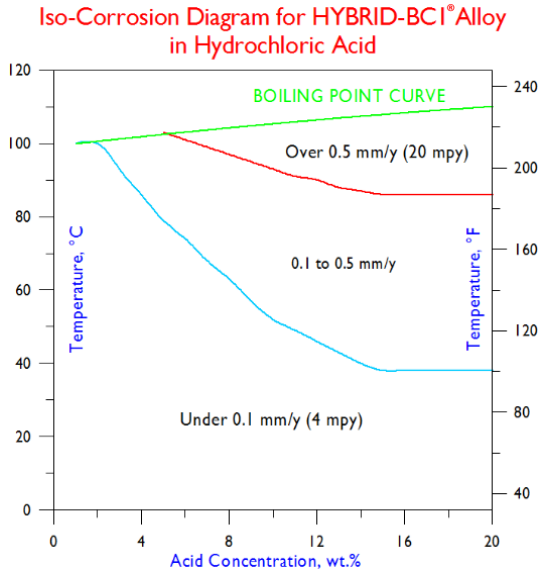

Two of the nickel-chromium alloys, namely 625 and HASTELLOY® G-35® alloy, contain sufficient molybdenum to provide good resistance to hydrochloric acid. The nominal molybdenum content of 625 alloy is 9 wt.%; that of G-35® alloy is 8.1 wt.%. The chief differences between these two materials are the chromium contents (21.5 wt.% for 625 alloy versus 33.2 wt.% for G-35® alloy) and the fact that G-35® alloy contains little else, whereas 625 alloy has deliberate iron (2.5 wt. %) and niobium (3.6 wt.%, including any associated tantalum) additions. The corresponding iso-corrosion diagrams for 625 and G-35® alloys are shown in the following two figures. The similarity of these two diagrams indicates that chromium content has little effect upon the performance of such alloys in pure hydrochloric acid.

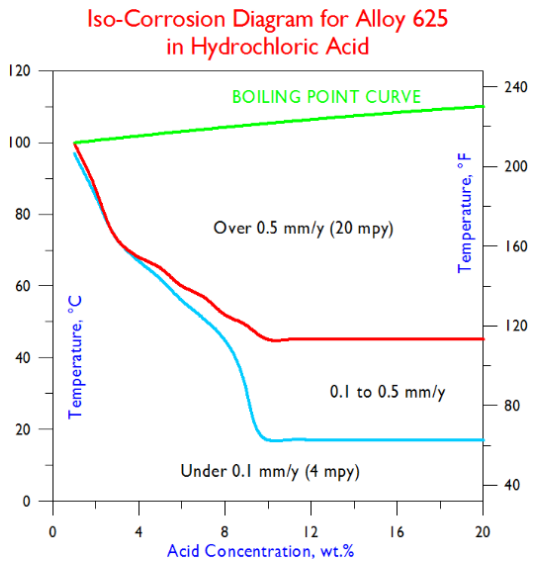

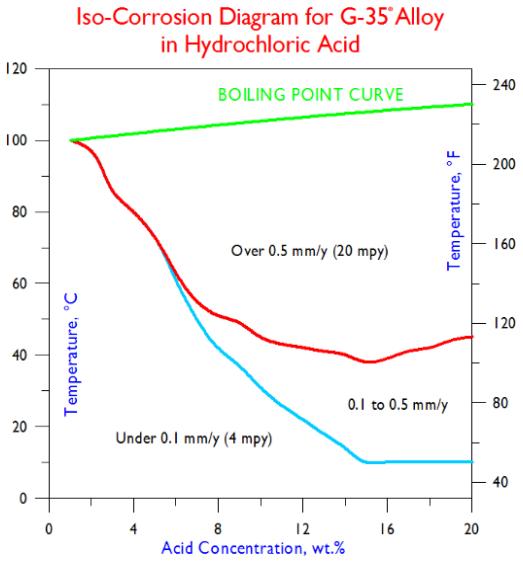

To compare materials, it is customary to plot their 0.1 mm/y lines, i.e. the lines separating the "very safe" and "moderately safe" regimes. This does not work for all materials, in particular B-3® alloy, which exhibits two 0.1 mm/y lines (one running horizontally at approximately 40°C), neither of which indicates that, unlike most other materials, B-3® alloy is safe to use up to the boiling point curve in pure hydrochloric acid, at concentrations up to 20 wt.%. Nevertheless, a comparative 0.1 mm/y line plot such as that shown below does provide perspective on the hydrochloric acid resistance of two nickel alloys (625 and C-276 alloy) versus that of two commonly used, austenitic stainless steels.

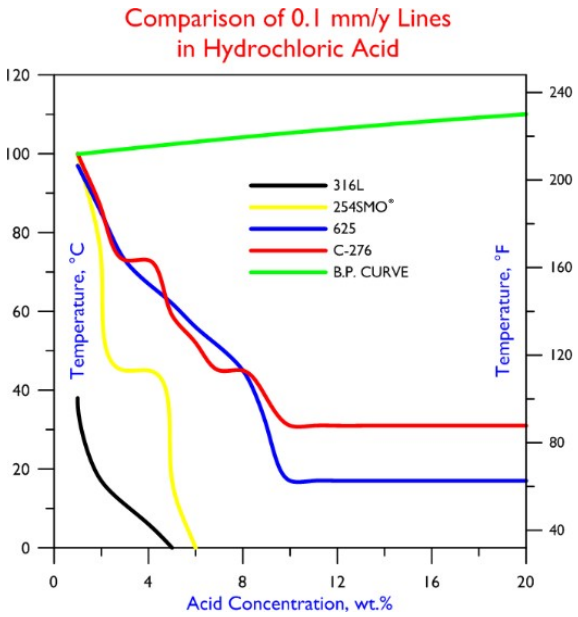

Plots of 0.5 mm/y lines can also be used to compare materials. Below is a comparative 0.5 mm/y chart for several chromium- and molybdenum-bearing, nickel-based HASTELLOY® alloys (including all of the versatile C-type materials), in reagent grade hydrochloric acid.

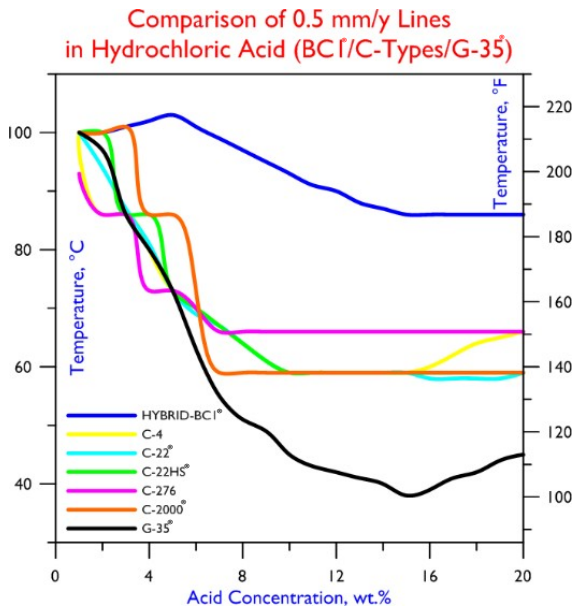

As already mentioned, copper is beneficial to the resistance of nickel alloys to reducing acids, of which hydrochloric acid is stereotypical. Hence it is relevant to present and discuss the iso-corrosion diagram for MONEL® 400 alloy, the most commonly used nickel-copper alloy, the nominal copper content of which is 31.5 wt.%. This diagram is shown in the following figure and indicates that, while the nickel-copper alloys possess some resistance to pure hydrochloric acid (higher than that of the common austenitic stainless steels), their performance is well below that of 625 and G-35® alloys (from the nickel-chromium group).

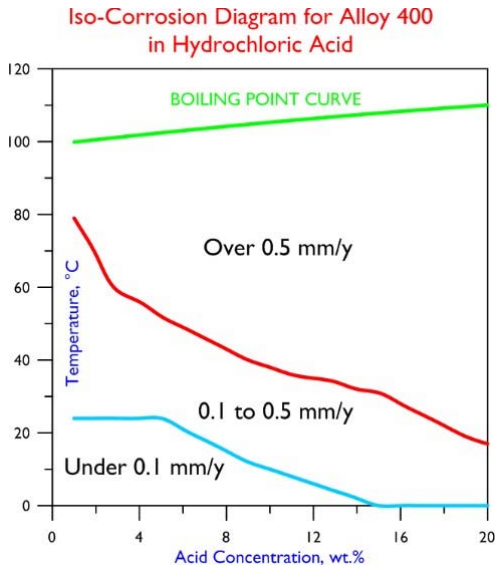

The only wrought, corrosion-resistant cobalt alloy that has been tested extensively enough in pure hydrochloric acid to enable the construction of an iso-corrosion diagram is ULTIMET® alloy. This is presented below. Interestingly, despite its relatively low molybdenum and tungsten contents (5 and 2 wt.%, which are equivalent to 6 wt.% molybdenum), its performance in pure hydrochloric acid bears some resemblance to that of 625 and G-35® alloys. The main difference is the narrower "moderately safe" regime at concentrations in the range 10 to 20 wt.%, indicating that it transitions from "safe" to "unsafe" over a smaller temperature range.

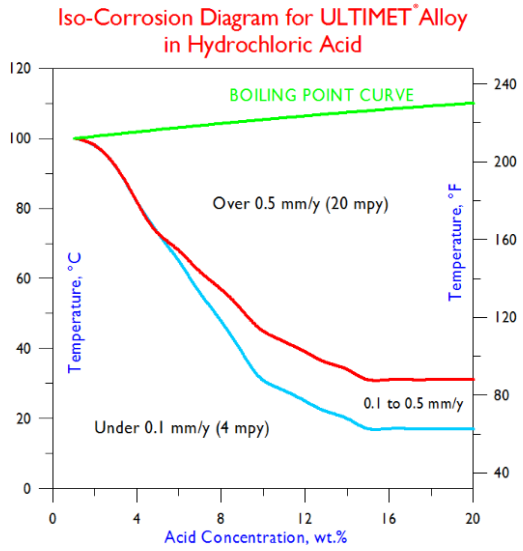

Uniform Corrosion in Sulfuric Acid

Sulfuric acid is also a very important and very corrosive industrial chemical. It is used in the manufacture of fertilizers, detergents, plastics, synthetic fibers, and pigments. It is also used as a catalyst in the petroleum industry. As with hydrochloric acid, the concentration and temperature dependencies can be strong for certain nickel- and cobalt-based materials. Also, "real world" conditions (in terms of chemical purity and flow) are unlike those in the laboratory used to generate the data in the following diagrams, so field trials are recommended. In pure sulfuric acid, again molybdenum is highly beneficial; copper is also advantageous.

Although the high-molybdenum alloys perform well across the whole concentration range in pure sulfuric acid, this is despite the fact that the nature of the cathodic reaction changes for many metallic materials at a concentration of approximately 60 to 70 wt.% (*Sridhar, 1987*). At lower concentrations, the cathodic reaction is believed to be the reduction of positively charged hydrogen ions (and the evolution of hydrogen gas), whereas mixed cathodic reactions

appear to be in play at high concentrations. This affects the behavior of metallic materials such as the zirconium alloys and nickel-copper alloys.

As with pure hydrochloric acid, the nickel alloys with the highest resistance to pure sulfuric acid are those of the nickel-molybdenum family, as indicated in the following iso-corrosion diagram for HASTELLOY® B-3® alloy. Note that this diagram covers a large concentration range (up to 90 wt.%), and that the "very safe" regime is extremely large for B-3® alloy. As with hydrochloric acid, however, the presence of oxidizing species in sulfuric acid negatively affects the nickel-molybdenum alloys.

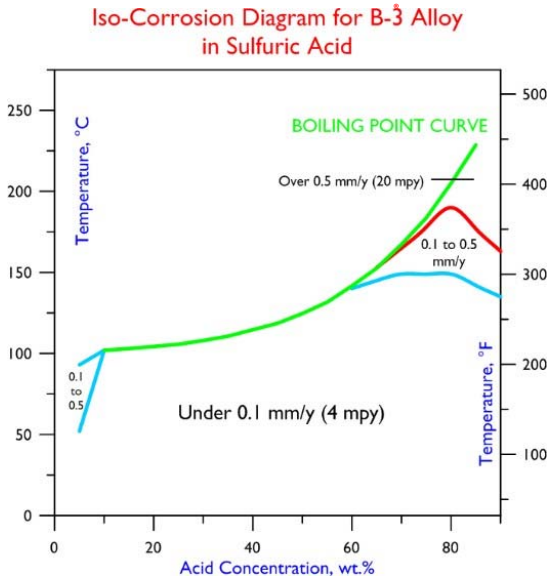

With their moderately high molybdenum contents (in the 13 to 22 wt.% range), the nickel-chromium-molybdenum alloys also possess high resistance to pure sulfuric acid. Moreover, they are somewhat protected from the oxidizing species that can occur in industrial solutions by chromium. Indeed, the higher the chromium content of the Ni-Cr-Mo alloys, the greater is the level of protection.

To illustrate the performance of the nickel-chromium-molybdenum alloys in pure sulfuric acid, the iso-corrosion diagrams for HASTELLOY® C-276 alloy and HASTELLOY® HYBRID-BC1® are shown below. Note that the temperature capability of both these nickel-chromium-molybdenum alloys does not vary much over the whole concentration range, in pure sulfuric acid. However, the higher molybdenum content of HYBRID-BC1® alloy (22 wt%) enables the material to be used at considerably higher temperatures.

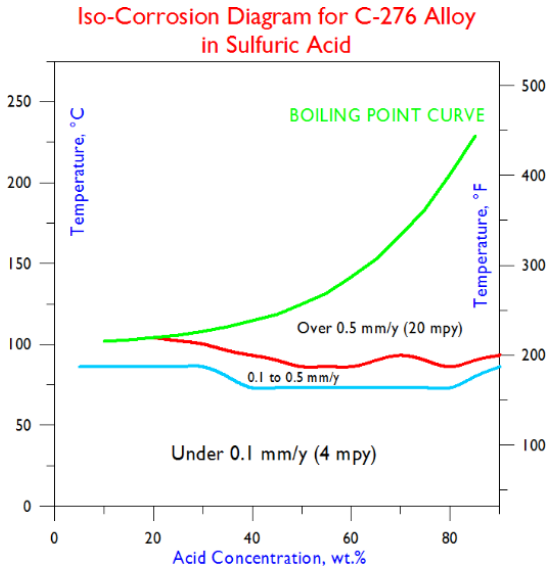

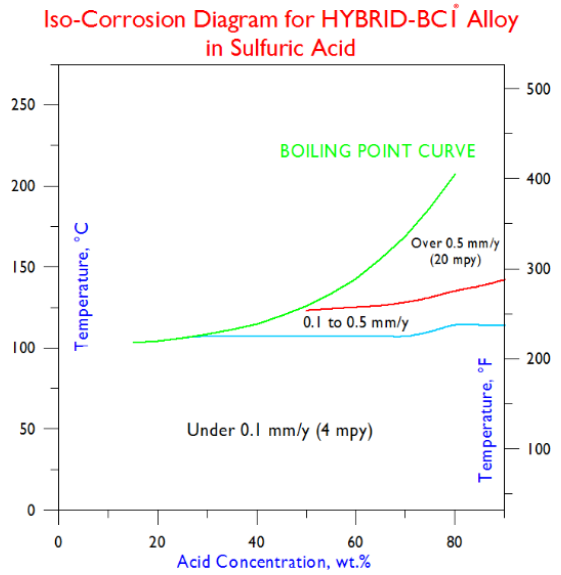

The iso-corrosion diagrams for 625 and G-35® alloys (from the nickel-chromium family of materials) in pure sulfuric acid are shown below.

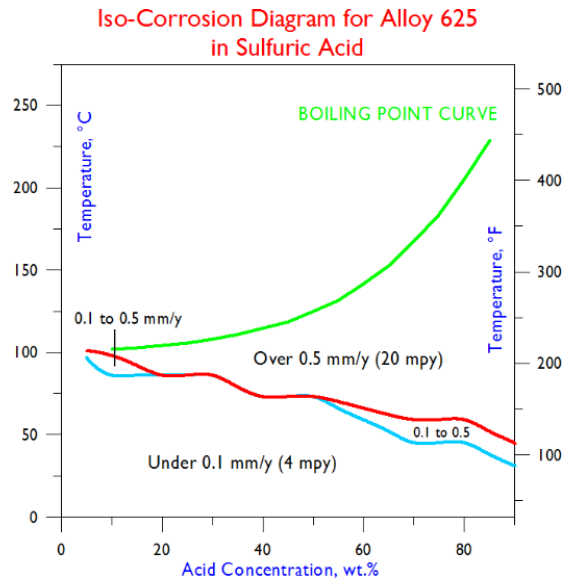

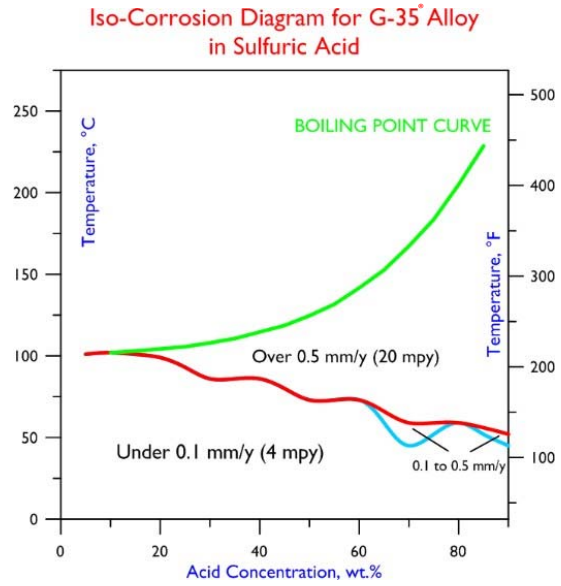

From these diagrams, it is evident that the characteristics of these two, molybdenum-bearing, nickel chromium alloys are almost identical in pure sulfuric acid and that temperature is critical to their performance. Indeed, at many concentrations, 625 and G-35® alloys exhibit no “moderately safe” regime. For perspective, their temperature capabilities in pure sulfuric acid are much higher than those of common, austenitic stainless steels, as indicated by the comparative 0.1 mm/y line plot shown below, which includes 625 alloy.

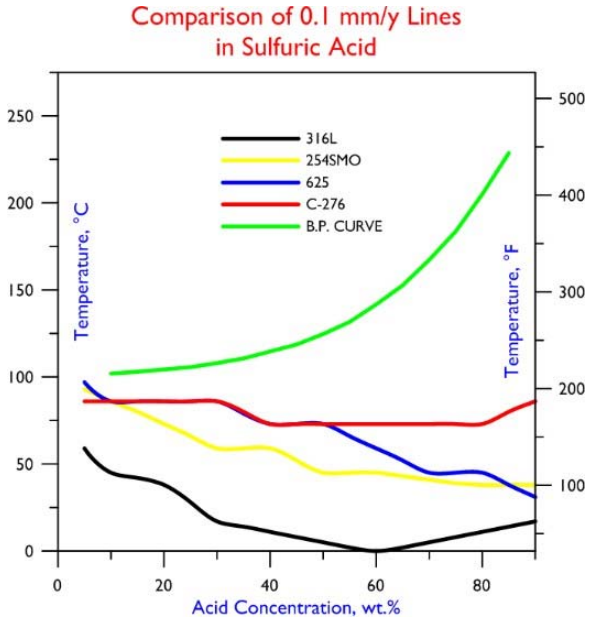

A comparative 0.5 mm/y chart for several chromium- and molybdenum-bearing, nickel-based HASTELLOY® alloys (including all of the versatile C-type materials), in reagent grade sulfuric acid is presented below.

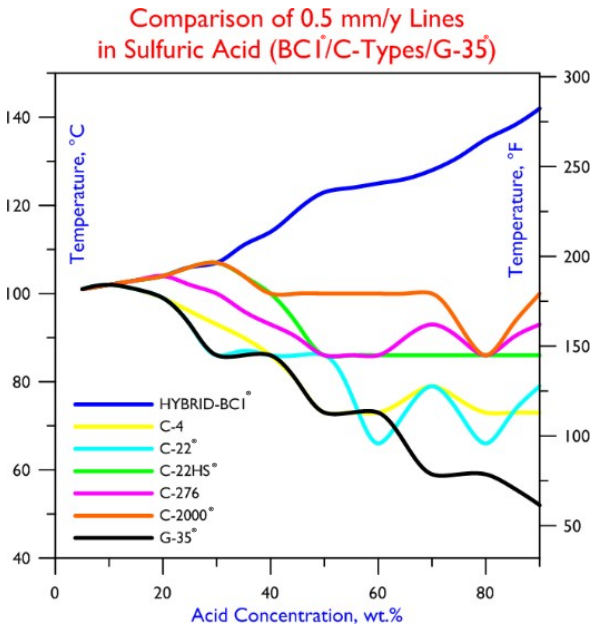

As already mentioned, the performance of the nickel-copper alloys in pure sulfuric acid is affected by the change in cathodic reaction at concentrations in the range 60 to 70 wt.%. This is illustrated in the following iso-corrosion diagram for MONEL® 400 alloy.

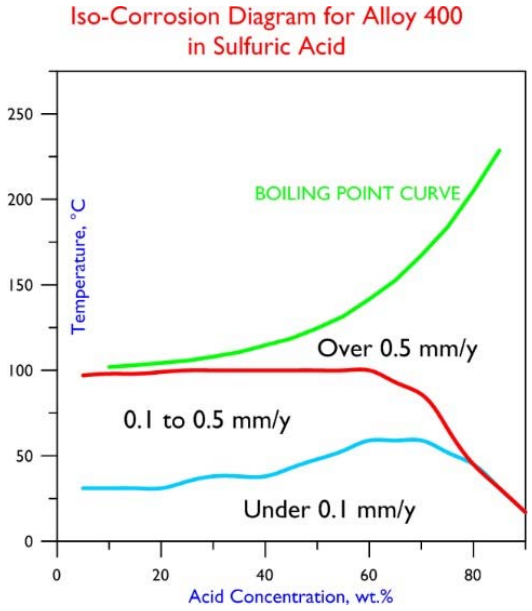

The iso-corrosion diagram for ULTIMET® alloy in pure sulfuric acid is shown below. Comparison of this diagram with those for 625 and G-35® alloys reveals many similarities, in particular the absence of a “moderately safe” regime at certain concentrations (i.e. there is a strong temperature dependency).

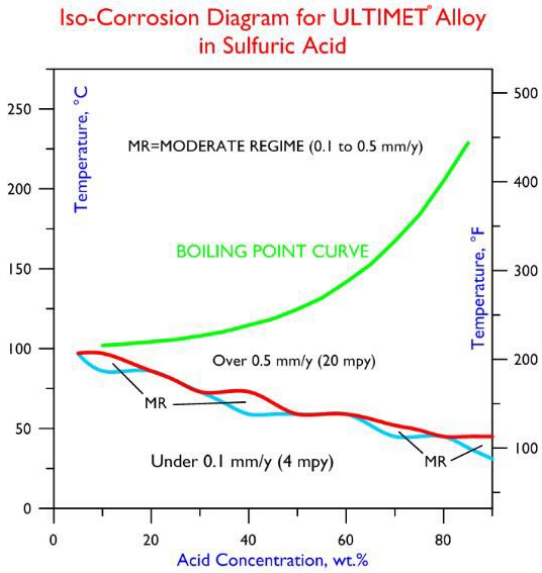

Uniform Corrosion in Highly Concentrated, Industrial Sulfuric Acid

A major source of sulfuric acid is the mining and metal extraction industry, which produces highly-concentrated solutions (typically 92-99 wt.%) from smelter off-gases. These solutions are described as “super-oxidizing” and induce cathodic reactions of very high potential, beyond the range capable of supporting chromium-rich passive films. Nevertheless, nickel-chromium-molybdenum alloys can be used in such solutions, up to about 95°C (*Sridhar, 1987*). For higher temperatures, materials which form alternate and sustainable protective films at these potentials are required.

Such materials include high-silicon nickel-based alloys and high-silicon stainless steels, both of which form protective silica films in solutions of this type. An example is HASTELLOY® D-205® alloy. Due to its weld mechanical properties, this wrought alloy is only available in thin sheet form for gasketed plate heat exchangers.

Uniform Corrosion in Hydrobromic Acid

Hydrobromic is another strong, reducing acid to which the molybdenum-bearing nickel alloys are resistant, within certain concentration and temperature ranges. It is not widely encountered within the chemical process industries, but is important in the production of inorganic bromides and of brominated organic compounds. The characteristics of the corrosion-resistant nickel alloys in pure hydrobromic acid are closely allied to those of the same materials in hydrochloric acid.

The iso-corrosion diagram for HASTELLOY® B-3® alloy in pure hydrobromic acid is shown below. Note that the azeotrope for hydrobromic acid is 40 wt.%, hence the extended concentration range. Comparing this diagram with the corresponding chart for hydrochloric acid, it is apparent that they are quite similar, in that they feature a large "moderately safe" regime, and no "unsafe" zone.

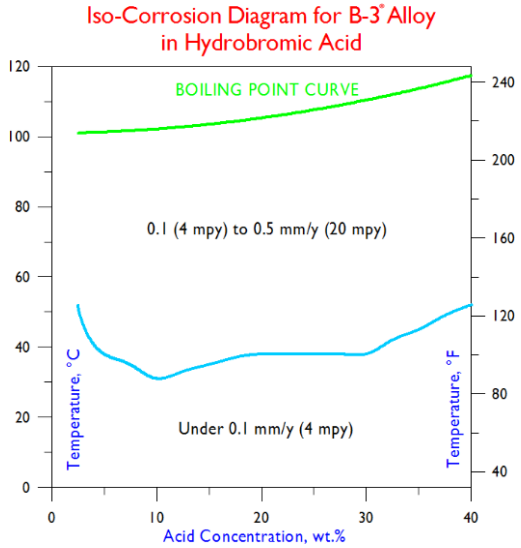

The iso-corrosion diagrams for C-276 and HYBRID-BC1® alloys in pure hydrobromic acid are shown in the following figures. Assuming the azeotropes for hydrobromic and hydrochloric acids to be equivalent, the diagrams are quite similar to those for the same alloys in hydrochloric acid, although C-276 and HYBRID-BC1® appear to be more resistant to hydrobromic acid. Particularly notable are the high position of the 0.5 mm/y line in the HYBRID-BC1® diagram, indicating a "moderately safe" zone to temperatures in excess of 100°C, and the increase in temperature capability of C-276 alloy in the concentration range 15 to 40 wt.%.

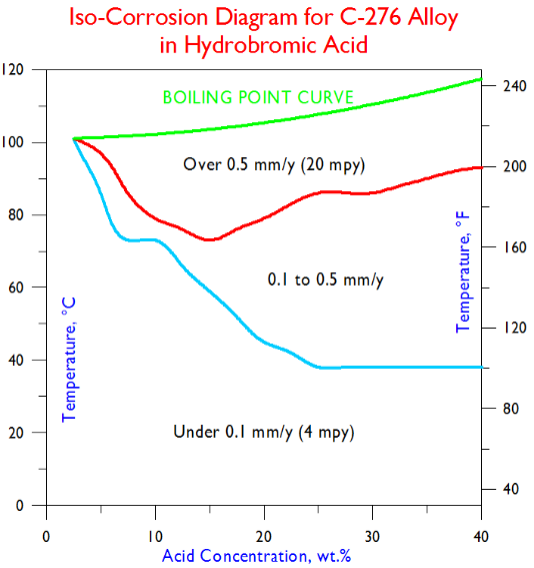

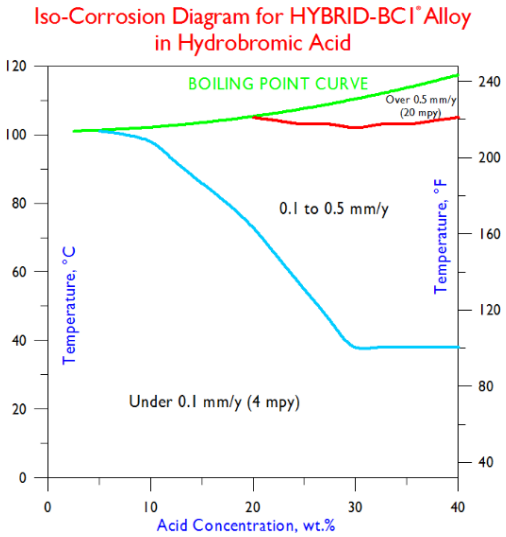

The molybdenum-bearing nickel-chromium materials, such as 625 and G-35® alloys also exhibit good resistance to pure hydrobromic acid, as indicated by the following iso-corrosion diagrams.

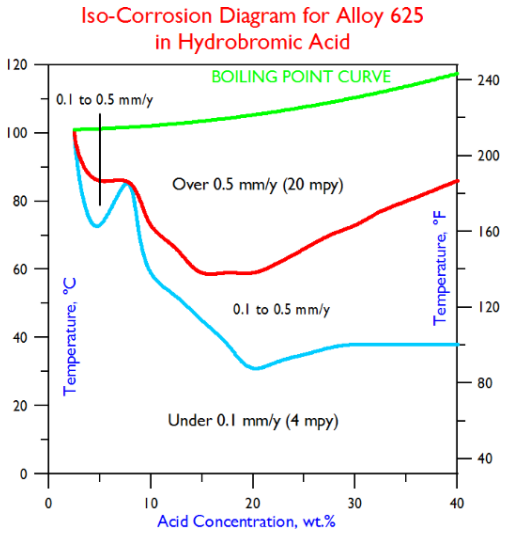

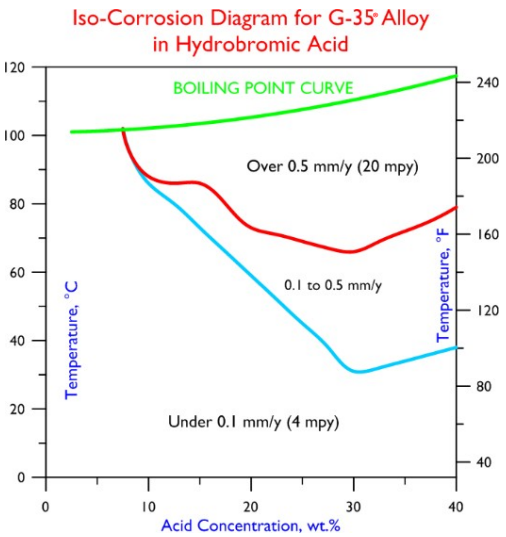

Comparing the diagrams for these two alloys in hydrochloric and hydrobromic acids, it is evident that hydrobromic is less corrosive. Also, comparing the hydrobromic acid diagrams for 625 and G-35® alloys, it appears that the latter is

considerably more resistant to this acid at concentrations up to about 25 wt.%. This infers that the high chromium content of G-35® alloy might be beneficial.

Uniform Corrosion in Hydrofluoric Acid

Aqueous solutions of hydrofluoric acid (HF) are among the most difficult to deal with. Not only can such solutions attack glass, but also alloys of elements such as titanium and zirconium, which are normally protected by oxide films, are rendered useless by hydrofluoric acid. In fact, select nickel alloys are among the few metallic materials resistant to hot hydrofluoric acid solutions, and even they have restricted temperature and concentration capabilities. Moreover, hydrofluoric acid can induce other forms of corrosion, such as internal attack and stress corrosion cracking (both of which will be discussed in later sections of this manual).

Hydrofluoric acid is also unusual (for a reducing acid) in that it can induce the formation of pseudo-passive films on nickel-based alloys. Indeed, the outstanding performance of MONEL® 400 alloy (from the nickel-copper family of materials) has been attributed to the formation of protective fluoride films on exposed surfaces.

As to industrial uses of hydrofluoric acid, it is found in the etching and cleaning of metals and ceramics, acid treating of oil and gas wells, and extractive metallurgy. Although beyond the scope of this manual, anhydrous hydrogen fluoride is used in the manufacture of the industrially important fluoro-chemicals (*Jennings 2006*). While all acids pose a safety issue, hydrofluoric acid is by far the most dangerous. No skin should be exposed when handling solutions of the acid, and fumes should be avoided.

Since glass is attacked by hydrofluoric acid, laboratory corrosion tests are carried out at Haynes International in TEFLON® flasks, with TEFLON® condensing systems. Due to the dangers of HF, tests (of 96 h duration) are normally carried out without interruption (tests in other acids involve four 24 h test periods, with interruptions for cleaning and weighing of samples, and replenishment of solutions, if needed).

Within the realm of corrosion-resistant nickel- and cobalt-based alloys, the nickel-copper alloys are the most commonly utilized for industrial applications involving hot, pure, aqueous solutions of hydrofluoric acid. However, they are negatively affected by the presence of oxygen. In such circumstances, the nickel-chromium-molybdenum alloys are used, although they are restricted to lower operating temperatures.

An iso-corrosion diagram for MONEL® 400 alloy in aqueous solutions of hydrofluoric acid is shown in *Crum et al, 1999*. Essentially, it indicates that the alloy generally exhibits rates of less than 0.5 mm/y at all concentrations up to 100 wt.%, and at temperatures up to boiling. *Jennings 2006* states that commercial aqueous hydrofluoric acid is available at concentrations of 49 and 70%; this is consistent with the experimental procedure of *Crum et al, 1999*, which states that their aqueous hydrofluoric acid tests involved solutions prepared from a concentration of 49 wt.%. It does not explain how the higher concentrations were attained, nor does it give the duration of the tests, which experience at Haynes International suggests is important. Tests of 24 h duration gave variable results, suggesting an incubation period, during which the pseudo-passive fluoride films are becoming established. Tests of 240 h (without interruption) resulted in concentration changes, due to the escape of hydrogen fluoride gas at the thermometer seals in the TEFLON® system.

A more important graph generated by Crum et al is reproduced in the following figure. It compares the positions of the 0.5 (or more precisely 0.51) mm/y lines of many nickel alloys on the iso-corrosion diagram for hydrofluoric acid. In particular, it indicates that the nickel-chromium-molybdenum alloys fall within a fairly narrow performance band, along with pure nickel, and well above that for the nickel-chromium, nickel-chromium-iron, and nickel-iron-chromium materials.

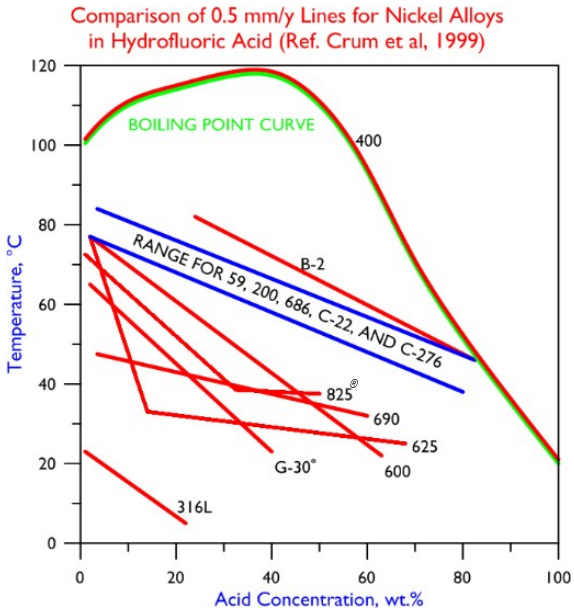

Much hydrofluoric acid testing was performed at Haynes International during the period 1995 to 2010, resulting in several technical papers, notably *Rebak et al 2001* and *Crook et al, 2007*. The former paper focuses on the behavior of HASTELLOY® C-2000® alloy versus MONEL® 400 alloy, both immersed in, and in the vapor phase above, solutions of hydrofluoric acid. The latter paper describes the internal attack that can occur in the nickel-chromium-molybdenum alloys (in particular C-22®, C-276, and C-2000® alloys).

Only one iso-corrosion diagram involving hydrofluoric acid is currently in use at Haynes International, and that is for C-2000® alloy (shown below). Note that it only covers concentrations up to 30 wt.%, and that there is considerable difference between the slope of the 0.5 mm/y line and the slope for the nickel-chromium-molybdenum materials in the Crum comparison, suggesting a greater temperature dependency.

One of the problems of using iso-corrosion diagrams for hydrofluoric acid is that they do not indicate whether or not internal attack is occurring. To remedy this, five alloys (from the Ni-Cr-Mo and Ni-Cr families) were subjected to extensive tests in hydrofluoric acid, then studied for internal attack. The results were used to create simplified corrosion rate charts, with indicators (black crosses) as to the temperatures and concentrations which can induce internal attack over 96 hours. These charts follow the iso-corrosion diagram for C-2000® alloy.

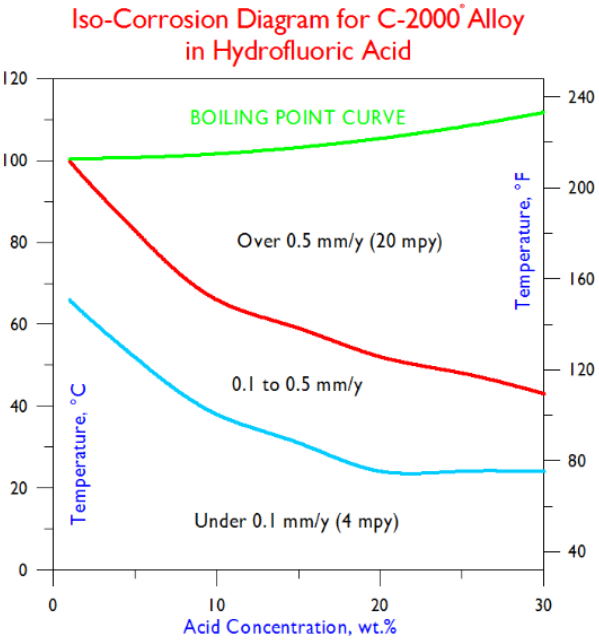

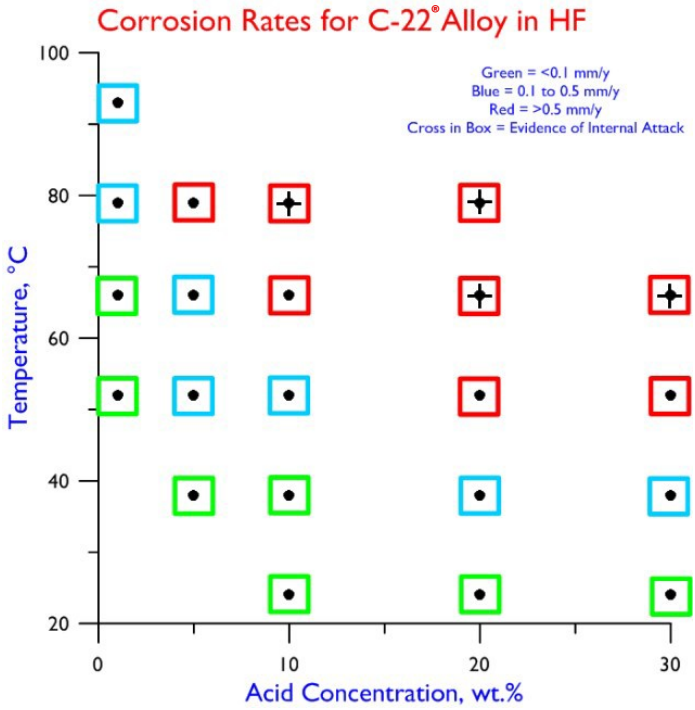
Corrosion Rates for C-22® Alloy in HF
Green = <0.1 mm/y
Blue = 0.1 to 0.5 mm/y
Red = >0.5 mm/y
Cross in Box = Evidence of Internal Attack
Temperature, °C
100
80
60
40
20
0
10
20
30
Acid Concentration, wt.%

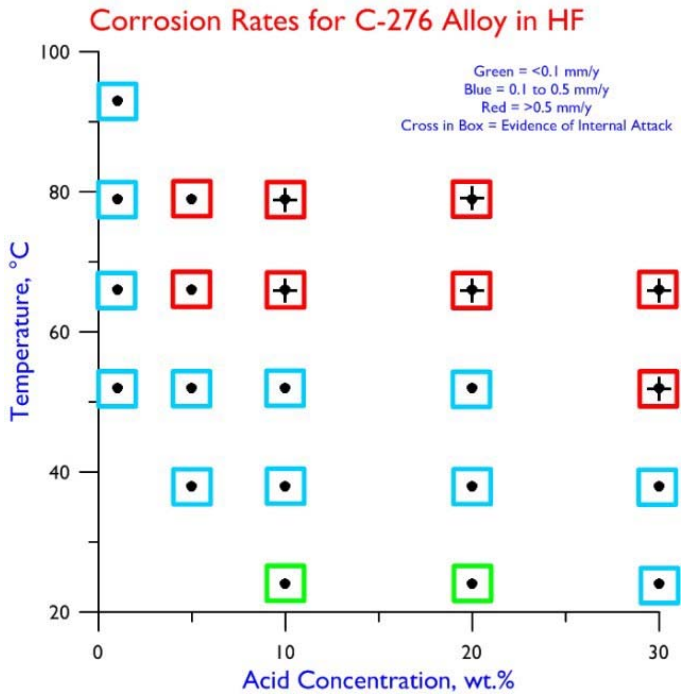
Corrosion Rates for C-276 Alloy in HF
Green = <0.1 mm/y
Blue = 0.1 to 0.5 mm/y
Red = >0.5 mm/y
Cross in Box = Evidence of Internal Attack
Temperature, °C
100
80
60
40
20
0
10
20
30
Acid Concentration, wt.%

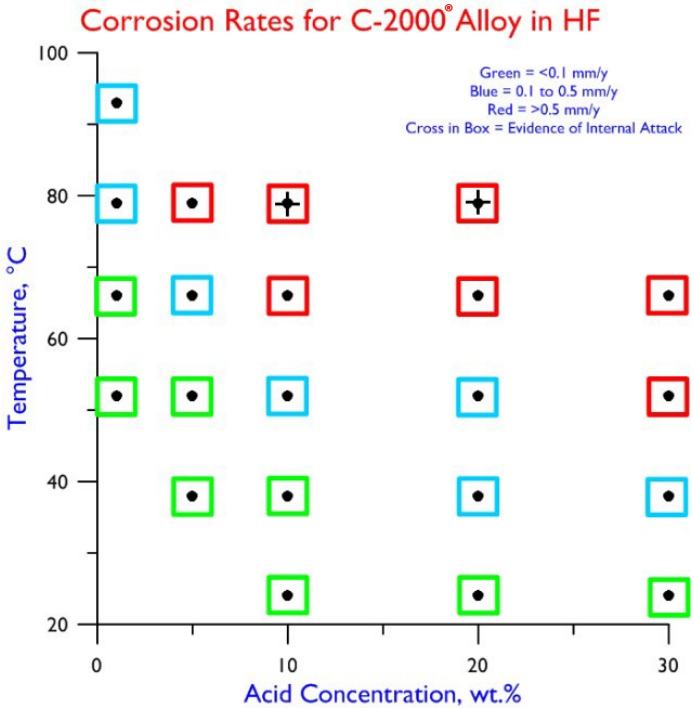
Corrosion Rates for C-2000® Alloy in HF
Green = <0.1 mm/y
Blue = 0.1 to 0.5 mm/y
Red = >0.5 mm/y
Cross in Box = Evidence of Internal Attack
Temperature, °C
100
80
60
40
20
0
10
20
30
Acid Concentration, wt.%

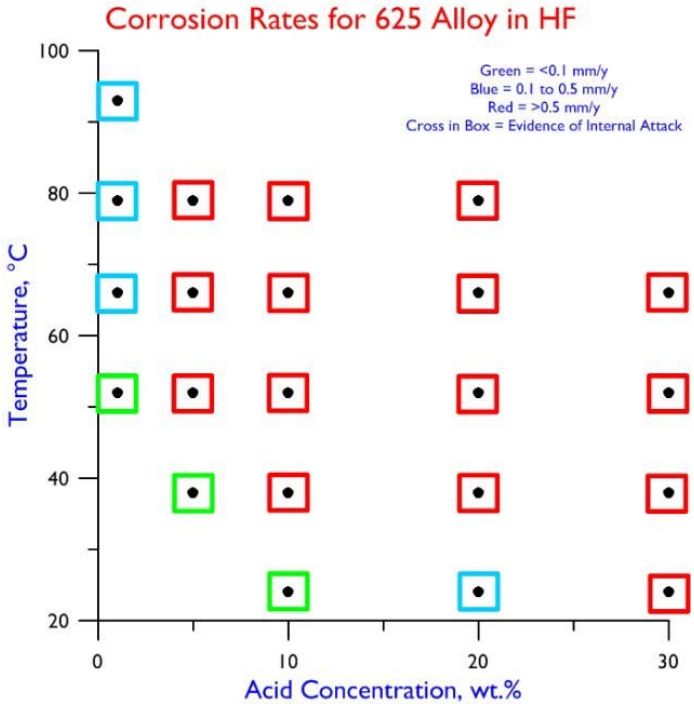
Corrosion Rates for 625 Alloy in HF
Green = <0.1 mm/y
Blue = 0.1 to 0.5 mm/y
Red = >0.5 mm/y
Cross in Box = Evidence of Internal Attack
Temperature, °C
100
80
60
40
20
0
10
20
30
Acid Concentration, wt.%

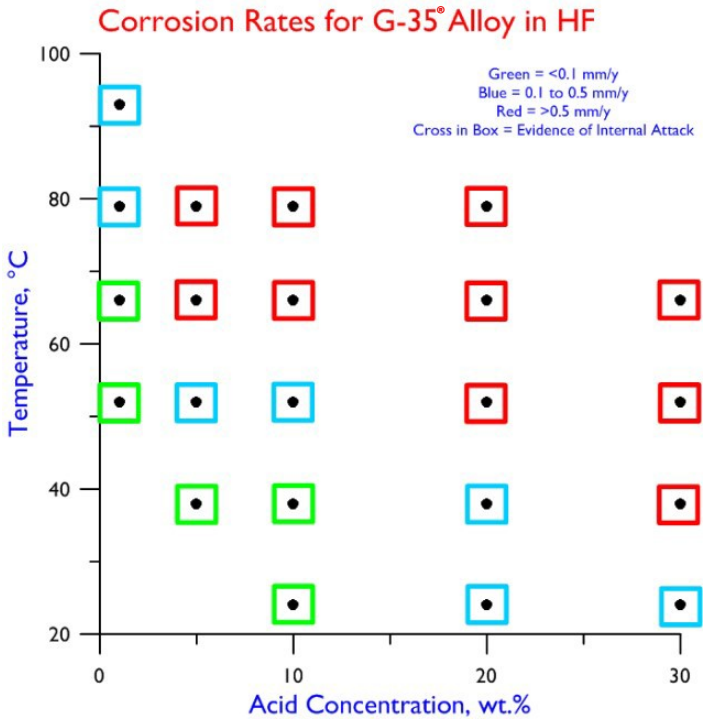

To indicate the “very safe”, “moderately safe”, and “unsafe” regimes for the five alloys, the enlarged squares (centered on the test concentrations and temperatures) have been colored green, blue and red, respectively.

From these charts, it is evident that:

1. Of the three nickel-chromium-molybdenum materials tested, C-2000® alloy is the least susceptible to internal attack; this might be because C-2000® alloy contains a small (1.6 wt.%) addition of copper.
2. The nickel-chromium materials are much less resistant to hydrofluoric acid; any internal attack is probably overwhelmed by the high rates of general attack in the “unsafe” zones.

Uniform Corrosion in Nitric Acid

Unlike the acids that have been discussed so far, nitric acid induces a high-potential, oxidizing, cathodic reaction with metallic materials. Under such circumstances, protective (passive) films form readily on materials containing sufficient chromium, such as the stainless steels, chromium-bearing nickel alloys, and chromium-bearing cobalt alloys.

For industrial applications involving only pure nitric acid, the stainless steels generally possess sufficient corrosion resistance. The chromium-bearing nickel alloys are only required if other chemicals, notably the halides and/or halogen acids, are present, or if the equipment has multiple uses involving different chemicals.

The performance of nickel-based alloys in pure nitric acid is very much a function of chromium content. Thus, HASTELLOY® G-35® alloy, which has a very high chromium content (33.2 wt.%), exhibits outstanding resistance, as shown below (the corresponding iso-corrosion diagram). In fact, a rate of less than 0.1 mm/y is expected at all temperatures below the boiling point curve, in the concentration range 0 to 70 wt.% (the highest concentration for which reagent grade, laboratory acid is available).

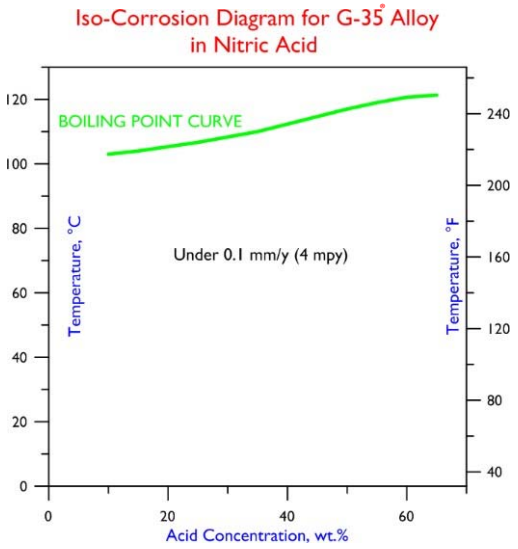

Two iso-corrosion diagrams showing the performance of nickel-chromium-molybdenum alloys in pure nitric acid are presented below. These relate to C-276 alloy (16 wt.% chromium) and C-2000® alloy (23 wt.% chromium). Note how the 0.1 mm/y and 0.5 mm/y lines have been pushed to higher concentrations and temperatures by the higher chromium content of C-2000® alloy.

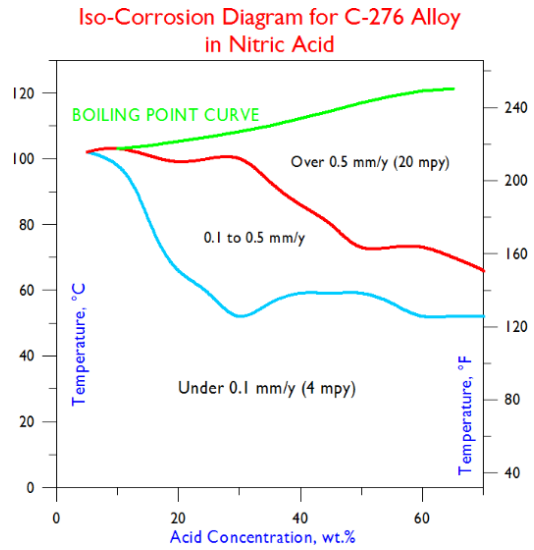

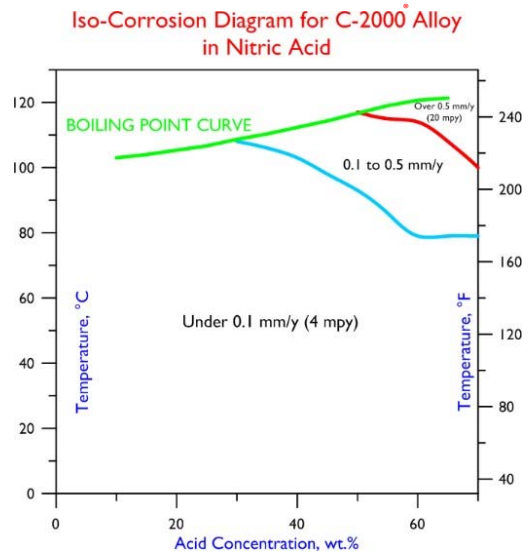

B-3® alloy, the chromium content of which is only 1.5 wt.%, corrodes rapidly in nitric acid. On the other hand, HYBRID-BC1® alloy, with a chromium content of 15 wt.%, can withstand even 70% nitric acid (i.e. exhibit corrosion rates less than 0.5 mm/y) up to a temperature of approximately 50°C.

Uniform Corrosion in Phosphoric Acid

There are two types of phosphoric acid, a pure, "food" grade made from elemental phosphorus, and an impure, "fertilizer" grade, which is made by reacting phosphate rock with sulfuric acid. Pure, "food" grade phosphoric acid is not nearly as corrosive as the other reducing acids, such as hydrochloric. Indeed, many alloys from the nickel-chromium, nickel-molybdenum, and nickel-chromium-molybdenum systems exhibit corrosion rates of less than 0.1 mm/y over large temperature and concentration ranges, as indicated in the iso-corrosion diagrams shown below for G-35® alloy, B-3® alloy, and C-276 alloy.

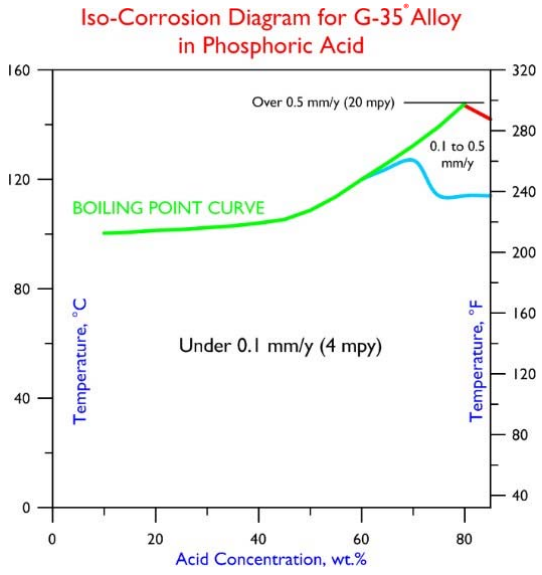

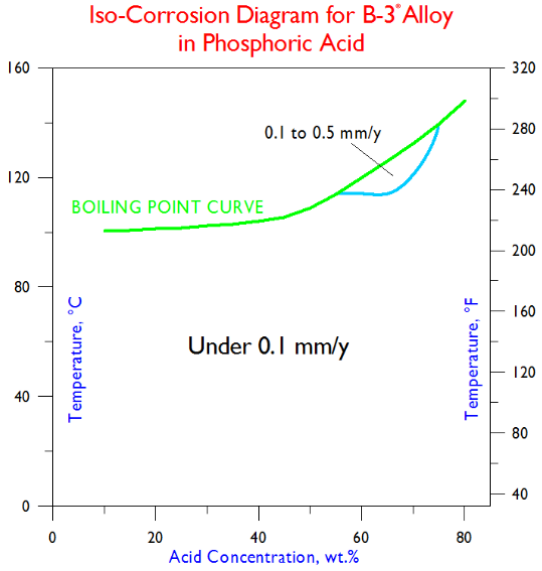

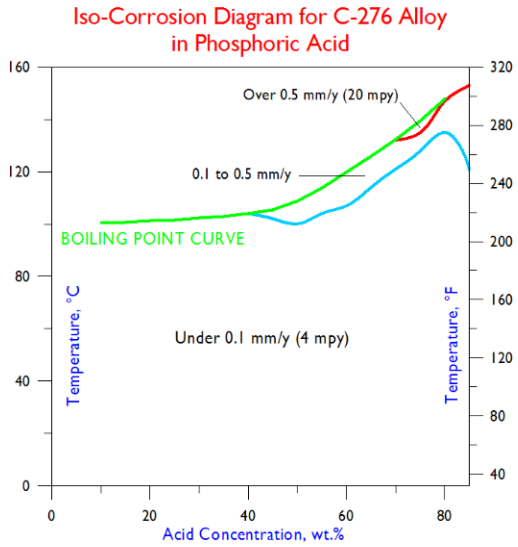

With regard to “fertilizer” grade phosphoric acid, important steps in the manufacture of fertilizers are the production and concentration of phosphoric acid. This acid is made by reacting phosphate rock with sulfuric acid, hence the alternate name “wet process” phosphoric acid. Not only does this fertilizer-grade/wet process acid contain traces of sulfuric acid, but also it contains impurities from the phosphate rock, which serve to increase its corrosivity.

The primary constituents of the phosphate rock are tricalcium phosphate (from which phosphoric acid and calcium sulfate are created), calcium fluoride (which generates hydrogen fluoride and calcium sulfate), and calcium carbonate (which yields carbon dioxide, calcium sulfate, and water). The concentration of the phosphoric acid (or rather the P_2O_5 content) is determined by the amount of rinse water needed to separate it from the calcium sulfate, and is normally in the range 30 to 32 wt.% (*Crook and Caruso, 2004*).

Impurities include fluoride ions, from the hydrogen fluoride (although these generally form complexes with metallic ions), chloride ions, silica, aluminum, iron (which serves to increase the oxidizing potential of the acid), calcium, and sodium.

A typical concentration sequence (to enable transportation and effective use) is:

Step 1: 30-32% to 37-39%

Step 2: 37-39% to 45-48%

Step 3: 45-48% to 52-54%

Step 4: 52-54% to 69-72%

The first three steps typically involve temperatures of 90°C or higher, and the fourth step typically involves temperatures up to 150°C.

Geographically, producers of fertilizer-grade/wet process phosphoric acid are located close to the largest accessible reserves of phosphate rock. In the United States, activity is centered in Florida, although there are also plants in the North-West. Across the Atlantic, most of the action is centered around North African and Middle Eastern deposits. Differences in impurity levels at the various locations result in differences in corrosivity.

The graph below compares the results for several materials in fertilizer-grade/wet process phosphoric acid (in the concentration range 36 to 54 wt.% P_2O_5). Acid 1 and acid 2 were from different locations in Florida. The tests were performed in autoclaves at 121°C, for a duration of 96 hours (uninterrupted). The choice of this temperature was based on previous tests of the high-chromium stainless steels (Alloys 28 and 31), for which 121°C was the upper limit. It should be noted that, for the nickel-based materials (i.e. C-2000® alloy with 23 wt.% chromium, G-30® alloy with 30 wt.%

chromium, and G-35® alloy with 33.2 wt.% chromium), there is a strong correlation between chromium content and corrosion resistance, due to the presence of oxidizing species.

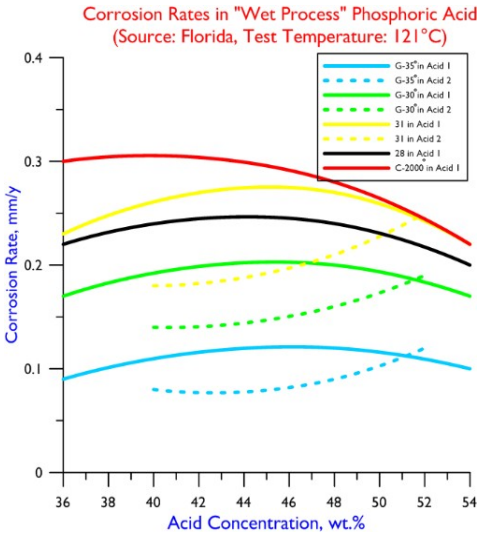

Uniform Corrosion in Sodium and Potassium Hydroxides

Sodium hydroxide (NaOH, caustic soda) and potassium hydroxide (KOH, caustic potash) are widely used chemicals. Applications include the manufacture of soap, paper, and aluminum. They are also used to neutralize acids, especially in the petrochemical industries. Molten NaOH is used to descale stainless steels and other alloys, in the metals industry. The materials most commonly used to resist NaOH and KOH are the commercially pure, wrought nickel products, Ni 200 and Ni 201 (*Dillon, 1994*, *Klarstrom, 1987*, *Friend, 1980*). The latter is a low carbon grade for use at temperatures above 315°C, where graphitization is a possibility with the higher carbon material (Ni200). Where greater strength is required, Ni301, which can be age-hardened, is used. The iso-corrosion diagram for Nickel 200 in sodium hydroxide (Ref. *Crum and Schumaker, 2006*) is shown below.

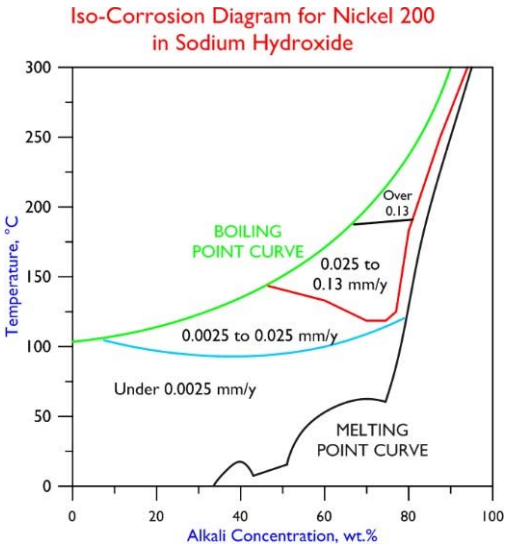

In many heat transfer systems, the material of choice must resist NaOH (or KOH) on one side and chlorinated or contaminated water on the other (*Rebak, 2005*). Worse still, some situations require that the material be exposed sequentially to both acids and alkalis. In such cases, nickel alloys containing chromium and/or molybdenum are necessary.

As to the resistance of these chromium and molybdenum bearing nickel alloys to NaOH and KOH, several are susceptible to “caustic dealloying” at high concentrations and temperatures (*Chambers, 2002*, *Crook and Meck, 2005*). This

phenomenon is characterized by the selective removal of elements other than nickel from near-surface regions of the microstructure. In tests involving 50 wt.% sodium hydroxide at temperatures up to 107°C, it was determined that B-3® and C-2000® alloys are susceptible to dealloying at 66°C and 79°C (and above), respectively, whereas G-35® alloy does not exhibit dealloying, at least up to the maximum test temperature, and over the 72 h test duration. This infers that molybdenum is a bad actor regarding caustic dealloying, and/or that a higher chromium content is beneficial.

Pitting and Crevice Corrosion

Pitting and crevice corrosion are forms of attack associated with the presence of chlorides (or other halides) in aqueous solutions. Pitting is typically initiated by the localized breakdown of passive films, or by the occurrence of localized electrochemical cells (normally the anodic and cathodic sites move around on a metallic surface, but metallurgical inhomogeneity can result in static conditions). As its name suggests, crevice corrosion occurs in crevices or narrow gaps between structural components. Both forms of attack are associated with the localized build-up of positive charge, and the attraction of negatively charged chloride (or other halide) ions to the pit or gap, followed by the formation of the corresponding acid (hydrochloric acid, in the case of chloride ions). This acid accelerates the attack, and the process becomes auto-catalytic.

It was once stated that the commercial success of the nickel-chromium-molybdenum alloys has been largely due to their resistance to pitting and crevice corrosion (i.e. chloride-induced localized attack). Indeed, this is a major attribute of this family of materials, another being their resistance to chloride-induced stress corrosion cracking, which will be discussed later.

The pitting resistance of a material is hard to assess. Short-term tests can result in miniscule pits or large pits, both of which are treated equally. Corrosion rates are generally misleading, since there is great random error associated with the time of pit initiation and progression; in a 24 h test of identical samples, for example, the first pit on each sample can start either early or late in the test, giving widely different corrosion rates for the two samples.

The pitting and crevice corrosion tests preferred by the author are those described in ASTM Standard G48: Pitting and Crevice Corrosion Resistance of Stainless Steels and Related Alloys by Use of Ferric Chloride Solution. Six test methods are described in this standard, two of which (Methods C and D) are related to nickel-based and chromium-bearing alloys. Method C enables determination of the critical pitting temperature (CPT) of a material, i.e. the lowest temperature at which pitting is observed in a solution of 6 wt.% ferric chloride + 1 wt.% hydrochloric acid, over a 72 h period. Method D requires a crevice assembly to be attached to the sample, to enable determination of the corresponding critical crevice temperature (CCT). In the inter-laboratory test program associated with ASTM Standard G48, a maximum temperature of 85°C was used. The standard does allow testing at higher temperatures, but does not address the equipment (i.e. autoclaves) required for tests above the boiling point.

Generally speaking, the ranking of alloys in Method C correlates well with the ranking in Method D, although crevice corrosion tends to be encountered at much lower temperatures than pitting. With this in mind, along with industry concerns about high temperature autoclave testing, the focus at Haynes International has been on Method D, and the associated CCT's of the nickel-based alloys (relative to stainless steels).

The CCT's of several nickel-chromium and nickel-chromium-molybdenum alloys are given in the following bar chart, along with those of 316L (CCT = 0°C) and 254SMO® alloy. They suggest that both molybdenum and chromium are important to chloride-induced pitting and crevice corrosion resistance, with the former being more influential (which is not surprising, since hydrochloric acid is the aggressive chemical of concern in chloride solutions).

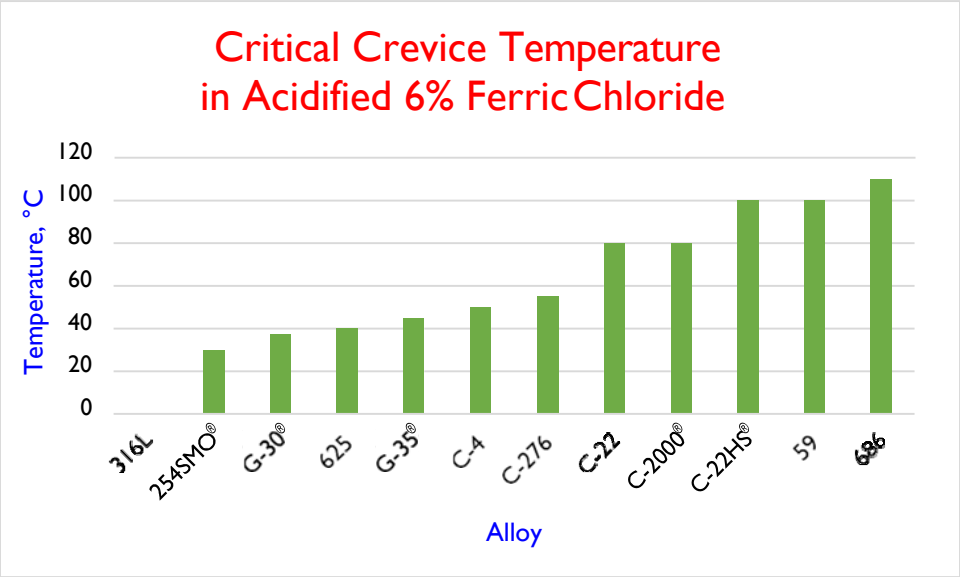

With regard to the pitting and crevice corrosion resistance of the cobalt-based alloys, only ULTIMET® alloy and HAYNES® 25 alloy have been seriously compared with the nickel-based CRA's. This is partly due to the fact that the tungsten-bearing, high-carbon cobalt alloys are not nearly as corrosion-resistant as the nickel-based CRA's, since portions of their chromium and tungsten contents contribute to carbide formation. Furthermore, from the standpoint of chloride-induced localized attack, their carbide-laden microstructures are inhomogeneous and therefore likely to cause localized electrochemical conditions. ULTIMET® alloy and HAYNES® 25 alloy, on the other hand, are homogenous wrought products, the former designed specifically to excel in aqueous solutions of corrosive chemicals.

Tests to determine the pitting resistance of ULTIMET® alloy were carried out in the early 1990's, before the ASTM G48 test became favored at Haynes International. At that time, the critical pitting temperature in Green Death (a solution designed to simulate condensates in flue gas desulfurization systems) was the definitive measure of a material's resistance to chloride-induced pitting. Green Death is similar to the ASTM G28B quality control solution and comprises 11.5% H_2SO_4 + 1.2% HCl + 1% $FeCl_3$ + 1% $CuCl_2$ (where all percentages are by weight). The duration of the Green Death test is 24 h.

Surprisingly, ULTIMET® alloy was equal to the nickel-chromium-molybdenum alloy with the highest critical pitting temperature (i.e. C-22® alloy), as shown in the table below, despite the much lower combined molybdenum plus tungsten level of ULTIMET® alloy. It perhaps indicates that these two elements are more effective in a cobalt, rather than nickel, base. Alternatively, nitrogen (which is more soluble in cobalt alloys than nickel alloys, and was deliberately added to ULTIMET® alloy to enhance its resistance to chloride-induced pitting) could be responsible.

Testing in Green Death revealed that HAYNES® 25 alloy also possesses high resistance to chloride-induced pitting. Its critical pitting temperature in this solution is close to that of C-276 alloy, despite that, in atomic terms, its combined molybdenum plus tungsten content is relatively low.

Note that HAYNES® 6B alloy, the wrought version of the most popular high-carbon cobalt-based alloy, has a Green Death critical pitting temperature of 45°C, which is significantly higher than that of 316L stainless steel.

Critical Pitting Temperatures in Green Death Solution

Alloy	Critical Pitting Temperature, °C
ULTIMET®	120
C-22®	120
C-276	110
25	110
625	75
6B	45
316L	25

Perhaps the most common chloride solution encountered by the wrought, corrosion-resistant nickel alloys is sea water. Sea water is encountered by marine vessels, oil rigs, and coastal structures and facilities (which typically use sea water as a coolant). As a chloride, it can induce pitting, crevice attack, and stress corrosion cracking of metallic materials, as well as uniform attack. Furthermore, marine equipment can become encrusted, leading to a form of crevice attack known as "under-deposit" corrosion; biofouling is also an issue.

Fortunately, the nickel alloys possess good sea water resistance. In particular, those with high copper contents, such as alloy 400, resist biofouling (copper being a poison to microbes). For stagnant or low velocity conditions, chromium- and molybdenum-bearing nickel alloys are favored, due to their higher resistance to pitting and crevice attack.

Some crevice corrosion data for sea water, generated as part of a U.S. Navy study at the LaQue Laboratories in Wrightsville Beach, North Carolina, are presented in the following table created by *Aylor et al, 1999*. Crevice tests were performed in both still (quiescent) and flowing sea water, at 29°C, plus or minus 3°C. Two samples of each alloy were tested in still water, for 180 days, and two samples of each alloy were tested in flowing water, for 180 days. Each sample contained two possible crevice sites. In quiescent sea water, the results mirror those generated in acidified ferric chloride, with C-22® and C-2000® alloys as the most resistant. In flowing sea water, crevice attack of the stainless steels was shallower, and none of the Ni-Cr-Mo alloys exhibited crevice corrosion.

	Quiescent Sea Water		Flowing Sea Water	
Alloy	Number of Attack Sites	Depth mm	Number of Attack Sites	Depth, mm
316L	2	1.80	2	0.32
254SMO®	2	1.25	2	0.01
625	2	0.11	2	<0.01
C-22®	0	0	0	0
C-276	1	0.12	0	0
C-2000®	0	0	0	0

Stress Corrosion Cracking

One of the chief advantages of the wrought, corrosion-resistant, nickel-based alloys is their high resistance to chloride-induced stress corrosion cracking (SCC), a form of corrosion to which the stainless steels are particularly prone. In fact, evidence points to the fact that the higher the iron content of the nickel alloys, the less is their resistance to this extremely harmful form of attack.

Chloride-induced SCC falls within the broader category of environmentally assisted cracking (EAC), which also includes hydrogen embrittlement, sulfide stress cracking, and liquid metal embrittlement (*Rebak, 2005*). All of these phenomena describe circumstances under which ductile materials exhibit embrittlement when subjected to tensile stresses in specific corrosive environments.

While chlorides, hence chloride-induced SCC, are the main concern of this manual, other halides (bromides, fluorides, and iodides) can be equally damaging. Also, hydrofluoric acid is known to cause stress corrosion cracking, especially in the presence of dissolved oxygen. Resistance to hydrogen embrittlement and sulfide stress cracking are important attributes for down-hole applications in the oil and gas industry; fortunately, the nickel-chromium and nickel-chromium-molybdenum alloys are very resistant to these forms of environmentally assisted cracking, and are consequently used in some of the most severely corrosive wells.

A test commonly used to assess the resistance of metallic materials to chloride-induced SCC is that described in ASTM Standard G36, which involves a boiling solution of 45 wt.% magnesium chloride. The following table gives the times required to cause cracking of U-bend samples (made from 3.2 mm sheet) of various alloys in this solution. For the low-iron nickel-based CRA's, which did not exhibit cracking, the test was stopped after 1,008 h (six weeks).

Alloy	Family	Time to Cracking, h
316L	Austenitic Stainless Steel	2
254SMO®	Austenitic Stainless Steel	24
28	Austenitic Stainless Steel	36
31	Austenitic Stainless Steel	36
G-30®	Ni-Cr-Fe	168 h
G-35®	Ni-Cr	No Cracking in 1,008
C-22®	Ni-Cr-Mo	No Cracking in 1,008
C-276	Ni-Cr-Mo	No Cracking in 1,008
C-2000®	Ni-Cr-Mo	No Cracking in 1,008
625	Ni-Cr	No Cracking in 1,008

EAC and chloride-induced SCC are complicated subjects. In the case of nickel-based alloys and stainless steels, and aqueous solutions, it is believed that local electrochemical conditions occur at crack tips, to ensure rapid crack propagation. Microstructure also plays a part, cold-worked materials being much more prone to cracking than solution annealed materials.

With regard to the propagation of cracks during chloride-induced SCC, a branching transgranular pattern is common with the austenitic stainless steels; however, other propagation paths are possible. Hydrofluoric acid, for example, can induce rather peculiar crack patterns in stressed nickel-based CRA's, as illustrated in the following photomicrographs, which show a) extremely fine/barely resolvable cracking in the outer surface of a C-2000® U-bend sample exposed to 20% hydrofluoric acid at 79°C for 240 h, an b) cracking of a more normal nature in a C-22® U-bend sample exposed to the same conditions.

Cracking in C-2000® U-Bend Sample Exposed to 20% HF at 79°C (*Crook et al, 2007*)

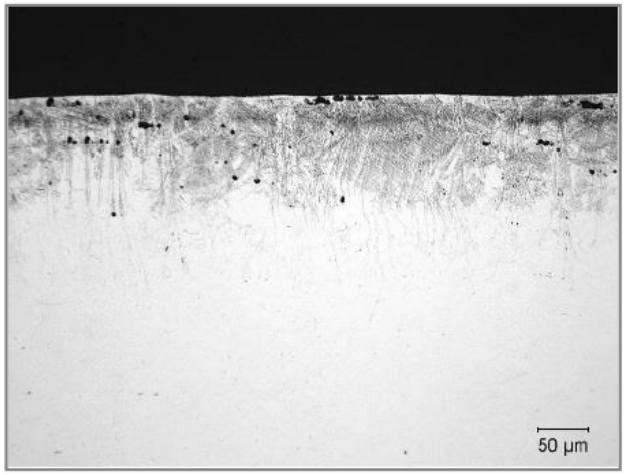

Cracking in C-22® U-Bend Sample Exposed to 20% HF at 79°C (*Crook et al, 2007*)

Wear Background

Wear can be described as the degradation of surfaces by mechanical means. This degradation can be caused by solid particle impact, liquid impact, relative motion between surfaces in contact, by solid particles forced against surfaces, and by solid particles trapped between surfaces in relative motion. Wear of metallic materials generally falls into one of three major categories, namely abrasion, erosion, or metal-to-metal sliding. However, many sub-categories exist. For example, four types of erosion are common, namely solid particle erosion, liquid droplet erosion, cavitation erosion, and slurry erosion. The important issues in a wearing system are the amplitude and direction of the applied stresses, and the response of the surface(s) to those stresses, in terms of deformation and fracture.

Many industrial systems are complex, involving more than just mechanical stresses. The presence of water or more corrosive liquids, in a system, can significantly change the nature of the degradation process. Stainless steels, for example, which rely on passive surface films for corrosion protection, can suffer accelerated corrosion if those passive films are damaged by mechanical stresses. At high temperatures, the interactions between mechanical stresses and protective oxide films are important. Of course, many sliding systems operate in the presence of lubricants, which completely alter the stresses to which surfaces are subjected.

From a materials standpoint, there is no universal panacea to industrial wear problems. While very hard materials (such as ceramics) resist certain types of abrasion, they are less suited to types of wear involving impact, where the ability of the material to absorb energy, without fracture, is paramount. Among the metallic materials, the tool steels, bearing steels, austenitic manganese steels, martensitic alloy steels, martensitic stainless steels, and high chromium irons are known for their resistance to certain types of wear, at low to moderate temperatures, and in the absence of corrosive chemicals. In the presence of corrosive chemicals, cobalt alloys are regarded as among the most wear-resistant of the metallic materials. They are also used to resist wear in hostile, high temperature environments.

Abrasion

Abrasion (or abrasive wear) is probably the most easily recognized form of wear. It is self-evident, for example, that hard particles will scratch softer surfaces, when they are forced against, and moved relative to, those surfaces. Not to be confused with solid particle erosion, which involves the striking of surfaces by gas-borne particles, abrasion is normally associated either with surfaces involved with the movement of packed particles (soil, sand, rocks, etc.), or hard particles trapped between machine surfaces. The former case is generally known as two-body abrasion or low stress abrasion; the latter is known as three-body abrasion or high stress abrasion. High stress abrasion is generally regarded as the more severe, because it can induce fracture of the abrasive particles, thereby ensuring the presence of sharp edges for the cutting action.

In the field of metallic materials, it has been found that alloys whose microstructures contain large volume fractions of hard precipitates (carbides, for example) provide the highest resistance to two-body (low stress) abrasion. Thus, the high-chromium irons, which contain large precipitates of chromium carbide, are favored for many earthmoving applications. For even higher resistance to low stress abrasion, mixtures of steel and carbide particles are available for co-deposition by welding. In this case, the steel melts in the welding arc, but the carbide particles are transferred intact from the welding consumable to the weld pool, where they become locked in place by the re-solidifying steel. These so-called composite materials normally contain tungsten carbide.

While a high volume fraction of carbides or intermetallics may be beneficial to low stress abrasion resistance, it is very detrimental to ductility. Consequently, it is common for weld overlays of the high chromium irons and tungsten carbide composites to crack during cooling, or upon impact in service. To cope with conditions requiring a modicum of ductility, therefore, alloys with moderate precipitate contents are available.

Cast cobalt alloys with different levels of low stress abrasion resistance are available, and, as with the high chromium irons, the higher the carbon content, the higher in general is the resistance to this form of wear (in the case of castings and weld overlays). In choosing cobalt alloys, however, the need for low stress abrasion resistance is often tempered by accompanying needs for corrosion resistance and crack-free overlays, both of which require the carbon content to be minimized.

To assess the low stress abrasion resistance of materials in the laboratory, the dry sand / rubber wheel test described in ASTM Standard G 65 is normally employed. The test procedure involves forcing a sample against a rotating, chlorobutyl rubber wheel (of diameter 229 mm), while feeding sand of a well-defined size and shape (rounded quartz grain sand, 212 to 300 µm diameter) to the wheel / sample interface at a specified rate. Data (relating to 2000 revolutions of the rubber wheel) for several wrought alloys are presented in the following chart, along with the corresponding value for STELLITE® 6 weld metal. These include 6B, which is compositionally similar to STELLITE® 6 alloy, but which exhibits much higher resistance to low stress abrasion by virtue of a more beneficial carbide structure. Other alloys include a tool steel (D-2), a carbon steel (1020), an austenitic stainless steel (316L), two low-carbon, cobalt-based materials (HAYNES® 25 and ULTIMET® alloys), and two nickel-based materials (625 and C-276 alloys). The difference in performance between Alloys 6 and 6B indicates the advantages of considering alternate product forms, in attempting to solve wear problems.

Low Stress Abrasion Data

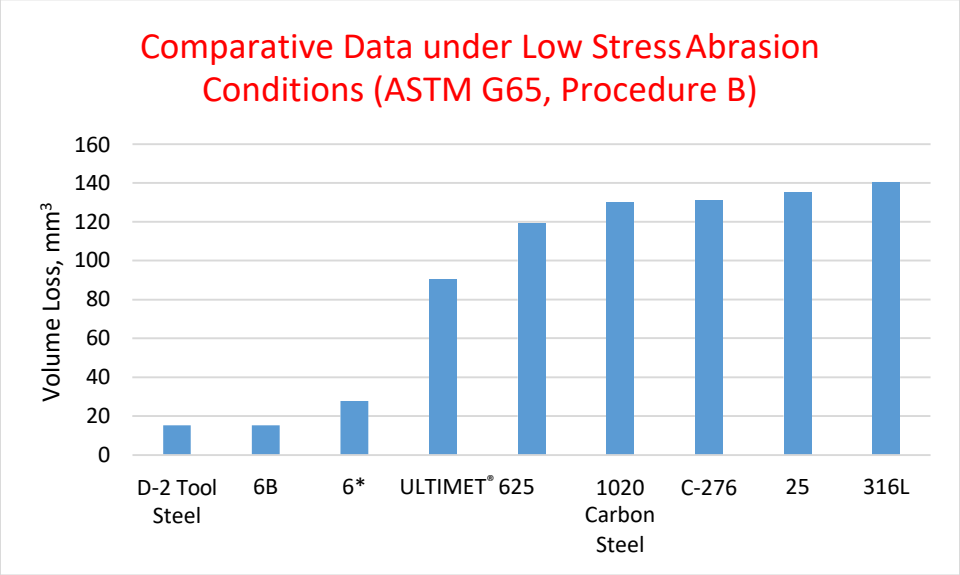

*All weld metal, applied by the TIG (GTA) welding process

2000 revolutions at 200 revolutions per minute

Load: 13.6 kg

Feed Rate: 390 g/min

Three-body (high stress) abrasion is not only a much more severe form of wear than two-body abrasion, but also it appears equally damaging to soft and hard metallic materials, as illustrated in the following chart. These data were generated using the ASTM B 611 test procedures, which involve forcing a sample against a rotating, high strength steel wheel (of diameter 165 mm), while stirring a sand/water slurry (1500 g of the 212 to 300 µm rounded quartz grain sand to 940 g of water) by means of paddles on both sides of the steel wheel, in an enclosed chamber. Test parameters include a load of 22.7 kg and a rotational speed of 245 revolutions per minute. The test results relate to just 250 revolutions of the steel wheel.

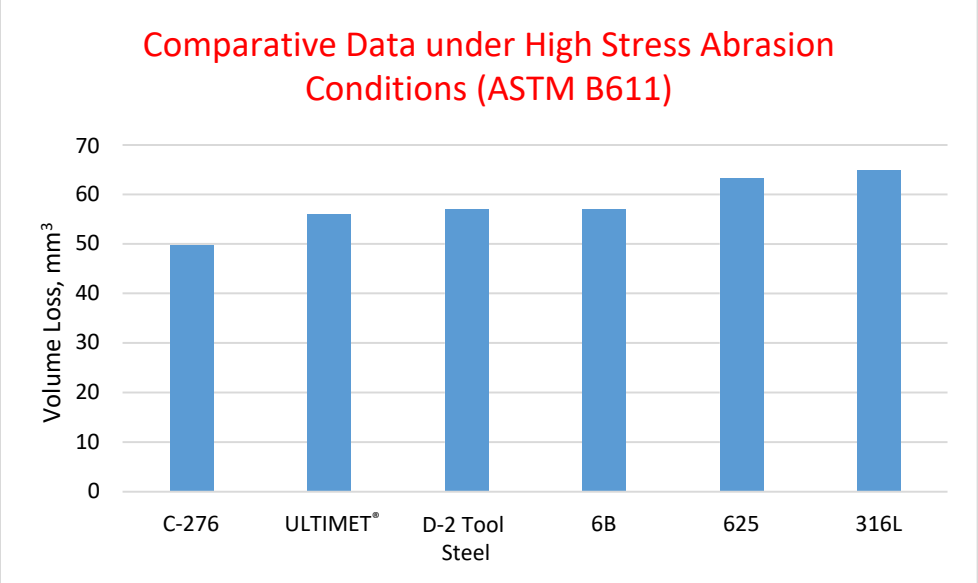

It is evident that the material ranking is quite different for low- and high-stress abrasion. For example, the two materials which perform extremely well under low stress abrasion conditions (hardened D-2 tool steel and Alloy 6B) are mediocre under high stress conditions. Evidently, performance in three-body abrasion is not related to material hardness, nor the presence of hard precipitates within the microstructures of metallic materials.

As to the effects of temperature upon abrasive wear resistance, data generated under three-body conditions are provided in *Berns and Fischer, 1993*, whose work involved abrasive particles of flint, ranging in size from 63 to 100 µm, with a mean value of 80 µm. The apparatus used by these workers had a ring-on-disc configuration, with outer and inner ring diameters of 24.9 mm and 18 mm, respectively. The disc (of diameter 30 mm, with a 5 mm diameter hole in the center) was rotated at 28 mm/s. The test load was limited to 0.82 MPa, so that the abrasive particles could be fed into, and flow within, the interface. Both the ring and disc were made from the test alloy, and weight losses of both used to determine a dimensionless wear rate, by considering the surface areas, densities, and wear path lengths. Tests were performed by these workers, under argon, at temperatures between 550°C and 1050°C, and at room temperature.

Two types of metallic material were tested by these workers, specifically materials with and without large (5 to 15 µm) particles within their microstructures. Some of the results related to the second group (no precipitates or precipitates less than 1 µm in size) are plotted in the figure below. Considering first the room temperature results for these selected (wrought) materials, namely ULTIMET® alloy (low carbon Co-Cr-Mo), NIMONIC® 80A (Ni-Cr), 316L (austenitic stainless steel), and 410 (martensitic stainless steel), these indicate that significant differences do exist between alloys, under three-body abrasion conditions. This is in contrast to the high stress abrasion results shown above, which infer that many metallic materials fall within a narrow performance band, under such conditions.

The Effect of Temperature upon High Stress Abrasion

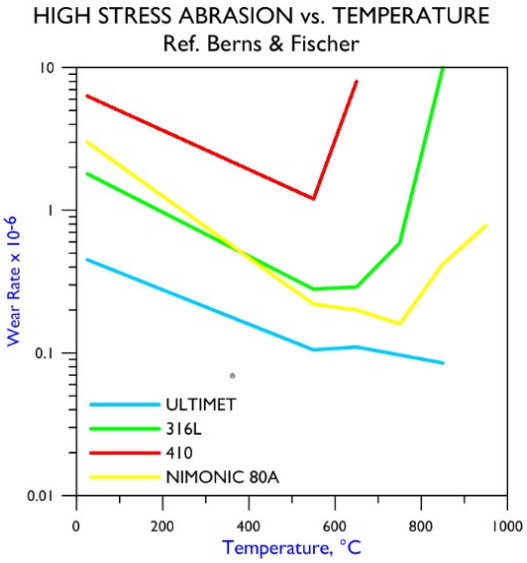

A possible explanation of the room temperature wear rate differences is that the test load is insufficient to cause massive fracture of the flint particles, thus placing the wear process in a pseudo-low stress abrasion category, rather than the high stress category normally associated with three-body abrasion. Among the other materials tested were hardened D-2 tool steel and Alloy 6 (in cast form). At room temperature, the wear rates for these materials were approximately 0.2 and 0.3, as compared with 0.45 for ULTIMET® alloy. At least in terms of ranking, these values correlate well with the low stress abrasion numbers generated using the dry sand/rubber wheel test, which, ironically, is a three-body system used to simulate two-body conditions.

Surprisingly, the wear rates of all the test materials from *Berns and Fischer, 1993* were significantly lower at 550°C than at room temperature. Also, it appears that there is a critical temperature, beyond which high rates of degradation are encountered. It was concluded by these workers that the wear rate up to the critical temperature is largely controlled by the solid solution strength and work hardening rate. The critical temperature is believed to be the temperature

(augmented by frictional heating) at which dynamic recrystallization of the surface supplants work hardening. Notably, the cobalt alloys exhibited relatively low wear rates, which is commensurate with their high strengths and work hardening rates at elevated temperatures, and exhibited relatively high critical temperatures.

In summary, two types of abrasion have been identified, although the lines of demarcation between them are somewhat blurred, and probably dependent upon the precise nature of the abrading species and the forces involved. Under so-called two-body or low stress conditions, at temperatures close to ambient, the abrading particles remain largely intact and can ride on hard microstructural outcrops (such as carbides), if these exist. Consequently, materials containing large quantities of hard microstructural precipitates are resistant to such conditions. Surfaces moving through packed abrasives (as commonly encountered in the mining and construction industries) give rise to this form of degradation. At high temperatures, it appears that the strength and work hardening characteristics of the solid solution (matrix) are critical to the abrasion resistance of metallic materials.

Three-body or high stress abrasion relates to abrasive particles trapped between surfaces in relative motion. At temperatures close to ambient, metallic materials appear to fall within a narrow band of performance, irrespective of their microstructure or hardness.

Solid Particle Erosion

Erosion has been defined as the progressive loss of original material from a solid surface due to the mechanical interaction between that surface and a fluid, a multicomponent fluid, or impinging liquid or solid particles (*Hutchings, 1983*). In solid particle erosion, the particle sizes are typically between 5 and 500 µm, and the relative velocities between 5 and 500 m/s. In most cases, the particles are traveling at high speed, when they strike the surface. However, the reverse is possible, as in the case of helicopter blades in dust-laden air.

In solid particle erosion, the impact angle (defined as the angle between the plane of the surface and the particle trajectory) is very important. Ductile materials appear to suffer most at impact angles between 20 and 30°, whereas brittle materials exhibit maximum rates of degradation when the impact angle is 90° (*Hutchings, 1983*). The former has been described as ductile erosion behavior, involving plastic flow as the primary mode of degradation. The latter has been described as brittle erosion behavior, with brittle fracture as the predominant degradation mechanism.

Rates of degradation during solid particle erosion are strongly dependent upon the velocity with which the particles strike the surface (or vice versa). In fact, for a constant impact angle, the rate has been found to be proportional to velocity to the power n, where n usually falls within the range 2.3 to 2.5 for ductile materials, and within the range 2 to 4 for brittle materials (*Hutchings, 1983*).

Except in the case of very fine particles, the relationship between the erosion rate of brittle materials and particle radius also appears to obey a power law, with exponents in the range 0 to 1. Fine particles, surprisingly, induce a response in brittle materials that is pseudo-ductile, i.e. the angular dependence is similar to that for ductile materials. The erosion of ductile materials is generally independent of particle size, with diameters above 100 to 200 µm. At smaller diameters, the relationship is approximately linear, though little erosion is experienced with particles of diameter 5 µm and less (*Hutchings, 1983*).

With regard to the nature of the eroding particles, sharp particles obviously cause more damage than rounded particles. Surprisingly, however, there is not a strong relationship between erosion rate and particle hardness, provided the particles are harder than the surface being eroded. For particles softer than the surface, the erosion rate falls sharply with reduced particle hardness (*Hutchings, 1983*).

With regard to metallic materials, attempts have been made to establish relationships between microstructural characteristics and solid particle erosion resistance. Several studies indicate, for example, an inverse relationship between the hardness of martensitic steels and their erosion resistance (*Gulden, 1979* and *Green et al, 1981*).

Likewise, carbides can be deleterious to the solid particle erosion resistance of white irons, if they are softer than the eroding particles (*Aptekar and Kosel, 1985*). If they are harder, the opposite is true. From these studies, it is evident that hardness, especially if due to the presence of martensite or carbides in metallic microstructures, is, if anything, a measure of lack of resistance to this form of wear.

Cobalt alloys have been included in several room temperature, solid particle erosion studies through the years, notably those described in *Ninham, 1987* and *Levy and Crook, 1991*. It is valuable to review some of these results, in light of the principles presented in *Hutchings, 1983*. In the *Ninham, 1987* study, Alloys 6, 6B, and HAYNES® 188 (a low carbon Co-Cr-Ni-W alloy designed for use in the hot sections of flying gas turbine engines) were tested, along with several chromium-bearing nickel alloys and stainless steels. Three variables were studied, namely the type of eroding particle (silicon carbide or quartz), the impact angle (30, 60, or 90°), and the condition of the material. One of the test alloys (718) was age-hardenable, so was tested in both the age-hardened condition and the annealed condition. Two of the alloys (188 and C-276) can be cold-reduced, to enhance their room temperature strength, so these were tested in both the annealed and cold-reduced conditions.

The apparatus used to assess the effects of these variables is described in detail in *Levy, 1981*. Essentially, it comprises a vibrating hopper, to feed the erosive particles into a high velocity air stream, and a test chamber, in which impingement occurs. A particle velocity of 60 m/s was used, and sample weight measurements taken every 20 or 40 g of erosive particles used. The silicon carbide particles were angular and had diameters between 250 and 300 µm. The quartz particles were between 75 and 200 µm diameter, and of an unspecified shape. The hardnesses of these two materials (taken from *Hutchings, 1983*) are 2100 to 2480 kgf/mm^2 for silicon carbide and 820 kgf/mm^2 for quartz (SiO_2).

One of the main conclusions of this work was that aging and cold-working have little effect upon the solid particle erosion resistance of alloys of this type. Also, the effect of impact angle was small. In the case of silicon carbide, the angle effects were in line with those defined for ductile erosion behavior in *Hutchings, 1983* (a 30° impact angle causing the highest rate, and 90° causing the lowest). In the case of quartz, however, the angle effects were both mixed and minimal. As might be expected, the angular silicon carbide particles did more damage than the quartz particles.

Perhaps the most important fact to emerge from the work described in *Ninham, 1987* was that there is not much difference between the various alloys (under these test conditions), irrespective of the alloy base (cobalt vs. nickel vs. iron), and irrespective of the microstructural condition (annealed vs. aged vs. cold-reduced). Although the carbides present in Alloys 6 and 6B did not appear to be of benefit, at least they were not detrimental, as they were for the white irons in *Aptekar and Kosel, 1985*.

The *Levy and Crook, 1991* study, involving many of the same wrought alloys tested under abrasive wear conditions, was limited in scope, but again provided evidence that alloy base and carbides are of little importance in solid particle erosion, at room temperature. One of the materials, ULTIMET® alloy, was tested at different impact angles, with two different types of eroding particle (400 µm angular silicon carbide and 80 µm aluminum oxide, of an unspecified shape). The erosion rates measured are shown below, as a function of impact angle. As in the *Ninham, 1987* study, silicon carbide induced ductile erosion behavior, whereas aluminum oxide produced a slightly different response, the erosion rate at an impact angle of 60° being equal to that at 30° impact. According to *Hutchings, 1983*, the hardness of aluminum oxide is similar to that of silicon carbide; however, the shape of the aluminum oxide particles was not specified.

An important part of the *Levy and Crook, 1991* study was some solid particle erosion testing at high temperature (850°C), using the same aluminum oxide particles and an impact angle of 30°. The alloy with the lowest strength, 316L stainless steel, exhibited the lowest erosion rates by far in this test, suggesting that the particles might have become embedded in the surface, rather than causing the surface to deform and fracture. Of course, oxides films are very important at such high temperatures.

The Effect of Impact Angle upon Solid Particle Erosion of ULTIMET® Alloy

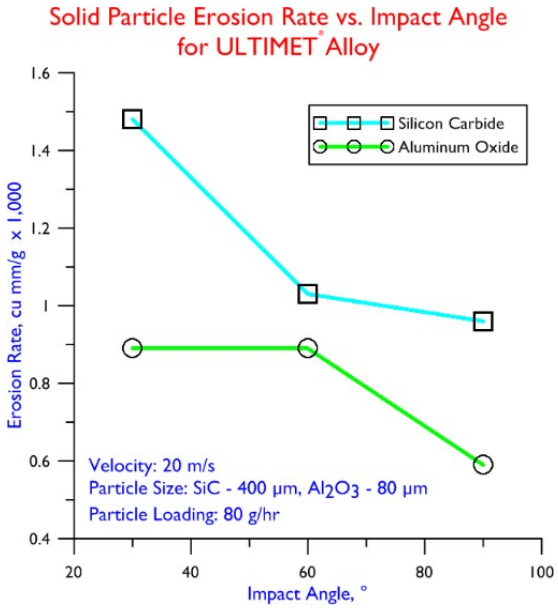

The solid particle erosion data presented in the following three figures were generated for Haynes International at Tallinn University (Estonia) in the 2006/7 time period, and illustrate the effects of impact angle, particle velocity, and temperature upon the performance of 25, 282®, and ULTIMET® alloys. 282® alloy (a nickel-based superalloy designed for high temperature service) was tested in the age-hardened condition. In reviewing these data, it should be borne in mind that the weight change measurements did not take into account the oxide scales that grew on surfaces not subject to erosion, nor was it possible to take into account the weight gains associated with the embedding of particles in the eroded surfaces. Nevertheless, the results provide considerable insight as to the effects of the aforementioned variables.

The single data points provided for HARDOX® 400 and 316L stainless steel in Erosion Figure 2 indicate that these materials are more resistant to erosion than the three Haynes alloys at 300°C and an impact angle of 60°. However, it is possible that the result for 316L was influenced by gains in weight due to embedding of silica particles, 316L being a relatively soft material.

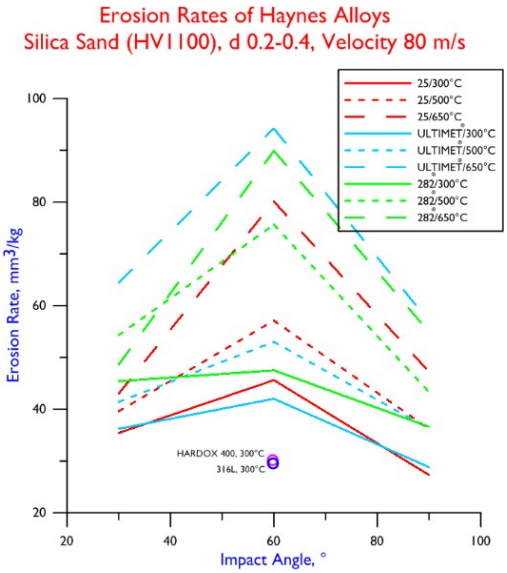

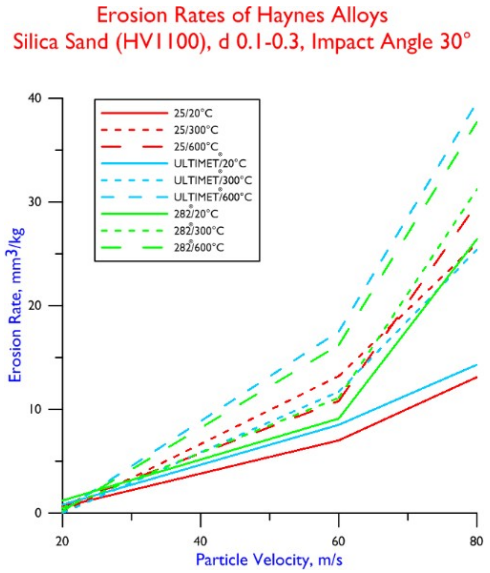

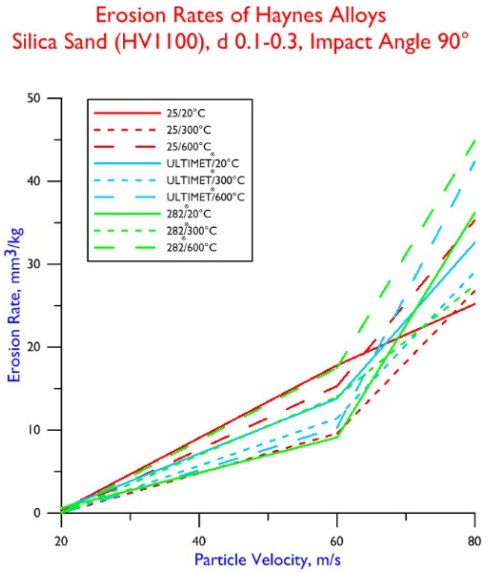

Cavitation Erosion

Cavitation erosion relates to the formation and collapse of near-surface bubbles, in liquids undergoing pressure changes. Surface damage is caused by the collapse of the bubbles, or, more precisely, by the liquid jets that occur during bubble implosion. The bubbles themselves are created when the pressure in a liquid falls below the liquid's vapor pressure; collapse is a result of subsequent pressure increases. This mode of degradation is common in valves and pumps.

Since the cavitation erosion resistance of materials depends upon their response to a succession of shock waves, it is common for the metallic materials to suffer from micro-fatigue. This is true of liquid droplet erosion also. In fact, these two types of erosion are so intertwined that tests for one type are often used to determine resistance to the other.

The cobalt alloys possess outstanding resistance to both cavitation and liquid droplet erosion (*Heathcock et al, 1979, Antony and Silence, 1979, and Woodford, 1972*). This has been attributed to the tendency of the cobalt-rich solid solution to transform (from fcc to hcp), under the action of mechanical stress, and the associated low stacking fault energy, which influences both the nucleation and propagation of cracks. Furthermore, cobalt alloys are known to absorb stress by twinning (*Rémy and Pineau, 1976*).

The remarkable resistance of the cobalt alloys to cavitation erosion is evident from the following figure, which indicates the depths of erosion recorded after 24 hours for several wrought cobalt alloys, nickel alloys, and stainless steels. Comparing the erosion rates of ULTIMET® alloy (which is carbide-free) with Alloy 6B (which contains approximately 13 wt.% carbide), it is evident that microstructural carbides have little effect on cavitation erosion resistance. More important is the transformation tendency, as indicated by the results for Alloy 25 and MP35N alloy, which are known to transform less than ULTIMET® alloy and Alloy 6B. The data in the figure were generated using the vibratory cavitation test described in ASTM Standard G32. Essentially, the apparatus comprises a transducer (the source of the vibrations), a tapered cylindrical member to amplify the oscillations, and a temperature controlled container, in which the test liquid (distilled water) is held. The specimens were shaped as cylindrical buttons of diameter 14 mm, with a 6.4 mm threaded shank that was screwed into a threaded hole in the end of the tapered cylinder. As recommended by the ASTM Standard, a frequency of 20 kHz and an amplitude of 0.05 mm were used during the tests, and the distilled water was maintained at 16°C.

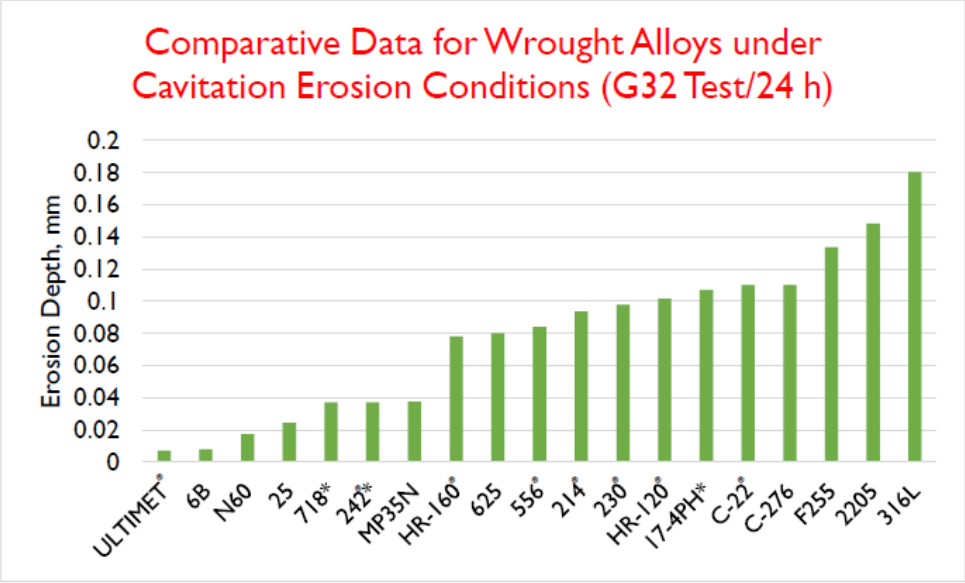

*Age Hardened

For all liquids, the maximum cavitation erosion rate usually occurs at a temperature midway between the freezing and boiling points (*Hutchings, 1986*). For example, *Zhou and Hammitt, 1983* describes a study of the effect of temperature

upon the cavitation erosion resistance of 304 stainless steel in water; a maximum was measured at about 50°C. As regards the effects of time, it is known that there is a short incubation period, prior to the loss of material, under cavitation conditions (*Hutchings, 1986*). In the case of the cobalt alloys, this incubation period is less than 8 hours. After longer periods, a reduction in the erosion rate has been observed with most materials. The effects of longer test durations upon the cavitation erosion resistance of ULTIMET® alloy are illustrated in the figure below, which also indicates differences between product forms.

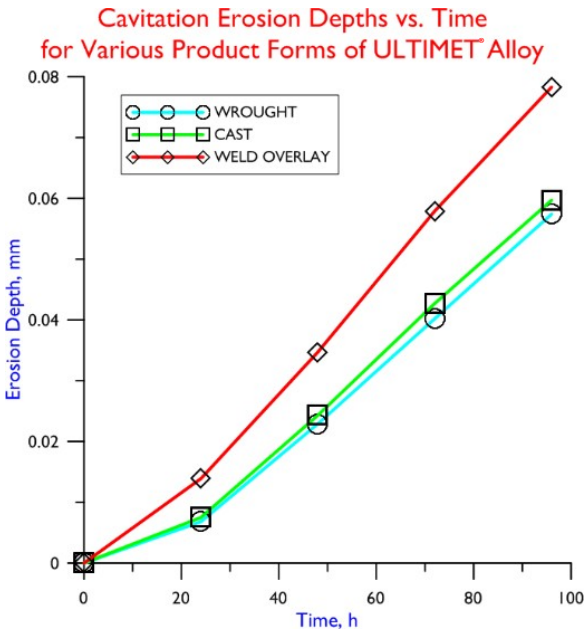

Many wear-related applications of the cobalt alloys involve the use of weld overlays. Unless multiple layers are applied, dilution (i.e. intermixing of the wear-resistant cobalt alloy with the substrate material, normally a steel or stainless steel, in the molten weld pool) can degrade the wear performance of the overlay material. The following figure depicts the results of *Crook, 1993*, who studied the effects of dilution upon ULTIMET® alloy (the experimental approach is described in the section on galling). From these results it can be ascertained that the effects of dilution (at least upon ULTIMET® alloy, and up to the 16.7% level with steel or stainless steel) are not extremely detrimental over a 96 h test period.

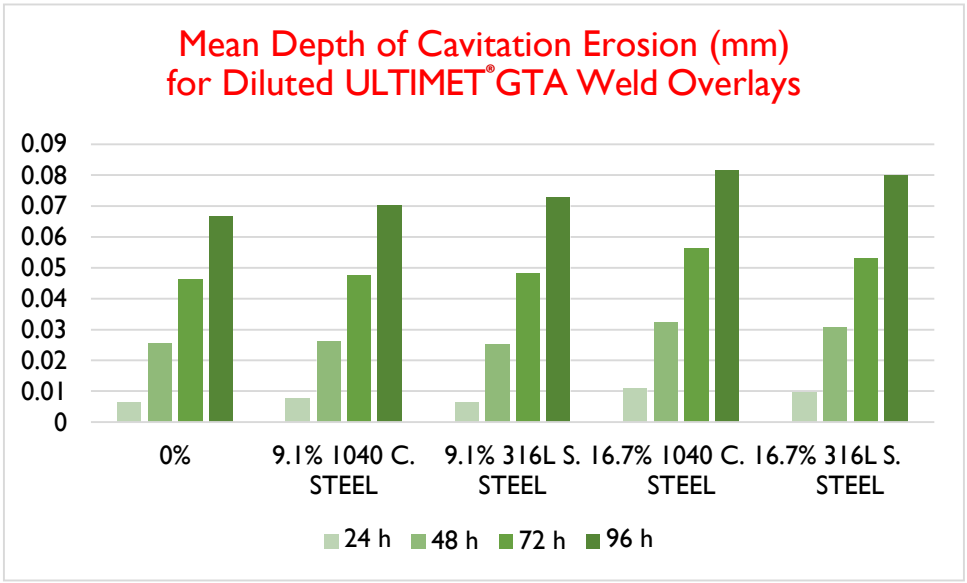

Slurry Erosion

Slurry erosion, caused by solid particles entrained in liquid streams, is a complex phenomenon. At high impact angles (i.e. perpendicular to the plane of the surface), the process bears some resemblance to solid particle erosion. In fact, the sand blasting of buildings is often carried out with a sand / water slurry, to minimize airborne debris. However, the impact forces are markedly affected by the presence of the liquid. At low impact angles, the process is more akin to low stress abrasion, with the particles forced against the surface hydro-dynamically. If the surface is metallic and the liquid is corrosive (and water can be corrosive to steels), then there is a high probability of erosion / corrosion, an allied process involving the mechanical stripping of passive films, leading to high rates of chemical attack.

The only slurry erosion test data generated by Haynes International (in conjunction with Lawrence Berkeley Laboratory) comparing 6B, 25, and ULTIMET® alloys is shown below (ref. *Levy and Crook, 1991*). The test, of duration 40 h, was carried out in an enclosed slurry pot, with samples and a propeller attached to a rotating shaft. The slurry was alumina (80 μm) in water at room temperature, with a particle loading of 0.12 kg/l. The impact angle was 30° and the impact velocity was 5 m/s.

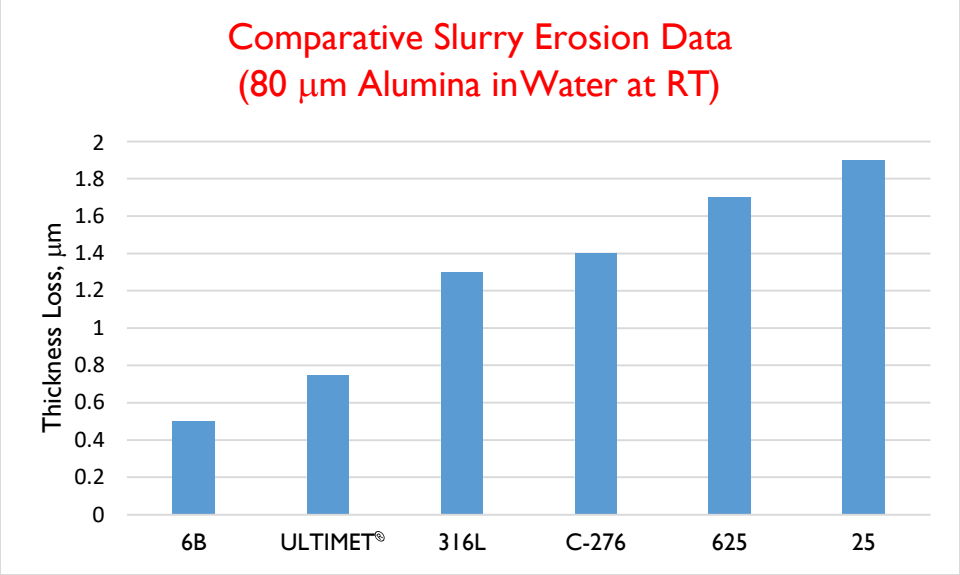

Metal-to-Metal Sliding Wear

Of the metallic materials, cobalt-based alloys are generally regarded as the most resistant to sliding wear at high loads, in the absence of lubrication. Under such conditions, a form of damage known as “galling” is common; this is thought to occur by gross plastic deformation, atomic bonding (or cold welding), then fracture on one or both surfaces, leading to material transfer. As will be shown, test results confirm that cobalt-based alloys are resistant to galling. Moreover, they indicate that the stainless steels are very prone to this form of damage, independent of their atomic structure.

Galling, however, is not the only form of damage encountered in unlubricated sliding systems. At lower loads, and particularly at high relative velocities (which induce considerable heating of the metallic surfaces), oxide growth and stripping is a possibility. Under such circumstances (sometimes termed “oxidative” wear), the characteristics of the base metal are somewhat masked. This is certainly true at temperatures in excess of about 500°C, where oxides tend to control the sliding wear process, as long as the underlying material is sufficiently supportive. At very high temperatures, very smooth oxide surfaces can be generated on sliding metallic materials; it has been surmised that these so-called “glazes” might involve some form of thermal transformation, or that fine oxide particulates are easily sheared and even out the contact surfaces.

The history of metal-to-metal wear testing at Haynes International (and former companies) spans 40 years. In the early years (1978 to 1986), galling and pin-on-block tests were used to evaluate and compare the characteristics of the cast and weld overlay materials (mostly cobalt- and nickel-based) in the company portfolio at that time (the hard-facing segment of the business was sold in 1986). A pin-on-disc (POD) unit, capable of elevated temperature testing, was built, but gave dubious results, and quickly fell out of favor. Some room and elevated temperature, metal-to-metal contract testing (at General Atomic, in California) was carried out in 1981 (*Crook and Li, 1983*), and gave clear indications of the benefit of cobalt, even though it was concerned with weld overlay (hard-facing) materials and not wrought products.

The second period of metal-to-metal testing at Haynes International coincided with the development and promotion of ULTIMET® alloy, the first wrought, cobalt-based, corrosion and wear resistant material to emerge from the laboratories of Haynes, following the sale of the hard-facing business. This period was from 1989 to 1992 and involved mostly galling tests of wrought material, although other forms of ULTIMET® alloy were tested, in particular weld overlays made from Haynes-produced wrought wire consumables.

Haynes International has only recently entered its third period of metal-to-metal testing, by virtue of the purchase of an ASTM G99 compliant pin-on-disc tester, plus the re-furbishing of Haynes' galling test fixtures. More importantly, Haynes International has acquired a wide-area, laser-based, 3D measurement system, to enable extremely accurate surface analyses.

The ASTM G99 compliant, pin-on-disc test and the Haynes galling test are at opposite ends of the metal-to-metal sliding wear spectrum. The pin-on-disc test simulates high speed/low load conditions (found in many bearings and rotating seals, for example), whereas the galling test simulates low speed/high load conditions (found during the high torque attachment and detachment of bolts, for example). In the absence of liquids, high surface temperatures can be generated during high speed/low load, metal-to-metal sliding; these can result in debris containing oxide particles. Galling, on the other hand, can result in seizure (due to bonding of the materials) and can generate relatively massive amounts of damage over small sliding distances (large chunks of material being transferred from one surface to the other, or released at the interface).

To illustrate the influence of alloy base and of strengthening mechanism on high speed/low load sliding wear, early work at Haynes International on the ASTM G99 compliant, pin-on-disc tester has been focused on (self-coupled) HAYNES® 25, 230®, and 282® alloys. HAYNES® 25 alloy is a cobalt-based alloy containing 10 wt.% nickel to adjust its transformation tendency. HAYNES® 230® alloy is a nickel-based alloy with remarkably similar alloying additions, at similar levels. HAYNES® 282® alloy is a gamma-prime strengthened, nickel-based material.

The extent of pin wear on the three alloys is shown in the following bar chart, which indicates that the cobalt-based, HAYNES® 25 alloy is the most resistant of the three alloys to wear at a load of 30 N, and a linear speed of 2 m/s.

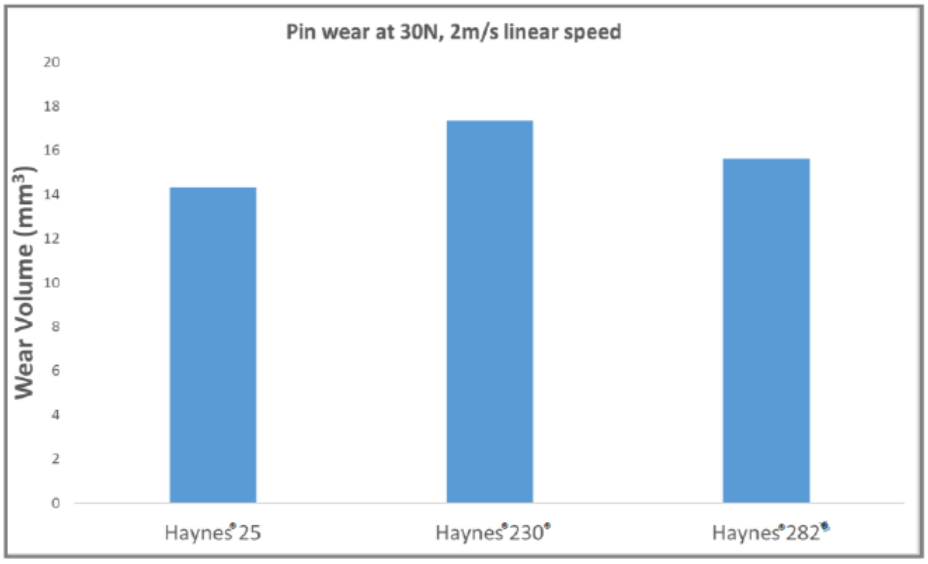

Gamma-prime strengthened HAYNES® 282® alloy was found to be significantly more resistant to wear under these conditions than the solid-solution strengthened, nickel-based, HAYNES® 230® alloy. Moreover, it was discovered that 282® alloy exhibits very low coefficients of friction at loads of 10 and 20 N, whereas the coefficients of friction for 25 and 230® alloys are generally independent of load in the range 10 to 30 N, as illustrated in the charts below.

Continuous Measurements of Coefficient of Friction for HAYNES® 282® Alloy at Loads of 10, 20, and 30 Newtons (Linear Sliding Speed 2 m/s)

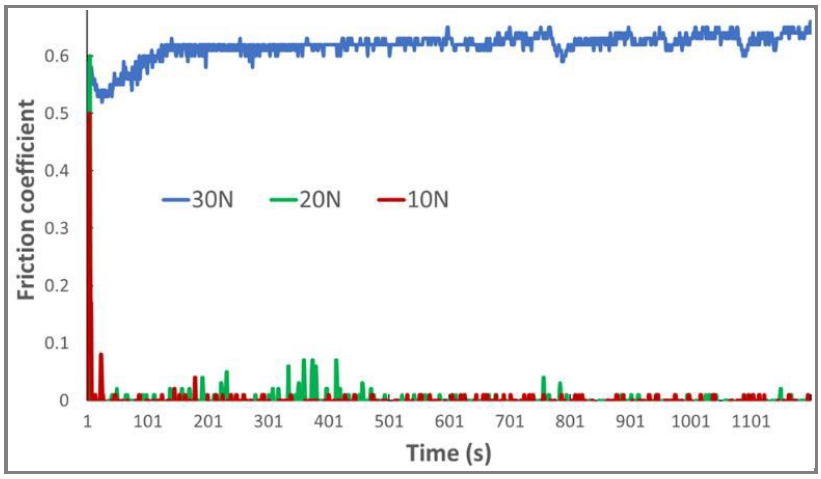

Continuous Measurements of Coefficient of Friction for HAYNES® 25 Alloy at Loads of 10, 20, and 30 Newtons (Linear Sliding Speed 2 m/s)

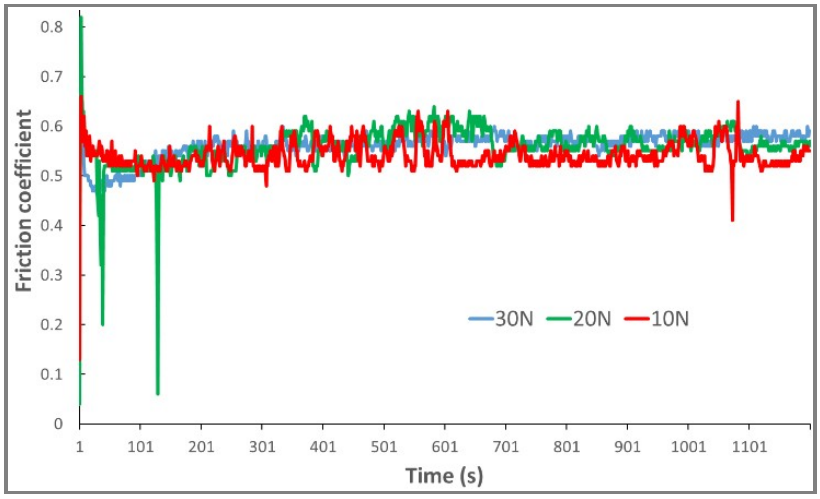

Continuous Measurements of Coefficient of Friction for HAYNES® 230® Alloy at Loads of 10, 20, and 30 Newtons (Linear Sliding Speed 2 m/s)

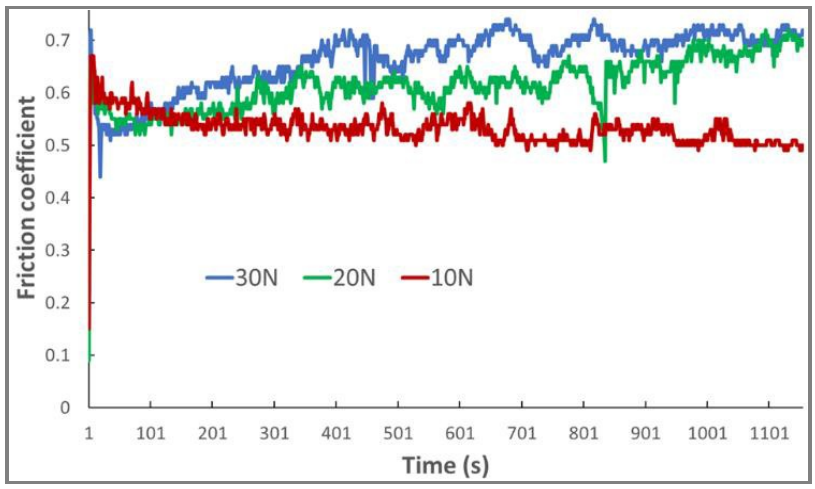

The first galling test used by Haynes International was of simple design, and involved the rotation (through 360°) of a 9.5 mm diameter pin (the sliding surface being a flat section, perpendicular to the cylindrical axis) against a block of dimensions 102 mm x 102 mm x 12.7 mm, under various loads (applied using a tensile testing machine, in compression mode). The main problem with this test, apart from load variations associated with deformation and fracture events at the sliding interface and the pin-to-machine coupling, was the subjective nature of the analysis.

Analysis involved visual inspection of the sliding surface and a determination of whether or not "galling" had occurred. Tests were performed at various loads, which were converted to stresses using the apparent area of contact, and a threshold stress (the lowest at which galling was observed) determined. This first test was unable to differentiate between the various wear-resistant, cobalt-based STELLITE® alloys in the Company's product portfolio at that time, and scanning electron microscopy suggested that the visual inspection was revealing only the scale of the damage, i.e. surfaces purported to be free of galling exhibited the same signs of damage, only on a micro-scale.

To remedy some of the limitations of this first test, changes were made (especially after a visit to the tribology laboratory of Armco, which was using a similar test, but using a clockwise-anticlockwise, multiple rotation technique). The most important change was to replace visual inspection with a quantitative determination of the change in peak-to-valley amplitude of the block surface, using surface profilometry. Generally, the pin and block surfaces appeared to exhibit similar changes; it was therefore deemed appropriate to analyze only the block surface, which was more amenable to profilometry (no edge drop-off). Other changes included a pin of larger diameter (15.9 mm) to accommodate a larger female cone shape on top (to hold the ball bearing used for load transfer from the tensile machine), and a 10-stroke clockwise-anticlockwise rotation technique over a 120° arc.

As an aside, the ASTM Standard (G98) Test Method for Galling Resistance of Materials is similar to that used by Armco, which had a strong ASTM representation. However, it requires a single revolution of the pin (which is termed a button in the standard) and a subjective judgement of threshold galling stress (which had been deemed unacceptable for ranking of the cobalt-based alloys).

Self-coupled/mated galling data (for many of Haynes International's current portfolio of wrought products) generated using the test introduced in 1981, and involving surface profilometry, are given in the following three figures (each corresponding to a specific load).

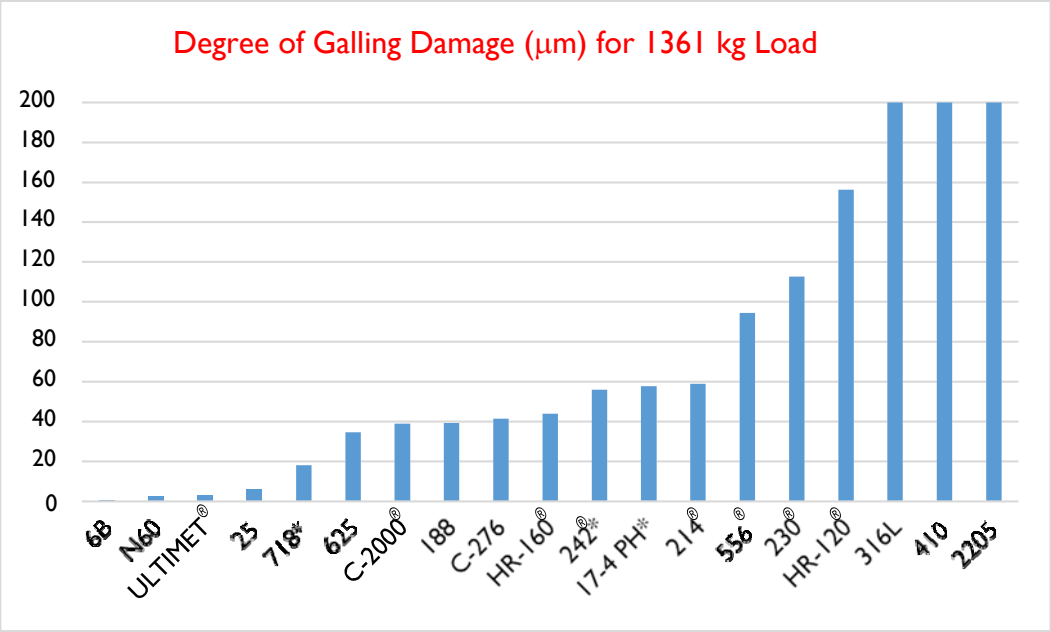

*Age Hardened

316L, 410, and 2205 suffered total seizure (with a degree of damage exceeding 200 μm)

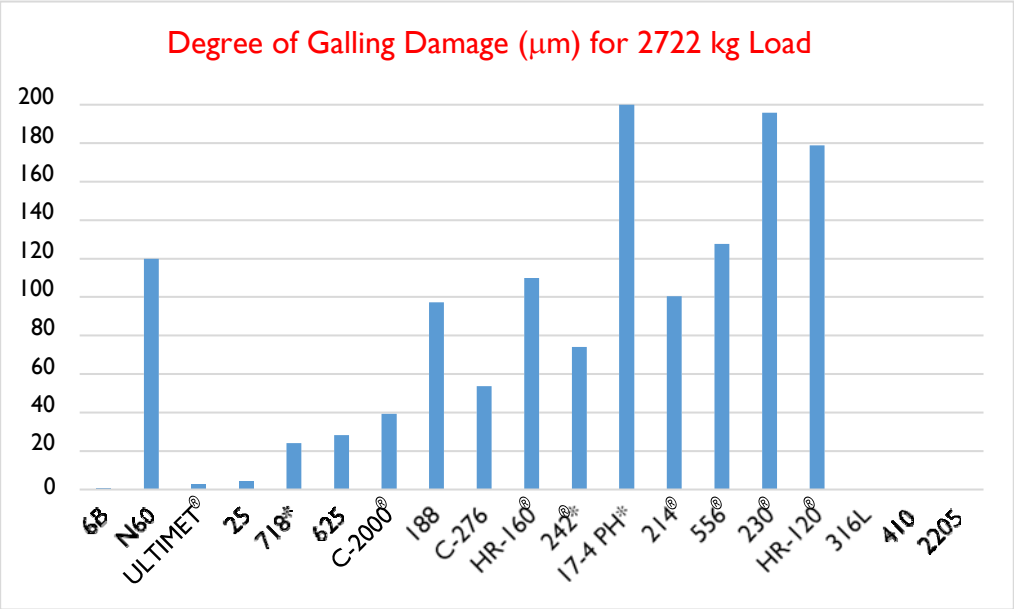

*Age Hardened

316L, 410, and 2205 were not tested at a load of 2722 kg

17-4 PH was too rough to measure (with a degree of damage exceeding 200 μm)

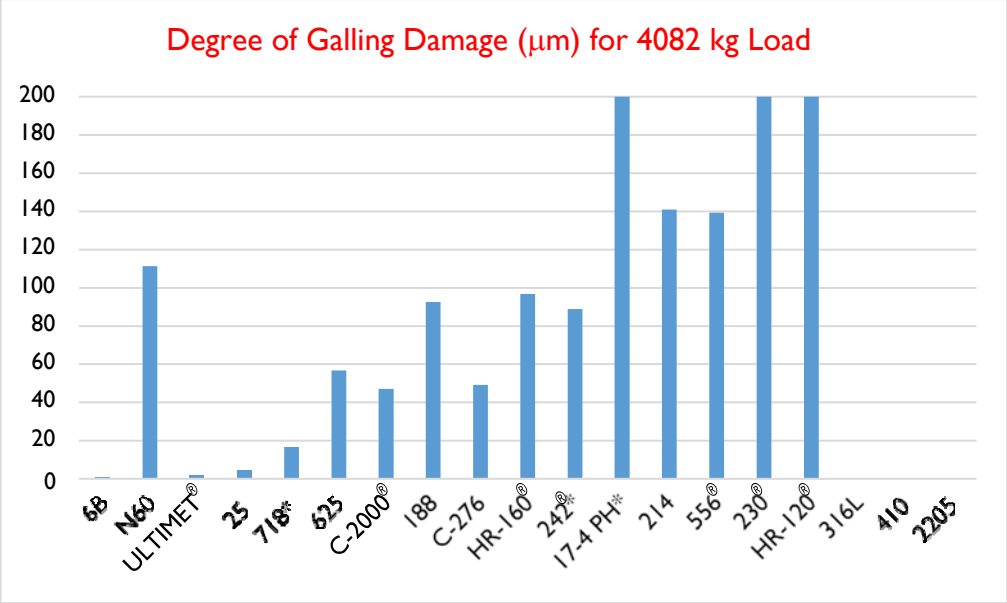

*Age Hardened

316L, 410, and 2205 were not tested at a load of 4082 kg

17-4 PH was too rough to measure (with a degree of damage exceeding 200 μm)

The values for 230® and HR-120® alloys exceeded 200 μm

Review of these figures indicates that:

1. The cobalt-based materials 6B alloy, ULTIMET® alloy, and 25 alloy exhibit very high resistance to galling, when self-coupled, at all three loads.
2. NITRONIC® alloy 60 (a high-silicon, 200-type, austenitic stainless steel, developed by Armco) exhibits very high resistance to galling at the lowest load, but offers poor resistance to galling at the higher loads.
3. Nickel is detrimental to the galling resistance of the cobalt alloys, as illustrated by the performance of 188 alloy (22 wt.% Ni) relative to those of ULTIMET® alloy (9 wt.% Ni) and 25 alloy (10 wt.% Ni).
4. Of the nickel-based alloys tested, the most galling-resistant is age-hardened 718 alloy; this bodes well for other gamma-double prime or gamma-prime strengthened super-alloys.
5. The nickel-chromium-molybdenum (C-type) alloys and 625 alloy exhibit moderate resistance to galling over the range of loads studied.
6. Apart from NITRONIC® alloy 60, the stainless steels are extremely prone to galling; indeed, with the exception of age-hardened 17-4 PH alloy, the stainless steels tend to bond so strongly that they seize up during self-mated testing (so much so that tests at the higher loads were not even contemplated).

As to the effects of different counterface materials, these are illustrated for wrought ULTIMET® alloy in the following figure. For all of these tests, the pin was made from ULTIMET® bar, and the block was made from plate of the counterface material (denoted along the x-axis). ULTIMET® alloy is compatible with many different materials in a galling sense; this is not necessarily true for other cobalt alloys. Note that the influence of load upon degree of damage is not strong, except in the case of 304 and 410 stainless steels.

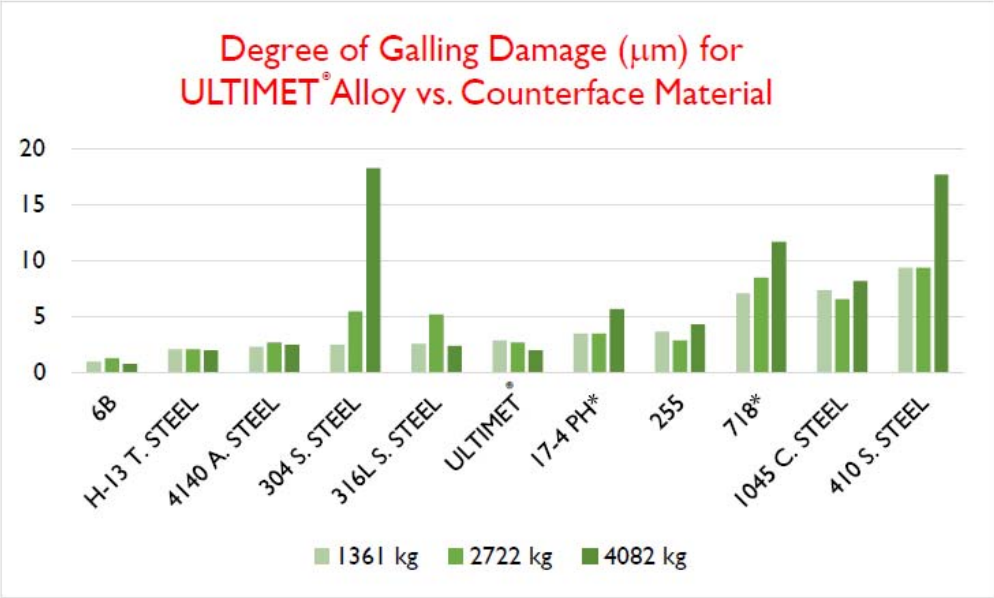

In recognition of the fact that many applications of the wear-resistant cobalt alloys involve weld overlays (of critical surfaces), the figure below depicts the effects of dilution upon the galling resistance of ULTIMET® welds, as applied by the gas tungsten arc (or TIG) welding process. These data (*Crook, 1993*) were generated using an unusual approach, involving the manufacture of pre-mixed consumables, and their deposition onto chilled copper blocks, to create "all-weld-metal" samples of known and homogeneous composition.

In acknowledgement of the fact that the effects of dilution are dependent upon the type of substrate, two compositionally dissimilar materials were selected for pre-mixing with ULTIMET® alloy. These were 1040 carbon steel and 316L stainless steel. With regard to the levels of dilution chosen for study (9.1% and 16.7%), these represent

"overlay to substrate" ratios of 10:1 and 5:1 (dilution is defined as the percentage of substrate in the weld bead). Undiluted samples of ULTIMET® alloy were also prepared and tested.

To make the pre-mixed consumables (welding rods of diameter 4.8 mm), a high frequency furnace and an overhead aspiration casting system were utilized. The charge materials were forged billet (in the case of ULTIMET® alloy), and cut pieces of wrought plate (in the case of carbon steel and stainless steel).

From these data, it is evident that dilution (at the 9.1% and 16.7% levels, which would be considered low to moderate) has little effect upon the galling resistance of ULTIMET® alloy.

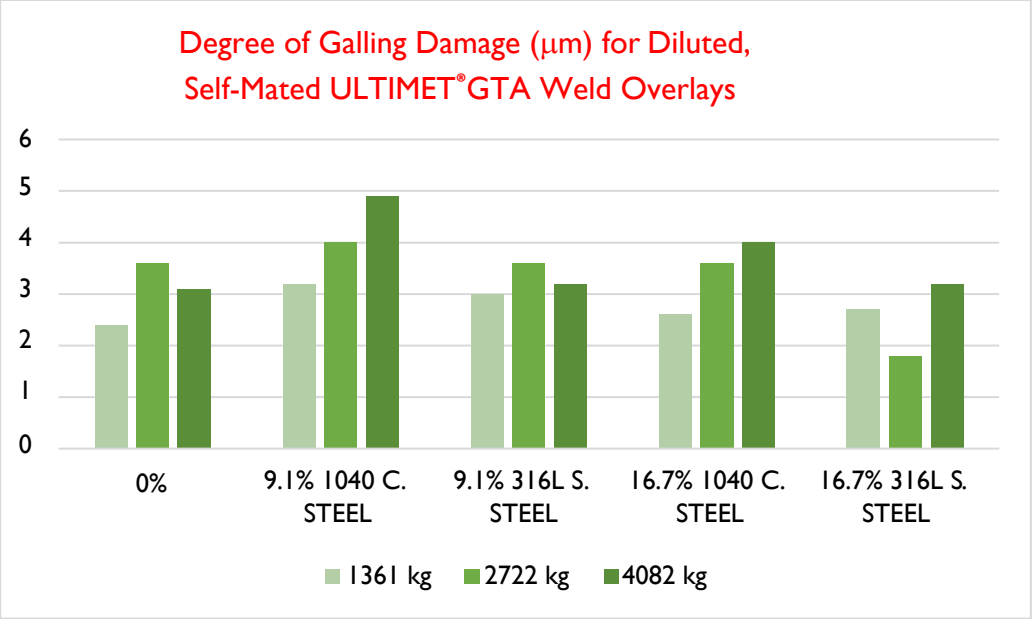

Although the aforementioned metal-to-metal sliding tests performed at General Atomic in 1981 concerned the performance of hard-facing (not wrought) materials, they did indicate the importance of alloy base and temperature. The resulting graphs are therefore of value, and are presented below.

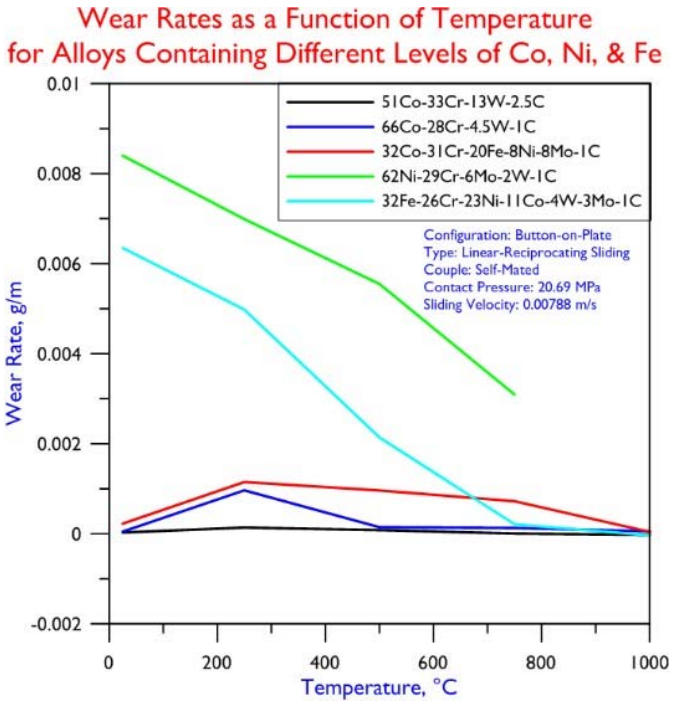

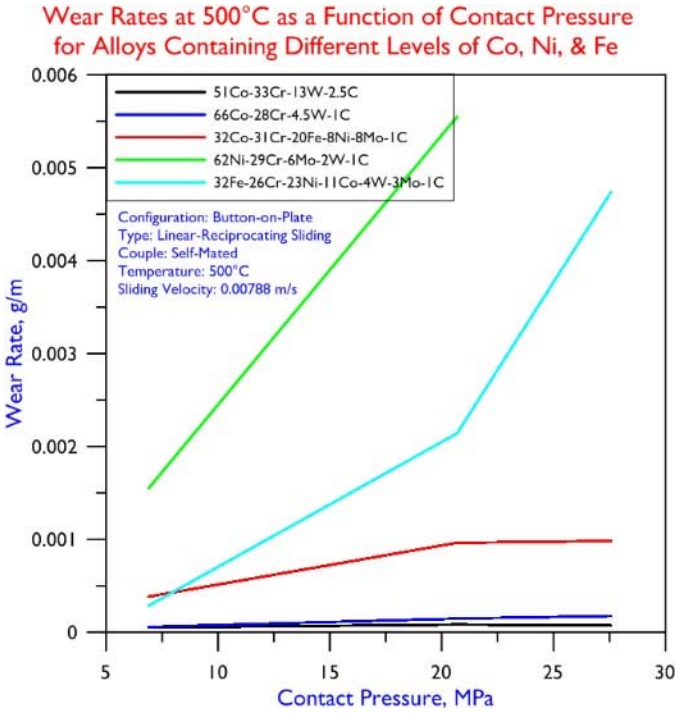

Finally, it is important to indicate the sophistication and accuracy of modern wear testing at Haynes International. Recently (*Krishnamurthy and Crook, 2018*), galling tests were performed to quantify the benefits of cobalt as a wear alloy base, and to study the advantages of gamma-prime strengthening (of nickel-based alloys). To accomplish this, HAYNES® 25, 230®, and 282® alloys were compared. The results, which were generated using the wide-area, laser-based, 3D measurement system, are shown in the following bar charts. These involved a load of 2722 kg (6000 lb) and the 1981 multi-stroke procedures.

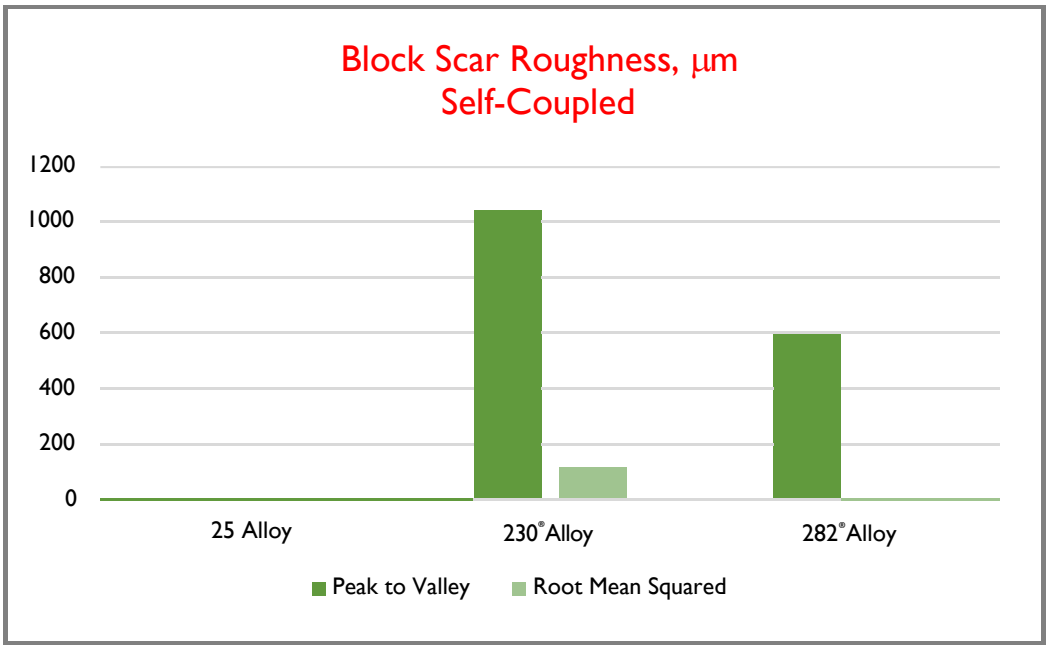

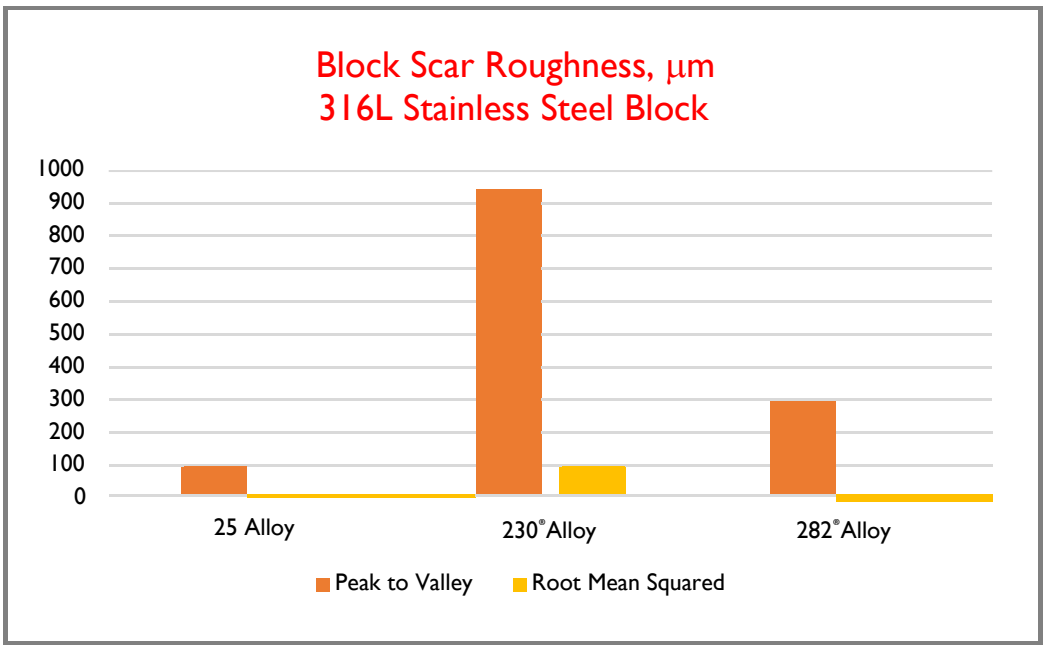

From these charts, it is evident that:

1. Cobalt (as a wrought alloy base) provides much higher resistance to galling than does nickel, whether measured in terms of peak to valley roughness, or root mean squared roughness, of the block scars.
2. This applies to self-coupled systems and to 316L counter-faces.
3. Gamma-prime strengthening is very beneficial to the galling resistance of high-temperature nickel alloys, both under self-coupled conditions, and versus 316L stainless steel.

Importantly, the values in the above bar charts represent laser-based readings over the total scar areas, rather than stylus-based readings along two diameters (as in previous times). Also, all couples were tested twice, and the results averaged.

The final figure, shown below, is a laser-generated image (magnified by 1500x) of the HAYNES® 230® block scar, color-coded to indicate the heights and depths of the surface features.

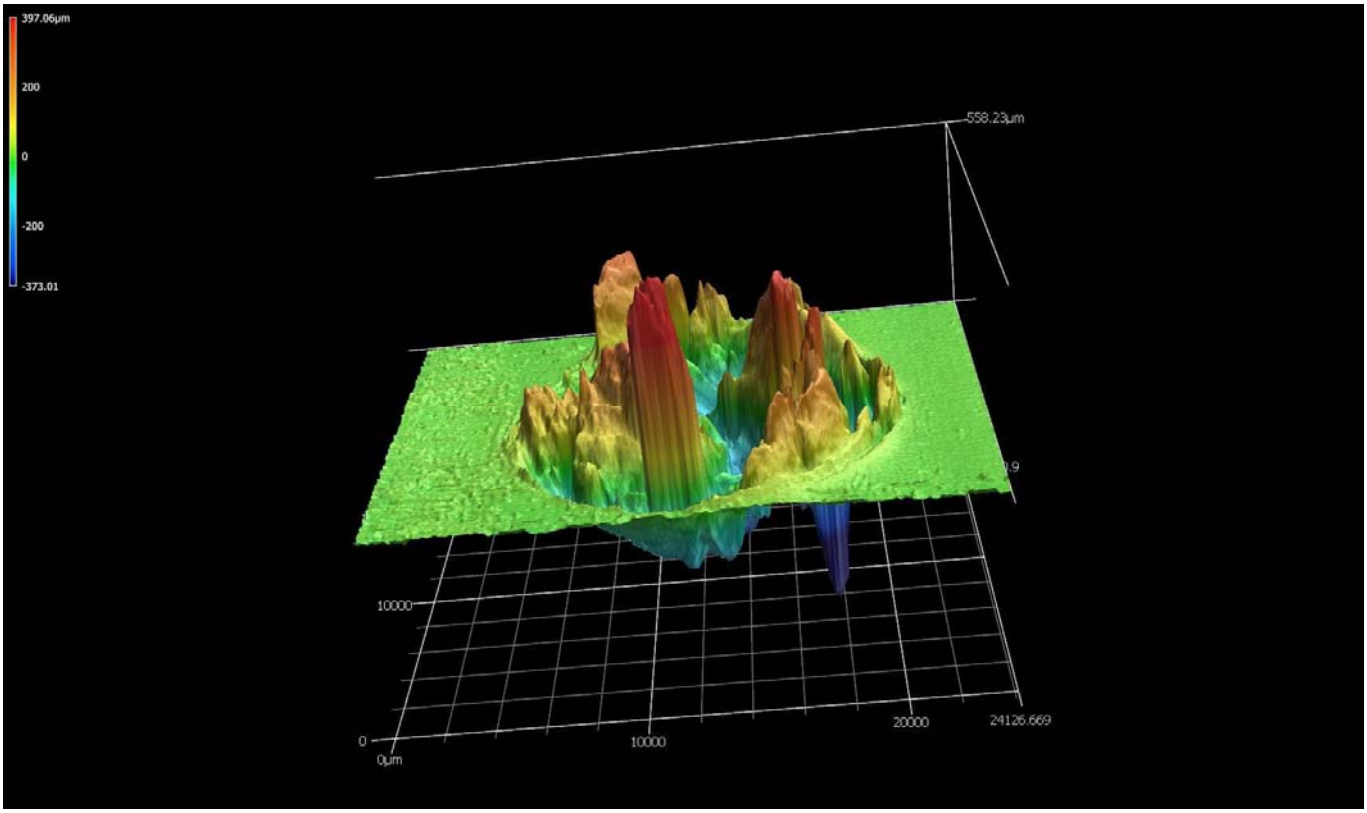

References

Antony and Silence, 1979 Antony, K.C. and Silence, W.L., Proceedings of the 5th International Conference on Erosion by Liquid and Solid Impact, Cambridge Press, 1979, Paper No. 67.

Aptekar and Kosel, 1985 Aptekar, S.S. and Kosel, T.H., Proceedings of the International Conference on Wear of Materials, 1985, ASME, p 677-686.

Aylor et al, 1999 Aylor, D.M., Hays, R.A., Kain, R.M., and Ferrara, R.J., Paper 329, Corrosion 1999, NACE International.

Berns and Fischer, 1993 Berns, H. and Fischer, A., Wear, Vol. 162-164, 1993, p441-449.

Chambers, 2002 Chambers, G., Proceedings of Stainless Steel World Conference, 2002.

Crook, 1993 Crook, P., Corrosion Science, Vol. 35 (Nos. 1-4), 1993, p 647-653.

Crook and Caruso, 2004 Crook, P. and Caruso, M.L., Paper No. 04221, Corrosion 2004, NACE International.

Crook and Li, 1983 Crook, P. and Li, C.C., Proceedings of the International Conference on Wear of Materials, 1983, ASME.

Crook and Meck, 2005 Crook, P. and Meck, N.S., Paper 645, Eurocorr 2005, Lisbon, Portugal.

Crook et al, 2007 Crook, P., Meck, N.S., and Rebak, R.B., Corrosion 2007, NACE International.

Crum et al, 1999 Crum, J.R., Smith, G.D., McNallan, M.J., and Hirnyj, S., Paper No. 382, Corrosion 1999, NACE International.

Dillon, 1994 Dillon, C.P., MTI Publication No. 45, 2nd Edition, NACE International, 1994, p 139-140.

Friend, 1980 Friend, W.Z., Corrosion of Nickel and Nickel-Base Alloys, Wiley, 1980, p 228-232.

Gulden, 1979 Gulden, M.E., Proceedings of the 5th International Conference on Erosion by Liquid and Solid Impact, Cambridge Press, 1979, Paper No. 31.

Gutherie and Stansbury, 1961 Gutherie, P.V. and Stansbury, E.E., ORNL Report 3079, 1961.

Green et al, 1981 Green, G.M., Taggart, R., and Polonis, D.H., Metallography, Vol. 14, 1981, p 191-212.

Hodge, 1973 Hodge, F.G., Corrosion, Vol. 29, No. 10, 1973, p 375-383.

Hutchings, 1983 Hutchings, I.M., Monograph on the Erosion of Materials by Solid Particle Impact, MTI Publication No. 10, MTI, 1983.

Hutchings, 1986 Hutchings, I.M., The Erosion of Materials by Liquid Flow, MTI Publication No. 25, MTI, 1986.

Jennings, 2006 Jennings, H.S., ASM Handbook, Vol. 13C: Corrosion – Environments and Industries, ASM International, 2006, p. 690-703.

Klarstrom, 1987 Klarstrom, D.L., ASM Metals Handbook, Vol. 13, Corrosion, ASM, 1987, p 647-650.

Klarstrom, 1993 Klarstrom, D.L., Proceedings of the 12th International Corrosion Congress, NACE International, 1993.

Krishnamurthy and Crook, 2018, Krishnamurthy, R. and Crook, P., Unpublished Work, Haynes International, 2018.

Levy, 1981 Levy, A.V., Wear, Vol. 68, 1981, p 269-287.

Levy and Crook, 1991 Levy, A.V. and Crook, P., Wear, Vol. 151, 1991, p 337-350.

Ninham, 1987 Ninham, A., Wear, Vol. 121, 1987, p 307-324.

Pike et al, 2003 Pike, L.M., Klarstrom, D.L., and Rothman, M.F., U.S. Patent 6,544,362, April 2003.

Raghavan et al, 1982 Raghavan, M., Berkowitz, B.J., and Scanlon, J.C., Metallurgical Transactions A, Vol. 13A, 1982, p 979-984.

Raynor and Rivlin, 1981 Raynor, G.V. and Rivlin, V.G., Intl. Metals Rev., Vol. 26, 1981, p 213-249.

Rebak, 2005 Rebak, R.B., Paper No. 05457, Corrosion 2005, NACE International.

Rebak et al, 2001 Rebak, R.B., Dillman, J.R., Crook, P., and Shawber, C.V.V., Materials and Corrosion, Vol. 52, 2001, p 289-297.

Sridhar, 1987 Sridhar, N., Paper No. 19, Corrosion 1987, NACE International, 1987.

Srivastava and Crook, 2016 Srivastava, S.K. and Crook, P., Unpublished Work, Haynes International, 2016.